DOTTORATO DI RICERCA IN SCIENZE CHIMICHE

XXVI CICLO

Tesi di dottorato

Approcci innovativi della chemoterapia a base metallica per la cura del mesotelioma pleurico maligno (MPM)

Relatore: Prof. Domenico OSELLA

Coordinatore: Prof. Domenico OSELLA

Candidato: Dr.ssa Ilaria BONARRIGO

Philosophiae servias oportet,
ut tibi continua vera libertas

SENECA
(4 a. C. – 65 a. C.)

The real voyage of discovery
consists not in seeking new landscape
but in having new eyes

MARCEL PROUST
(1871 – 1922)

Index

Abstract

Malignant pleural mesothelioma (MPM) is a highly aggressive tumor that originates from mesothelial cells of the pleura, a serous membrane that lines and lubricates the lungs and the inside of the rib cage. The main risk factor for mesothelioma is prolonged exposure to asbestos. Redox stimuli caused by asbestos trigger to a strong and prolonged inflammation, which leads to altered gene expression inducing, *inter alia*, an increase of antioxidant enzymes and glutathione (GSH), and to the selection of cells characterized by proficient DNA-repair and anti-apoptotic ability. The interplay of all these mechanisms is at the basis of the by intrinsic chemoresistance of MPM.

An extensive meta-analysis indicated cisplatin, a platinum(II) complex, as the most effective single agent for MPM treatment, despite an objective response rate of only 23%. The current gold-standard protocols are based on cisplatin combined with the antifolate pemetrexed. However, this chemotherapy regimen improves the median overall survival for patients with MPM of very few months. Furthermore, the tumor recurrence, due to chemoresistance, and the cisplatin heavy side effects limit the therapeutic efficacy.

For this reason, we carried out several research lines in order to discover novel metal- based drug candidates.

We mainly focused our investigations on **platinum(IV) complexes** aimed to improve the **selectivity,** the **antitumoral activity,** and to **bypass the pharmacological resistance to Pt(II)-based drugs, as cisplatin, oxaliplatin and picoplatin**. It is widely believed that reduction from Pt(IV) to platinum(II) is essential for the anticancer activity of these complexes, that are otherwise rather inert; therefore, they behave as pro-drugs. Moreover, they could be functionalized with several bioactive molecules (obtained the so-called bi-functional drugs), joining the cytotoxic activity of Pt-based drug with a further biological property.

Since MPM arises from a chronic inflammation, the inducible isoform of cyclooxygenase (COX-2) represents a good pharmacological target. Therefore, in a further research line we investigated a **cobalt-based complex** (called Co-ASS), derived from a well-know COX-2 inhibitor, aspirin. The obtained results showed that the biological activity of the candidate drug mainly depends on the cellular context, as it acts as CO-releasing molecule (CO-RM), which retains a NSAID effect.

The second approach aimed to optimize platinum-based combinatorial chemotherapy, in order to reduce cisplatin dosage and therefore, its side effects.

Apoptosis resistance in MPM cells is ascribed to the overexpression of proteins activating key pathways, such as c-myc. Thus, we aimed to drop **c-myc expression** by means of an epigenetic agent, JQ1. We analyzed the pharmacological pattern of the **cisplatin-JQ1 association** and investigated the better schedule of treatment.

Furthermore, in order to have more reliable results , we developed a protocol to perform drug screening on 3D cellular models (**spheroids**), that more accurately mimic the conditions of the tumor tissue.

Introduction

Exploring general pharmacology

What is pharmacology?

Pharmacology (from Greek *pharmakon, "*drug", and *–logos,* "knowledge of") is a branch of science that examines the interactions of bioactive molecules (*i.e.* neurotransmitters, hormones, toxins, small molecules) with living systems, their properties and the mechanisms of action through which they elicit biological effects. Bioactive molecules are generally defined **drugs**.

Pharmacological studies dissect the processes at molecular, subcellular and systemic level; these investigations are intended for both therapeutic and non-therapeutic purposes (e.g. toxicological studies). Pharmacology has evolved over the years, and nowadays is especially focused on *drug discovery*, the process by which novel drug candidates for treatment and prevention of a specific disease are synthesized, and then selected on the basis of their activity and safety. Within this scenario, pharmacology shares intimate connections with other disciplines including chemistry, physiology, biology, medicine and genetics.

The pharmacological sciences can be further subdivided in several subgroups, depending on the discipline of interest (neuropharmacology, cardiovascular pharmacology, chemotherapy, molecular pharmacology etc…)

Characteristics of drug - receptor interactions

Usually, drugs are designed or to mimic or to block the physiological action of bioactive endogenous molecules. To generate a biological effect, a drug has to interact with its target defined *receptors, i.e.* macromolecules (usually proteins or nucleic acids) located on the cell surface or within the cytoplasm.

In the broad sense, a molecule that binds to a receptor is called *ligand*. Ligands bind to precise receptive macromolecular regions of the target, called *recognition sites* or *binding sites*. Ligand binding to a receptor alters its conformation and modulates its functional status leading to changes in biochemical processing or chemical signaling that trigger the biological response.

The interaction between the ligand and its target molecule mainly involves ionic, hydrophobic, hydrogen bonds and Van der Waals forces. The combination of this forces leads the molecule to reside in a certain position within the complementary binding region. Irreversible covalent bonds are rare in biological systems: for this reason, the *classical theory of drug-receptor interactions* assumes reversible binding at 1:1 stoichiometry based on the *mass action law* (Equation 1)*:*

$$[R] + [X] \overset{K_{on}}{\longleftrightarrow}_{K_{off}} [RX] \qquad (1)$$

where [R],[X] and [RX] represent the molar concentration of receptor, drug, and receptor-drug adduct (or complex), respectively, and where it is assumed that the reaction components are in dynamic equilibrium (that means the rates at which ligand-receptor adduct is formed and dissolved are equal). The ligand-receptor interaction is limited by the available binding sites, thus, it is saturable. K_{on} and k_{off} in Equation (1) represent the rate constants for association and dissociation of the ligand-receptor complex, respectively.

The *condicio sine qua non* a particular drug-target binding occurs in living organisms, where several types of ligands and receptors exist, is the attractiveness of a given molecule to a receptor, depending on the strength of the chemical forces between the two species; this property is defined **affinity**.

The affinity constant (K_a) indicates how the equilibrium (1) is shifted towards the complex formation; it means that higher the affinity is, the lower the drug concentration required to reach receptor saturation is (Equation 2):

$$K_a = \frac{K_{on}}{K_{off}} = \frac{[RX]}{[R][X]} \qquad (2)$$

However, the binding affinity is usually defined by the K_a reciprocal, the equilibrium constant of dissociation (K_d) (Equation 3):

$$K_d = \frac{K_{on}}{K_{off}} = \frac{[R][X]}{[RX]} \qquad (3)$$

K_d is inversely proportional to ligand affinity for the receptor [1].

From equation (3), with appropriate replacements, it is obtained that the concentration of bound drug (B) to the maximal available binding sites (Bmax) is:

$$B = \frac{([X]B_{max})}{K_d + [X]} \qquad (4)$$

This hyperbolic dependence (Equation 4) is called *binding isotherm* or *Langmuir isotherm* and expresses the values of fractional receptor occupancy as a function of drug concentration and receptor units occupied (Figure 1).

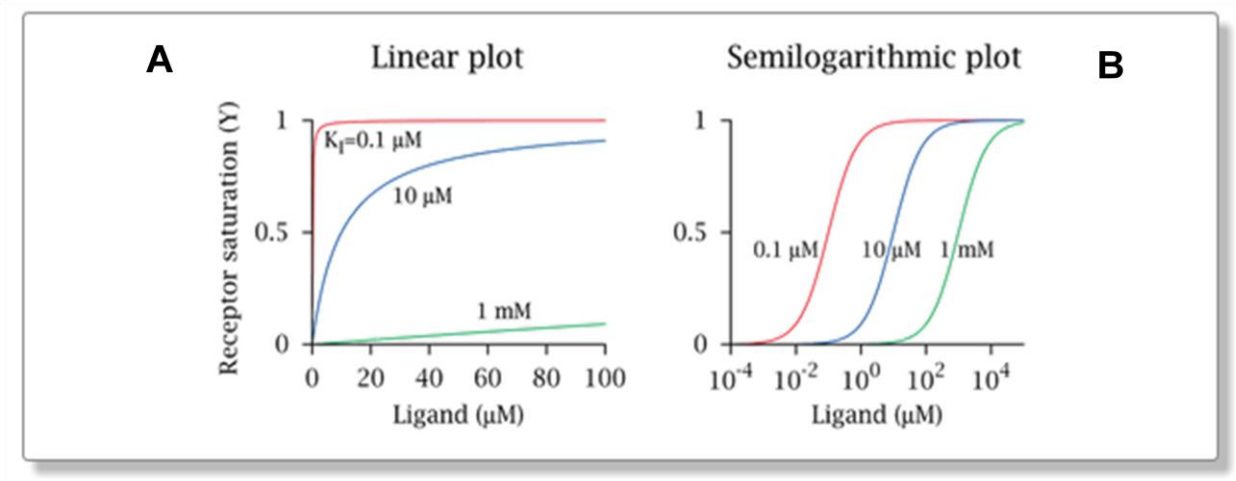

FIGURE 1. Binding isotherm or Langmuir isotherm: concentration of drug-receptor complex as a function of drug concentration (concentration-occupation curve) in presence of a limited number of receptive sites. B_{max} correspond to asymptote value of the curve. K_d stands for the drug concentration that induces half occupancy of total receptors. **A.** Linear plot (arithmetic scale). **B**. Same data plotted in semi-logarithmic scale [1].

As shown in Figure 1, the kinetics of binding is initially fast in keeping with the fact that there are many unbound sites for the drug; as the occupancy of receptor population occurs, there is a reduction of binding until reaching the maximal value of occupied sites.

B_{max}, corresponding to the asymptote value of the curve, stands for the maximal number of binding sites available, whereas K_d represents the concentration at half maximal binding (binding to 50% of receptor population) occurred. *Langmuir isotherm* model was adequate to depict and quantify affinity of a molecule for a single class of receptors (namely *homogeneous receptors*) [2]. However, in most cases a receptor exists in more subtypes (defined as *heterogeneous receptors*). Scatchard model is obtained through linear transformation of equation (4). Graphically, it plots the ratio of unbound ligand to bound ligand versus the bound ligand concentration. The plot depicts a straight line of slope, corresponding to $-1/K_d$, which intercept on X axis is B_{max}. As depicted in Figure 2, Scatchard model loses linearity in presence of multiple binding sites [3].

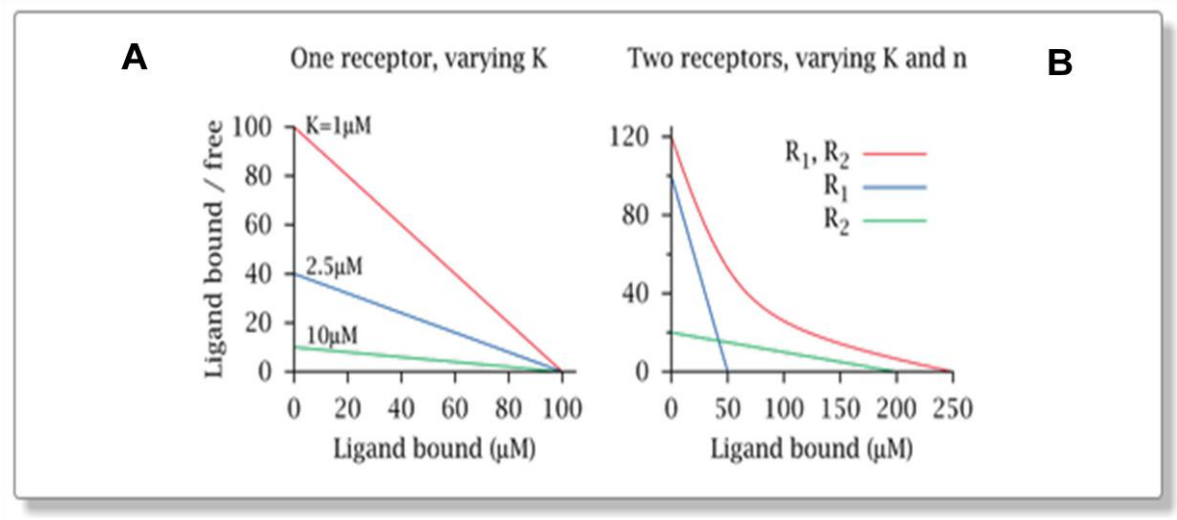

FIGURE 2. Scatchard plot. In order to construct this plot, the concentrations of both receptor-bound ligand and free ligand are measured, and the ratio of bound to free ligand is plotted against the concentration of free ligand. **A.** Linear fitting of data. The point where the line cuts the X axis represent B_{max}, while K_d stands for the value of the slope. If all drug molecules bind to a single class of receptors with uniform affinity, all data points will fall on a straight line. **B** If the plotted line is not straight, the binding sites (*n*) are inhomogeneous and vary in affinity [1].

As shown in Figure 1, if the curves are expressed in the arithmetic form, the data appear "compressed" and it would be difficult to correctly estimate fractional binding at various ligand concentration. The semi-logarithmic form is preferred because allows better extrapolation of the values, especially K_d, in accordance to the fact that places the midpoint in a linear portion of the graph. So, linear data regression models are inaccurate because distort experimental error and can be misleading; non-linear fitting plots are preferred because guarantee better parameter estimation. It is worth to underline that these considerations are not only true in this context, but could generalized for all mathematical models used in pharmacology.

Ligand binding affinity for particular receptor/s makes interaction **selective and specific**; selectivity is a property of the ligand, while specificity is a property of the receptor. Selective ligands bind preferentially few subtypes of receptors, while non-selective ligands bind to several types of targets. Selectivity plays an important role in pharmacology, because non-selective drugs tend to generate heavier side effects.

Specificity measure the discrimination of a receptor against other for a ligand binding and is determined by its spatial geometry. Non-specific drug binding also occurs (*i.e.* to plasma protein molecular sites), preventing the drug from binding to the desired target and prohibits it to exert its therapeutic effect [4].

Agonism and antagonism

Depending on the type of induced response, a drug is labeled with different denomination.

A molecule that binds to a receptor, alters its functional state and stimulates a functional activity is called an *agonist*. The bioactive molecule could be a *full agonist*, which leads to the maximal possible response in the system under study (α=1), or a *partial agonist (*$0 < \alpha < 1$*), i.e.* an agonist that under specified conditions does not elicit an effect as large. Finally, *inverse agonist* is a molecule that may actively reduces basal response. The binding sites for a drug may be the same or different from that of an endogenous agonist (hormone or neurotransmitter). Agonists that bind to a different site on a receptor are sometimes called *allosteric agonists.*

A compound that reversibly binds to a receptor and preventing binding with its own ligand, is called *antagonist* ($\alpha = 0$). Consequently, an antagonist inhibits or lowers the full response induced by drug.

There are several forms of antagonisms: competitive, non competitive and uncompetitive.

In competitive antagonism, antagonist "competes" with agonist for common binding site (so-called *orthosteric*) placed on the same receptor. Displacement of the agonist from its receptive unit lows its potency and, therefore, shifts concentration-response curve to the right. It is also known as *surmountable antagonism,* because if given at higher concentration, agonist will increase the number of occupied sites.

Because simultaneous binding of both ligand it is no possible, classic competitive antagonism is defined *mutually exclusive.*

At the contrary, non competitive antagonism is called *mutually inclusive,* because both species may interact simultaneously with their respectively receptive sites (known as *allosteric sites*); antagonist interaction prevents conformational changes in receptor, required to elicit a response, after agonist binding one its active sites. Unlike competitive antagonism, non competitive one depresses the magnitude of maximal response in a non surmountable way.

Lastly, in the uncompetitive antagonism, an antagonist requires receptor activation by agonist binding [1] [5].

Relationship between drug-receptor and pharmacological response

Intrinsic efficacy and affinity

Binding of a molecule with another receptive molecule is not sufficient to trigger a biological response: the interaction of the two species have to be processed in various way through a cascade of biochemical reactions ending to an observable functional effect. Indeed, a drug bound to a receptor site possesses pharmacological activity only if perturbs processes that regulate the physiologic equilibrium of the system by means of stimulation or blockage of the target.

The pharmacological activity of a drug is defined by two parameters: efficacy and potency.

Efficacy is the degree at which a drug activates receptor and prompts to a cellular response. The *receptor occupancy model,* suggested by A.J. Clark in 1940s [6], was one of the firsts attempts to explain the relationship between ligand-receptor interaction and the pharmacological response. It argued that the magnitude of the observed effect is directly proportional to the grade of receptor occupancy (and therefore, to drug-receptor complex concentration) and that the maximal response would be elicited once all receptors were occupied at equilibrium. With the introduction of the concept of intrinsic activity (α) by Ariëns in 1960s, the biological effect was expressed as a product of occupancy and intrinsic activity of the drug (Equation 5):

$$B = \frac{([X] \bullet B_{max})}{K_d + [X]} \bullet \alpha \qquad (5)$$

This theory was further revolutionized by Stephenson [7], who introduced the concept of **intrinsic efficacy** (e) (Equation 6), stating that efficacy is a molecule-related property, because different ligands have different capabilities to induce pharmacological effect, with various magnitude, trough a biological stimulus (the so-called *stimulus-response* relationship).

$$B = \frac{([X] \bullet B_{max})}{K_d + [X]} \bullet e \qquad (6)$$

This theory explained how a drug can elicit the maximal response without full receptor saturation [7].

Lastly, in 1990s Black and Leff introduced the revolutionary **operational model**, which states that the stimulus-cascade response is a hyperbolic relationship, without taking in account any intrinsic parameter referred to the drug [8].

The other drug parameter, **potency,** is the amount of a drug required to elicit an effect of given intensity. This parameter is used to compare biological activity of a series of drugs. Bioactive molecules differ in potency and maximum efficacy. These are two inter-dependent parameters: drugs combing with the same targets could share similar potency but show different efficacy (and vice-versa*).* Potency is indicated by drug concentration (or dose) causing 50% inhibition of a biological or biochemical function: in *in vitro* assay, IC_{50} or EC_{50} ("C" stands for concentration) are used, while in *in vivo* experiments ED_{50} ("D" stands for dose) is employed [1]. These parameters are calculated by means of concentration-response or dose-response curves.

Hill function and dose-response curves

The original Hill equation was first introduced by A.V. Hill [9] to describe the equilibrium relationship between oxygen tension and the saturation of hemoglobin, indicating *y* as the observed saturation, *x* as the free ligand concentration and relating *K* to an equilibrium association constant (Equation 7):

$$y = \frac{Kx^n}{1 + Kx^n} \qquad (7)$$

The power *n* designs *the Hill Coefficient*, that is a parameter equal to the number of binding sites on receptor; it is also called *Hill Coefficient of sigmoicidity*, a value that describes the slope of the curve.

The pattern of ligand interaction is called *cooperativity*. For:

- n>1, binding of a molecule ligand increases the receptor's apparent affinity, and hence increases the chance of another ligand molecule binding (positive cooperativity);
- n<1, once that one molecule ligand is bound to the target, its affinity for other ligand molecules decreases (negative cooperativity);
- n=1, binding of a molecule ligand doesn't influence receptor interaction with another ones (non cooperative binding).

In his experiment, Hill observed that the hemoglobin saturation against oxygen tension gave a hyperbolic rectangular concentration-response relation, that resembles positive cooperative.

On the rational basis of the receptor occupancy theory, Hill gave the following general equation (Equation 8):

$$y = \sum_{r}^{n} a_r \frac{K_r x^r}{1 + K_r x^r} \qquad (8)$$

Where *y* is the total fractional occupancy, factor a_r is the maximal fraction of receptive units with a number of *r* ligands bound, and K_r is the association constant for ligand binding with (r-1) ligands already bound.

Since its first introduction, because its effectiveness in fitting experimental data, Hill's equation was modified and transformed into several equations widely used in order to describe the effect derived from several biological processes, such as enzymatic activity, cellular growth and the biological response to the drugs, that are non-linear and saturable relationships [10].

Linearizing Hill equation (Equation 8) by means of logarithmic transformation of both *x* and *y* parameters, Equation 9 is obtained, also known as the median-effect equation [11]. It describes a straight line having slope of *n* and a intercept at ordinate axis of *n*logK. The term "log[y/1-y]" is called the "logit" and linear plots of Equation 9 is called "logit" plot.

$$\log\left[\frac{y}{1-y}\right] = n\log[x] + nlogK \qquad (9)$$

However, this linearization decreases the accuracy of estimation of the parameters, since the line is rarely straight and its the slope of is deeply influenced by the extreme values of both parameters.

Usually, the resultant effect (*y*) is represented as *a fraction of maximum effect (i.e.* E/E_{max}) or a percentage of maximum effect E_{max} (the full range of response that can be affected by the drug)[10] [12]. At the same time, if *x* is substituted by C, the drug concentration at time *t*, the value K, representing the flex of equations 8 and 9, represents is the drug concentration corresponding to 50% of maximum effect, namely the IC_{50} value. $Log[x]$ might also be log(IC_{50}). Therefore, this equation describes the concentration of drug required to bind a receptor to produce a functional effect.

Therefore, the previous function is transformed in the follow general Hill equation:

$$E = E_{max} \frac{C^n}{IC_{50}^n + C^n} \qquad (10)$$

When n=1, as in a simple binding isotherm, or a first-order enzyme kinetics, the graphical representation of the data is a rectangular hyperbola (Figure 3A). The semi-logarirthmic transformation of the *x* value data (drug concentration, C) yields to sigmoidal curves with symmetric shape. However, when n≠1, high-order of kinetics curves are obtained, described by Hill equation (Figure 3C).

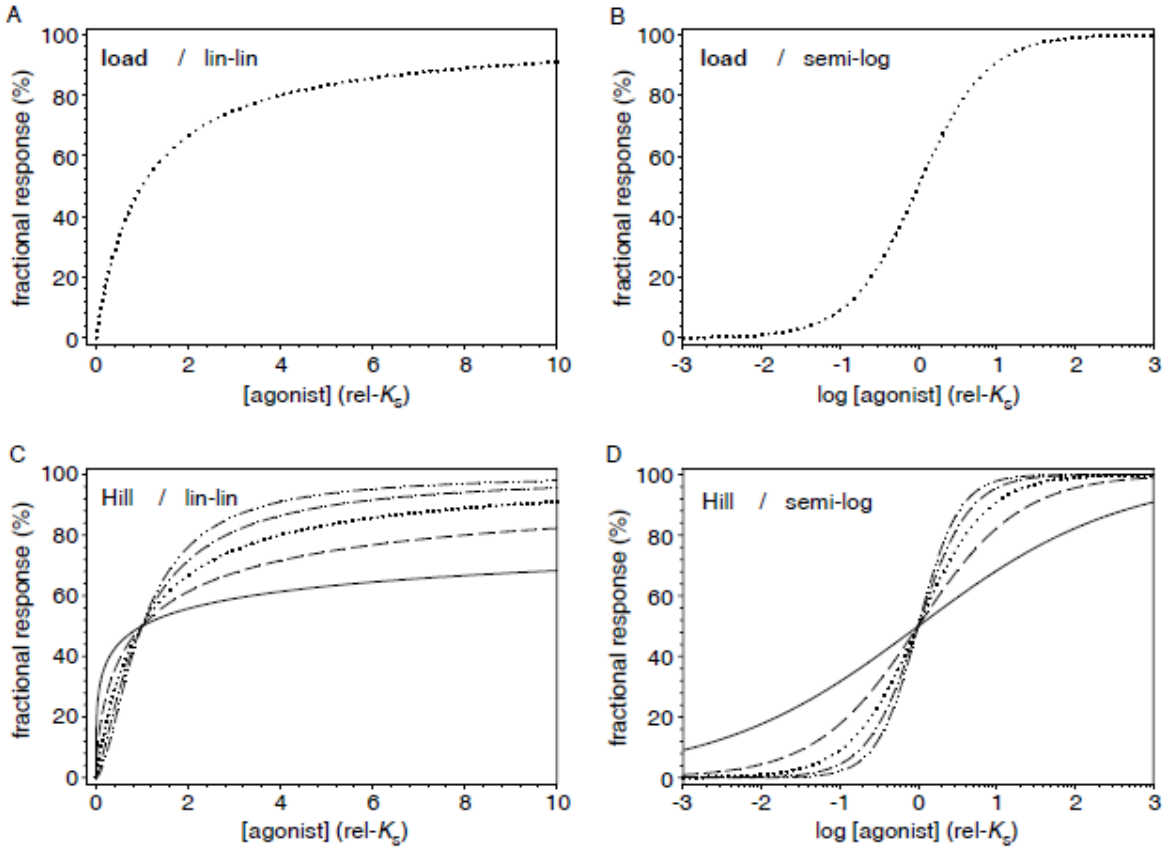

FIGURE 3. Examples of binding curves. The dependent variable, fractional response (%), is a function of drug concentration (independent one). **A**. "Load" is referred to a general binding isotherm or an enzymatic activity having first-order kinetics. Its semi-logarithmic transformation yields to (**B**) sigmoidal curves with symmetric shape. **C**:Hill equation is a hyperbolic rectangular dose-response relation, that describes the response of a system having multiple binding sites or higher-order of kinetics. The different binding sites and described by Hill coefficient *n,* also called *Hill Coefficient of sigmoicidity* **D**: Semi-log ("logistic") fitting of Hill curves , that display sigmoidal curves with symmetric shape [12].

Within this context, the most commonly used equation is a semi-log reversed Hill, so-called "logistic" function (Equation 11):

$$y = \frac{1}{1 + 10^{n([K_x] - \log [x]}} \qquad (11)$$

The expression "logistic" stands for logit (semi-log) plotting of data, because of logarithmic transformation of the axis for the independent variable *x*. Graphically, semi-log fitting of the data displays sigmoidal shape curve with slope indicated by *n*.

The function that describes the biological responses evoked by drugs are known as *concentration-response* (if performed *in vitro*) or *dose-response* (if performed *in vivo) curves.* However, often the term "dose" is used to be employed as synonymous of "concentration", although in a improper way.

Dose-response curves are the basis of pharmacology, since they describe drug activity evaluating response observed at molecular, cellular or tissue level as a function of the logarithmic dose of an active molecule. In Figure 4, sigmoidal curves with asymmetrical shape of the fitting of the data are depicted: a growth curve (Figure 4a) and a dose-response curve (Figure 4b). In Figure 4b, the magnitude of maximal asymptote stands for the intrinsic efficacy of the molecule, while the location of the curve along the concentration axis establishes its potency. IC_{50}, or EC_{50}, (*i.e.* the half maximal inhibitor concentration), is the parameter used to compare the potency of several tested drug and stands for the inflection point of the curve. Briefly, while efficacy is a relative measure on the concentration scale, efficacy is a relative measure on the response scale.

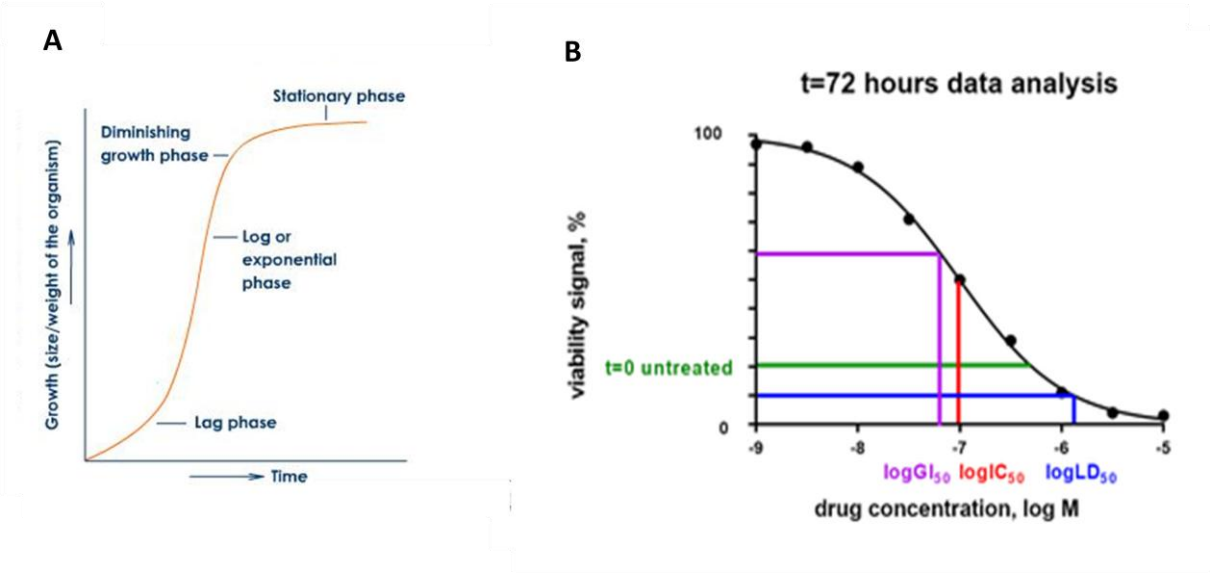

FIGURE 4. **A**. Example of a growth curve, that resemble a sigmoidal curve. **B**. Sigmoidal dose-response curve of a drug that affect cell viability [13].

Analyzing the pharmacological effect of drugs interactions

Why drug combination?

The resultant effect of a combination of two or more agents may be defined as:

- *additive*, if it is the same as the sum of the individual effects;
- *synergistic*, if it is greater than the sum of the individual effects;

- *antagonist,* if one drug counteracts the physiological action of the other one, diminishing its effect.

In pharmacology, the most favorable outcome is the synergy, because it offers several therapeutic benefits:

- increasing the efficacy of the therapy;
- decreasing the dosage, ensuring the same efficacy but minimizing the adverse effects of the individual agents;
- reducing the development of drug resistance.

A plethora of medical conditions is often treated with combination therapy, especially infectious diseases and cancer (polychemotherapy). Drug association is necessary when therapeutic response after monotherapy is not expected or is not so beneficial. In fact, anticancer polychemotherapy is the standard regimen to cure all tumors.

Therefore, during the past century several mathematical theories were developed to analyze the biological effects of combinations of drugs applied simultaneously o sequentially, in order to identify the best therapeutic regimen, to optimize the treatment schedule and to define the optimal dose ratios.

The application of these models allowed the optimization of the costs of experiments, to avoid useless ones and to minimizing use of laboratory animals.

Moreover, it should be reminded that the mathematical models solved the problem that the pharmacological outcome of a combination is not a simple sum of effects. For example, if drug 1 and drug 2 each inhibits 70%, then the combined additive cannot be 140%.

Unfortunately, mathematical models that analyze the effect resulting from a drugs combination *per se* are unable to explain *how* and *why* the underlying mechanisms ascribed to pharmacological effects occurs.

Among the available models, great dissonance exists. It is possible to generate widely different conclusions if different methods are applied to the same data set. Moreover, some methods are considered questionable and inaccurate.

To analyze pharmacological effect of drugs combination, additive interaction was conventionally established as standard reference in order to discriminate between synergy and antagonism.

Webb model and Bliss independence criterion

Webb states that the additive effect for a combination of drug 1 (dose = 1) and drug 2 (dose = 2), is given by the product of their fractional activities (Equation 12):

$$f_{1,2} = f_1 * f_2 \qquad (12)$$

Webb model is based on the assumption that the two drugs act in a indipendent way, that means that they do not cooperate with each other (*i.e.* have different modes of action), but each one contributes to a common result. However, Webb model does not consider the slope of dose-response curves of both drugs combination and single drugs [14].

Bliss independence model is based on the idea of probabilistic independence too. It states that the combined effect for two drugs was formulated as a sum of the fractional effect for each individual agent minus their product. For the combination of drug 1 (dose = 1) and drug 2 (dose = 2) , the fractional response f of the combinations is expressed by Equation 13:

$$f_{1,2} = f_1 + f_2 - f_1 * f_2 \qquad (13)$$

Positive or negative values from Bliss prediction describe synergistic and antagonistic interactions, respectively.

Graphically, it generates an isobologram called *non-interaction surface* that defines the additivity effect [15].

Bliss independence is a simplicist model, derived only from the potency and efficacy information obtained from dose-effect relationship. It may be properly applied to mutually non-exclusive drugs. Finally, it does not offer a reliable measure of the intensity of interaction and often misleads into data analysis. In particular, these model leads to a possible synergy overestimation when the dose-response curves are steep (cooperativity coefficient > 2) [16].

Loewe additivity model

Loewe additivity model is based on an assumption that is the opposite to the Bliss independence criterion: all the drugs in a mixture acts on the same biological target (*mutually exclusive drugs*). Graphical representation of Loewe additivity model is an isobologram, which is a cartesian plot having the doses of two drugs as the axis values. The straight and parallel lines, connecting the individual doses of drugs that yield the same and specific effect,

are so-called *lines of additivity (*or *non-interaction surface),* or *isoboles*. Their linearity is based on the assumption of *fixed-ratio dose* (known also as *constant dose ratio, dose equivalence or interaction index),* that means that the ratios between the equally effective doses of the drugs ever gives the same and specific value. So, every dose pairs defines exclusively one isobole. Therefore, the general equation of Loewe additivity assumes that, for a combination of drug 1 and drug 2:

$$\frac{D_1}{(D_x)_1} + \frac{D_2}{(D_x)_2} = 1 \qquad (14)$$

The term *(Dx)* stands for the effect *x* triggered by the drug D in single treatment, whereas in the numerator *D* indicates the concentration of the drug in the drug combination that induces the same effect.

Applying the concept of *fixed-ratio dose* the relative potency of both drugs is kept constant.

After the determination of additive isobole, it is possible to assess both antagonist and synergistic interactions of the mixture. Antagonism (also called subadditivity) and synergy (also defined superadditivity) are indicated when combination data points are located above or below the line, respectively [17] (Figure 5).

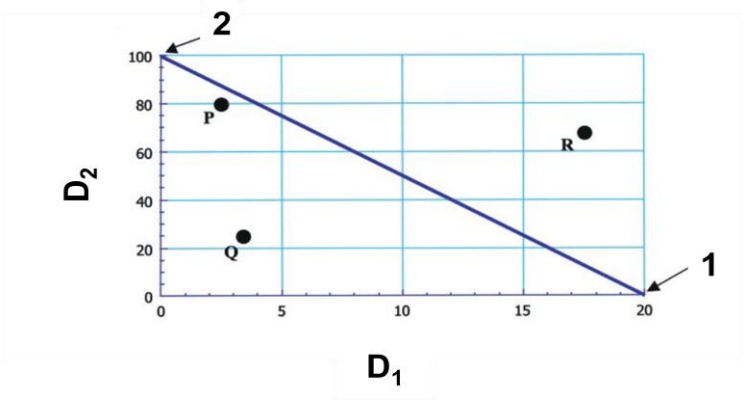

FIGURE 5. The isobologram plot. Each axis represents the doses of drugs 1 and drug 2 that "alone" induce a specific effect (20 and 100, respectively). Matching these intercept points, the additivity line is obtained, which represents all dose pairs that, based on drug potencies, should give the same effect. An actual dose pairs denoted as Q is superadditive (or synergistic), whereas R is subadditive (or antagonist) [18].

It should be noted that Loewe's isobologram shows a lot of weakness. First, it has limited application since it is suitable for mutually exclusive drugs only. Despite of the simple visual display of data, it is a fallacious and empirical method because it lacks any statistical precision, and it offers a rough measure of the type of interaction. It was demonstrated that it could give to distorted lines.

Combination Index (CI) and dose reduction index (DRI)

In 1960s Chou, a pharmacology Ph.D graduate student, derived the Michaelis-Menten equation (*i.e.* the equation that describe the first-order enzyme kinetics). Attracted to the complexity of the process substrate-product reactions, he extended the analysis to other systems, in particular in the drug-effect context, obtaining several deduction and equations.

In 1980s, he derived the *median-effect equation*, that correlates "dose" and "effect" in a simple form [11]. The *median-effect* function is also called *general (*or *unified) theory of dose and effect* because it derives from the principles of *mass action law* and, by means some derivations, it can substitute the Michaelis-Menten equation, the Hill equation, Scatchard-plot and the Henderson-Hasselbach equation, chancing f_a in fractional saturation, fraction occupancy, fractional binding and fraction ionization, respectively, The *Median-effect equation* is given by Equation (15):

$$\frac{f_a}{f_u} = \left(\frac{D}{D_m}\right)^m \qquad (15)$$

Where D is the dose of a drug, f_a stands for the fraction affected by D and f_u is the fraction unaffected (i.e $f_u = 1 - f_a$), giving a specific level of effect; since f_a is the ratio of the measured parameter affected over the control, its values range from 0 to1. *Dm* represents the median-effect dose that inhibits the system under study by 50% (e.g. IC_{50}), thus, it stands for drug potency; the coefficient *m* indicates the shape of the dose-effect curves (hyperbolic, sigmoidal and flat sigmoidal with m=1, >1, and >1, respectively) (Figure 6).

Defining x=log(D) and y=log(f_a / f_u) and plotting *y* versus *x* , and rearranging Equation (13), is obtained a linear function, the so-called *median-effect plot* which is the logit linearization, as described above (Equation 16):

$$log\frac{f_a}{f_u} = mlog(D) - mlog(D_m) \qquad (16)$$

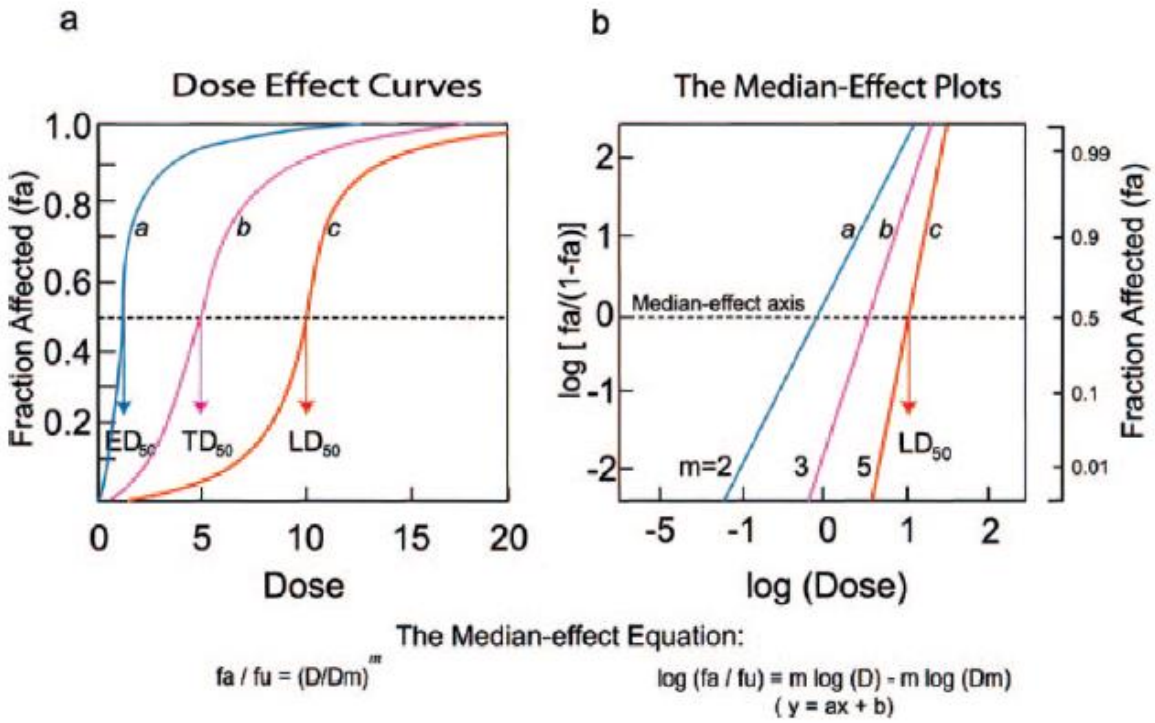

FIGURE 6. Sigmoidal dose-effect curves (**a**) transformed into the corresponding linear forms (**b**) by means of the median-effect plot. The line slopes, indicated with m, stand for the degree of sigmoicity, and the antilogs of the X-intercepts gives the Dm values, which indicate the potency of each drugs [19].

The median-effect equation allowed to analyze the a combination of two drugs, namely as Drug 1 and Drug 2. Based on Equation (16), Chou and Talalay in 1983 derived the *Combination Index* (CI) *theorem* [11].

Assuming that the two agents are *mutually exclusive* (*i.e.* share similar mode of action), the CI is described by equation 17:

$$CI = \left[\frac{(f_a)_{1,2}}{(f_u)_{1,2}}\right]^{1/x} = \left[\frac{(f_a)_1}{(f_u)_1}\right]^{1/x} + \left[\frac{(f_a)_2}{(f_u)_2}\right]^{1/x} = \frac{(D)_1}{(D_x)_1} + \frac{(D)_2}{(D_x)_2} \qquad (17)$$

The term *(Dx)* stands for the effect *x* triggered by the drug D in single treatment, whereas in the numerator *D* indicates the concentration of the drug in the mixture that induces the same effect. To detect these values, dose-effect curves for each single drug have to be performed and compared with that one of the combination.

The assumption of mutually exclusive drugs had been previously proposed by other researchers; Chou and co-workers introduced the condition of non mutually exclusive drugs, postulating that the two agents are *mutually non-exclusive* or *inclusive* (*i.e.* act trough mechanisms know or supposed to be different): a further term was added to equation (17)

equation because the combination mixture of the two agents is regarded as a third component, obtaining Equation (18):

$$CI = \frac{(D)_1}{(D_m)_1} + \frac{(D)_2}{(D_m)_2} + \frac{(D)_1(D)_2}{(D_m)_1(D_m)_2} \qquad (18)$$

CI is a a-dimensional value that allows to discriminate additive effect from antagonism and synergism (with CI=1, CI > 1, CI < 1 respectively). Equation (17) and (18) may be expressed in the following general form, in the case of two drugs that show x% effect:

$$(CI)_x^n = \sum_{j=1}^{n} \frac{(D)_j}{(D_x)_j} \qquad (19)$$

Where $(CI)_x^n$ is the combination index for *n* drug at *x%* effect.

When drugs in combination are in fixed- constant ratio classic isobologram is constructed (Figure 7a); conversely, if the agents are in non constant ratio, plotting of data yield to normalized isobologram (Figure 7b). In the latter procedure, doses in combination are normalized with their ED50 "alone". Normalized isobologram is adopted in order to determine the optimal combination ratio for maximum synergy [19].

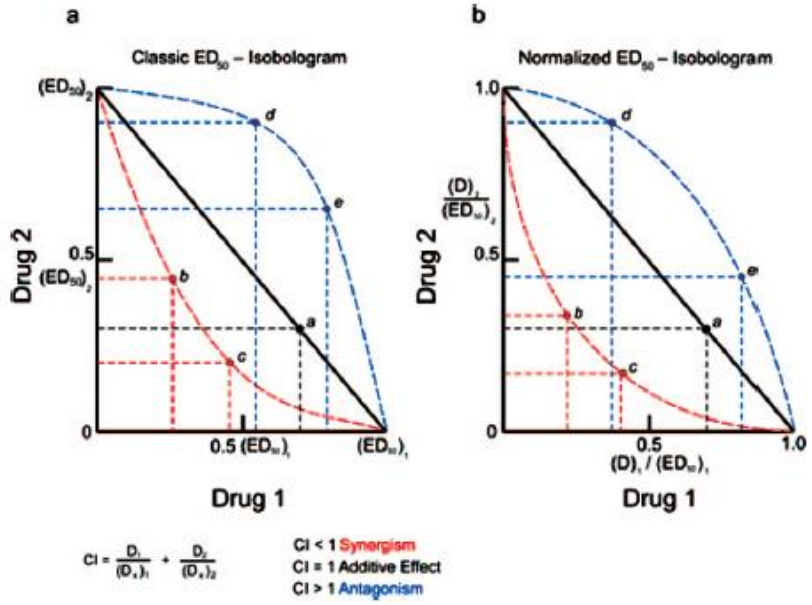

FIGURE 7. The ED50 (or IC50) isobologram for two drugs. When CI=1, combination data points fall on the hypotenuse drug-interaction result in additivity. If combination data points fall on the lower left, synergism is indicated (C < 1). Finally, their presence in the upper right indicates antagonism (C > 1). **a**. Classic isobologram, where the drugs in combination are in constant dose ratio (equipotency ratio). On X- and Y-axis are indicated the equipotency mutual doses that prokove a specific effect in the mixture. **b**. Normalized isobologram for two agents, at non-constant combination ratios, whose doses in combination are normalized with their ED50 "alone". Classic isoblogram is suitable for mutally exclusive drugs, whereas normalized isobologram is adopted for mutually nonexclusive ones [19].

So, proposing the median-effect principle and the CI theorem, Chou and Talalay gave theoretical basis to isobologram model, that was absent in Loewe's one.

In addition to isobologram, Chou and Talalay introduced a novel approach for drug-interaction analysis based on the same mathematical bases. It consists of a F_a-CI plot (Figure 8), where the CI values are expressed as a function of the effect levels. Whereas isobologram is a dose-oriented graphic, the F_a-CI plot could be regarded as an effect-oriented graphic.
Use of F_a-CI is preferred for a lot of reasons. First, because the isobologram is a bi-dimensional system, is indicated only for two-drugs combinations. Also, if it is constructed for a lot of effects, lines overlap and graph becomes too messy to read. Conversely, F_a-CI plot shows all f_a simultaneously, whatever the number of drug tested in association. Between the plethora of models available, F_a-CI based methods is the most popular for drug combination studies, because is the most accurate and offer a quantitative estimation of the extent of synergy and antagonism.

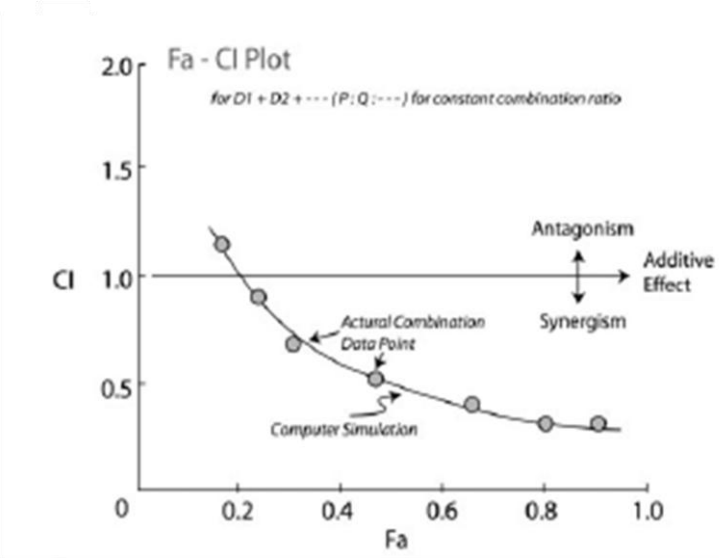

FIGURE 8. F_a-CI plot for *n* drugs combination given at fixed dose ratio. Experimental data closely fit those predicted by means of computer simulation using CompuSyn, a software performed by Chou and Martin [19].

For clinical purposes, high effect levels of synergy mean therapeutically promising mixtures. Moreover, it is worth to keep in mind how these theories are simplified models of the more complex cell system, and the whole organism, consequently, synergy depends on the context; for example, selective synergy is relevant against the target but antagonism is desired

towards the off-targets in order to minimize side effects. Therefore, synergy is not a property merely of a drug combination: it relies on ratio of the mixture constituents.

One of the major advantages of having a synergistic drug combination is the possibility to reduce the dose of the drug used, maintaining the same efficacy with reduced toxicity.

The *dose-reduction index (DRI)* is the reciprocal of CI terms and is a measure of how many-fold the dose of each drug in a synergistic combination could be reduced exerting the same effect (Equation 20).

$$CI = \frac{(D)_1}{(D_x)_1} + \frac{(D)_2}{(D_X)_2} = \frac{1}{(DRI)_1} + \frac{1}{(DRI)_2} \qquad (20)$$

In Figure 9, Fa-DRI plot expressed DRI as a function of the effect levels.

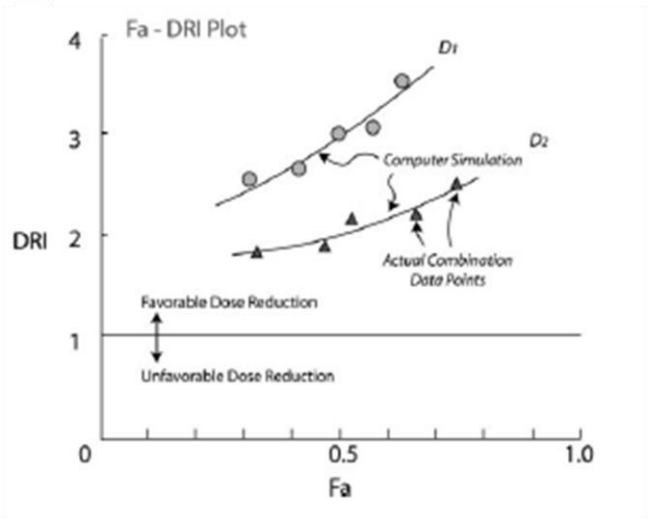

FIGURE 9. F_a-DRI plot for *n* drugs combination given at fixed dose ratio. At the same effect levels, computer simulation (by CompuSyn, software ideated by Chou and Martin) does not predict with precision experimental data [19].

However, it should be noted that DRI is not a parameter for synergy and antagonism [19] [11].

Polygonogram

It is a graphical representation of multidrug combinations that shows the pharmacological effect of each drug pairs (Figure 10). It as merely a tool of practical utility, because it allows an overall visualization of the outcomes by means of colorful lines; usually; synergism is presented by a solid line and antagonism is depicted by a dashed one and their thickness reflects the strength of observed effect [19].

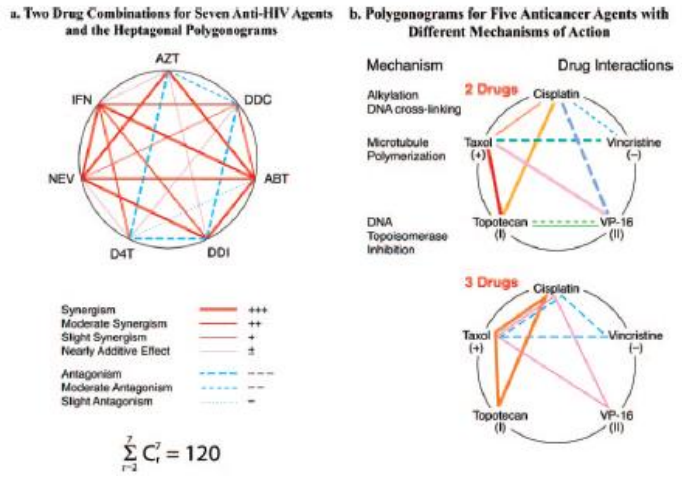

FIGURE 10. Sample illustration of polygonograms. a) Heptagonal polygonogram for 7 anti-HIV agents using two drug-combination *in vitro*, for which are 120 possible combinations. Synergism and antagonism are depicted with different colour lines (solid red-tone and broken blue-tone line, respectively). The thickness of the line represents the degree of interaction effect. b) Polygonogram for 5 anticancer drugs with different mechanism of action [19].

Response surface modeling

The effects of a combination could be plotted against the dose pairs in a three-dimensional coordinate system generating a surface in the plane, the so-called *response surface*. Graphically, the doses are scaled in the X-Y axis, while the effect is plotted as the vertical distance above the planar point (Z-axis). They are built by means of mathematical equations represent surface of isoboles in three-dimensions, integrating all the doses, all the effects given by single treatments, and the effects given by the mixture (Figure 11). The simplest model is based on Loewe additivity response surface analysis. The surface created stands for the additive interactions and become the reference to discriminate the experimentally determined effects. If the combination data fall in the area above this surface, they indicate synergism, whereas if they drop below mean an antagonist response.

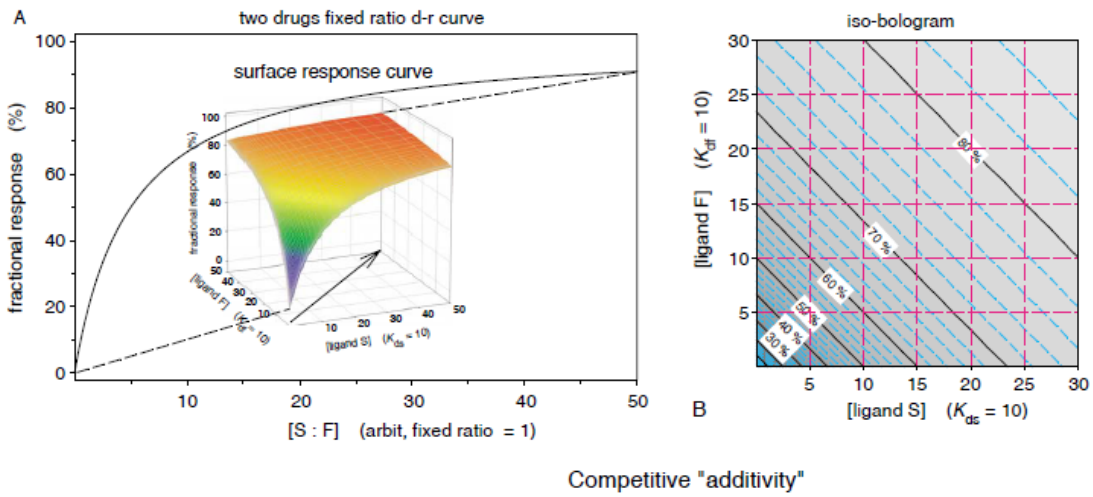

FIGURE 11. Loewe aditivity response surface: Illustration of dose-response curves for two drugs with their surface plot and related isobologram for simple competitive additivity. (A) A 3-D surface plane with the related dose-response curve for increasing concentration of both drugs in a fixed ratio (1:1), (B) its related contour plot that drops under the 3-D surface [12].

In addition to Loewe additivity response surface, during the last decades further theoretical approaches have been proposed. Greco et al., Machado, Plummer and Carter introduced equations with a single interaction parameter that summary the nature and the magnitude of the pharmacological effect. Otherwise, Minto and Kong introduced differents approach using a polynomial function [20] [21].

However, these models do could generate biases: indeed, if applied to the same data set they are likely to generate widely different conclusions.

However, the response surface analysis is not largely employed because it is a complicated procedure. A reliable fitting of response surface to combination data is often not possible because of an inappropriate experimental design or simply because of the poor number of available data.

Antitumoral pharmacology

The tumorigenesis

In physiological conditions, the balance between cell proliferation and cell death is preserved and strictly regulated to maintain normal tissue homeostasis. However, in some circumstances this order is disrupted and tumorigenesis occurs. Most cancers do not rise from a single event: tumorigenesis is a complex and multistep process in which acquisition of multiple abnormal functions are required to evolve through a series of premalignant stages into an invasive cancer. These changes are the result of hereditary mutations or of lesions induced by exogenous factors as UV light, X-rays, chemicals and viruses.

The efficiency of repair of premalignant lesions of DNA is one of the most critical events in cancerogenesis. If they can't be corrected, cells undergo cell suicide (*i.e* apoptosis, that is described in the next paragraphs). However, some cells may survive to uncompleted or uncorrected DNA lesions in key genes, *i.e.* proto-oncogenes, accumulating mutations and/or and genomic instability. These alterations give to mutant cells a selective advantage that allows them to duplicate out of control, that is the hallmark of the tumor. During this process, cells gain new characteristics which consequently are given to descendent cells. Growth and selection of first transformed cells is a process so-called *clonal selection*.

Several theories were proposed about the origin and the behavior of tumor-initiating cells, that are not still well understood. It was argued that stem cells acts as progenitors for tumor initiation because of their inherent capacity for self-renewal and their longevity, which promote the sequential accumulation of mutations. However, this thesis remains to be proven. It is compatible with observations obtained from some tumors, while it is elusive for other cancer types [22].

Relevant abnormalities that lead to tumorigenesis result from mutations in protein-encoding genes that regulate cell division and growth, which can be broadly classified into two groups: proto-oncogenes and tumor suppressor genes. *Proto-oncogenes* encode proteins that promote cell growth enhancing cell division (such as tyrosine kinase receptors, kinases, GTPase regulators, transcription factors extracellular and growth factors). Their mutated forms are called *oncogenes*. On the other hand, tumor suppressor genes encode for proteins that control and stop cell division or induce cell death. Therefore, mutations that produce oncogenes favor growth while those that affect tumor suppressor genes hold back ability to inhibit cell growth. In both circumstances, uncontrolled proliferation occurs. Consequently, cancer cells acquire

defects on regulatory circuits that rule tissue homeostasis [23] [24]. Generally speaking, malignant cells exhibit the follow capabilities:

- aberrant and unchecked growth;
- loss of capacity for senescence and limitless replicative potential;
- evasion of cell death, in particular apoptosis;
- sustained angiogenesis;
- tissue invasion and metastasis;
- altered mechanism of DNA damage repair;
- conversion from aerobic to anaerobic metabolism (the so-called *Warburg effect*).

Cell growth control

Cellular replication is ruled by cell cycle, that is a series of unidirectional, repetitive and tightly regulated events. It is composed of four stages: G_1, S, G_2 (which form the interfase) and finally, M. Upon receipting the mitogenic stimulus, cell enters the cell cycle in G_1 phase: the cell becomes actively a rise in cell metabolism and in the expression of proteins and organelles creates the conditions needed for the next stage, *i.e.* the S (synthesis) phase, characterized by DNA replication. In the G_2 phase, the accuracy of DNA replication is checked and proteins needed for the imminent cell division are then synthesized. During the M (mitosis) phase, the chromosomes separate in the nucleus and finally the cytokinesis, the division of the cytoplasm, occurs (Figure 12). The cell cycle can be arrested in checkpoints, close to critical events, to control the accuracy of the preceding processes and to prevent the progression of cell cycle in case of abnormalities. This block allows the cell to restore the normal conditions and, if it is not possible, to induce apoptosis in the damaged cells . So, checkpoints prevent the transmission of aberrant traits to daughter cells. Loss of this regulation is an hallmark of cancer [25].

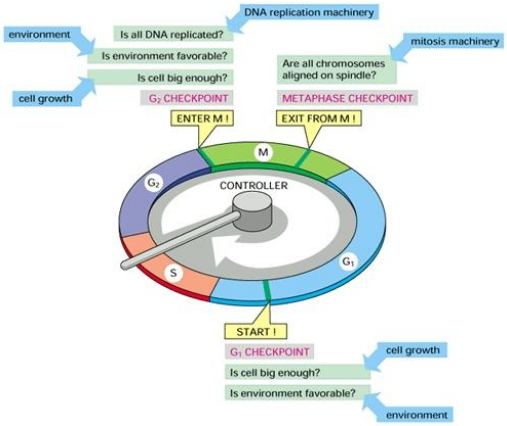

FIGURE 12. The events of cell cycle. The checkpoints, shown in yellow boxes, act as a central control system in order to regulate progression of cell cycle [26].

Cell cycle control system is based on two key families of proteins. The first is the family of *cyclin-dependent protein kinases* (CdKs); the second is a family of activating proteins, called *cyclins. Cyclins* bind to CdKs and control their ability to phosphorilate appropriate target proteins. There are different classes of cyclins and CdKs, each one defined by the stage of the cell-cycle at which they are assembly (Table 1).

CYCLIN-CDK COMPLEX	VERTEBRATES CYCLIN	VERTEBRATES CDK PARTNER	BUDDING YEAST CYCLIN	BUDDING YEAST CDK PARTNER
G_1-Cdk	cyclin D*	Cdk4, Cdk6	Cln3	Cdk1**
G_1/S-Cdk	cyclin E	Cdk2	Cln1, 2	Cdk1
S-Cdk	cyclin A	Cdk2	Clb5, 6	Cdk1
M-Cdk	cyclin B	Cdk1**	Clb1, 2, 3, 4	Cdk1

* There are three D cyclins in mammals (cyclins D1, D2, and D3).
** The original name of Cdk1 was Cdc2 in both vertebrates and fission yeast, and Cdc28 in budding yeast.

TABLE 1. The main classes of cyclins and CdK molecules are listed, referred to vertebrates (middle column) and budding yeast (such as *Saccharomyces cerevisiae*, that is a popular "model" organism) (right column). A specific cyclin-Cdk complex is activated at the entry point of each cell-cycle phase [25].

Some somatic cells (as neurons, muscle cells) do not undergo cell division and persist in a quiescent state, out of the cell cycle, called G_0. Other normal adult cells can duplicate, under the stimulation of external growth signals, as growth factors and hormones, in restricted cases only. Furthermore, they can replicate for a limited number of times, known as the Hayflick limit, that is about 60-70 doublings, given by the gradual erosion of telomeres, (the ending of chromosomes, whose role is maintaining integrity of inner part), that become shorten after every cell cycle. Eroded chromosomes can lead to a permanent escape from the cell cycle, in G_0, called senescence, or can trigged apoptotic cell death.

Adult stem cells as those of the derma, the hematopoietic progenitors and cells of the germinal lines actively proliferate to solve their physiological role, under a fine-tuned stimulation.

On the contrary, cancer cells proliferate under misleading stimulation, which can be also generated by themselves (autocrine stimulation), reducing their dependence on external stimulation and control [25].

Tumor suppressors

Regulatory circuits of cell cycle are controlled by two critical tumor supressors frequently mutated, that are ***P53*** and ***RB*** (for sake of clarity, in according to HUGO gene nomenclature, genes are named in italicized). P53 is a transcription factor that triggers the cell cycle arrest,

apoptosis and senescence. Since its crucial role in the maintenance of genomic stability, it was called "the *guardian of genome"*. Indeed, p53 functional inactivation has been observed in more than 50% of tumors. If DNA damage is so extensive that it cannot be repaired, P53 leads the cell to suicide eliciting apoptosis. p53 functional inactivation leads to failure of this machinery, that may be worsen by defective bcl-2, a proto-oncogene that counteracts programmed cell death [27]. Along with p53, another tumor suppressor, the product of *RB* gene, RB**,** is mutated in several cancers. Its functional inactivation has a central role in retinoblastoma, that is a children-affecting tumor. If hypophosphorylated, RB prevents the proliferation by sequestering and altering the function of E2F transcription factor, that controls the expression of genes fundamental for progression from G1 into S phase. So, defective RB is persistently iperphosphorilated and promotes cell proliferation. Similarly, oncogenes activation, stress inputs or DNA damage, trigger the transcription of a protein called **p21**. It blocks the activity of CdK required for progression through G_1, giving the chance to repair the DNA before it undergoes duplication.

Oncogenes and signal transduction

Tyrosine kinase receptors

Proto-oncogenes encode proteins that belong to an interwined network of cascade signals (pathways) involved in the processing and amplification of the mitogenic signals. So, it is intuitive that the acquisition of multiple defective products fosters aberrant cell behavior.

This could be envisaged in the context of tyrosine kinase receptors (RTKs) pathways, which are frequently mutated in cancer. RTKs are cell-surface receptors that play a key role in cell proliferation, differentiation, survival, metabolism and migration. The RTK family includes 20 subfamilies; some example of members are the epidermal growth factor receptor (EGFR), the vascular endothelial growth factor receptor (VEGFR), the platelet growth factor receptor (PDGF), the fibroblast growth factor receptor (FGFR) and the insulin receptor. Because their activity depends on the binding of growth factors, are also know as growth factors receptors. Aberrant growth factor receptors activity in cancer is mediated by four main mechanisms: autocrine activation, RTK overexpression, gain-of-function mutations that make the receptor constitutively active, or chromosomal translocations [28]. RTKs activation prompts to a series of downstream events transmitted to the nucleus, generally leading to cells division (Figure 13). Many proto-oncogenes take part to these signal transductions pathways. They consist of two groups: non-receptor tyrosine kinases (TKs), such as *abl* and *src*, and guanosine triphosphate (GTP)-ase (e.g. *ras*) [29].

Abl is a cytosolic tyrosine kinase. The mutated form of its proto-oncogene *ABL* results from chromosome 9 and 22 translocation, that yields to an hybrid chromosome, called Philadelphia Chromosome, and to the *BCR-ABL* oncogenes, coding for a fusion protein **BCR-ABL** that is constitutively active, yielding to uncontrolled cell cycle. This translocations occurs in many cases of chronic leukemia [30].

The oncogene coding for the GTP-ase RAS is one of the most common sites of mutation in the array of cancer types. The SOS-Ras-Raf-MAP kinase (MAPK, mitogen activated protein kinase) cascade is stimulated by a lot of stimuli (as cytokines, growth factors, oxidative stress). The MAPK family includes three subfamilies: ERK, JNK and P38. This signaling cascade cross-talks with other molecular pathways, such as PI3K-AKT cascade, promoting the transmission of pro-survival signals (Figure 13).

Moreover, growth factor receptors and non-receptors tyrosine kinases interplay with the Janus Kinase/ signals transducers and activators of transcription (**JAK/STAT**) pathway, that contributes to cancerogenesis stimulating cell proliferation and preventing apoptosis. JAK belongs to a family of non-receptor protein tyrosine kinase that, after activation, recruits and activates STAT proteins inducing their dimerization, nuclear translocation and DNA-transcriptional activity [31].

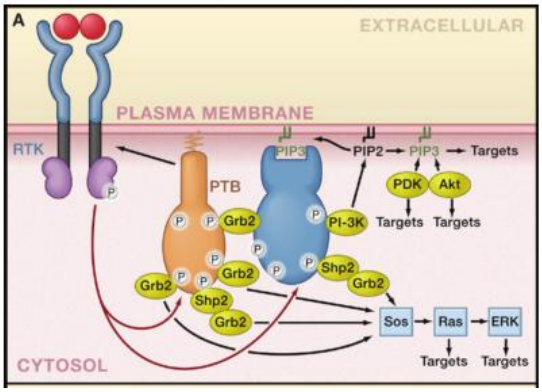

FIGURE 13. RTKs have a characteristics structure consisting of three principal domains: the extracellular ligand-binding domain, the transmembrane domain and finally, the intracellular catalytic domain. They are activated by ligand-induced oligomerization (mainly dimerization), that thus induces autophosphorilation of the tyrosine located on catalytic domain. After RTKs activation, Grb2 binds SOS, that interchange GDP bound to Ras, with GTP. It triggers a complex network of downstream signals. Several proteins are involved, ultimately activating one or more transcription factors, stimulating the expression of the genes that are under their control [28].

Transcription factors

Transcription factors (TF) are nuclear proteins that regulate the expression of target genes by means binding to specific DNA sequences, called responsive elements, which can be found in regulatory parts upstream and/or downstream the target genes, the promoters and the enhancers, respectively. The mechanism of actions of TF involves binding to other proteins, forming homo- and/or heterodimeric complexes.

The signaling of the TF Nuclear factor-*k*B **(NF-*k*B)** has a central role in cancer. It exerts a pleiotropic effect that is context-dependent, ranging from tumor promoting actions (such as

triggering proliferation, mestastasis, inflammatory response, angiogenesis, pro-survival signals) to tumor suppressor activities (as inducing apoptosis, senescence and promoting DNA repair). It should be noted that NF-*k*B aberrant activity is not due to oncogenic mutations in the genes itself, but is mainly a consequence of its induction by "upstream" oncogenic signals [32].

There are five subunits that belong to the mammalian NF-*k*B family, which all share a related DNA-binding and dimerization domain, termed the REL domain. The subunits RelA (also known as p65), RELB and REL contains domain that mediates gene transcription, while the subunits p50 and p52 modulate DNA-binding.

NF-*k*B resides, in the cytosol as a dimer, bound to an inhibitor called I*k*B. NF-*k*B activation requires phsphorilation of I*k*B by IkB kinase (IKK), which thus becomes ubiquinated and destroyed by proteasomes. This event allows NF-*k*B to translocate into the nucleus where acts as a transcription factor, ruling the expression of many genes [33].

FOS, JUN, c-MYC are some examples of oncogenic transcription factors that regulate many crucial genes involved in tumor initiation.

C-MYC is broadly involved in many human malignancies and its functional alteration was found in up to 70% of human cancer, resulting from both its deregulation and overexpression. It harbors a central role in many cellular processes such as the cell cycle, energy metabolism, stem cells differentiation and apoptosis [34].

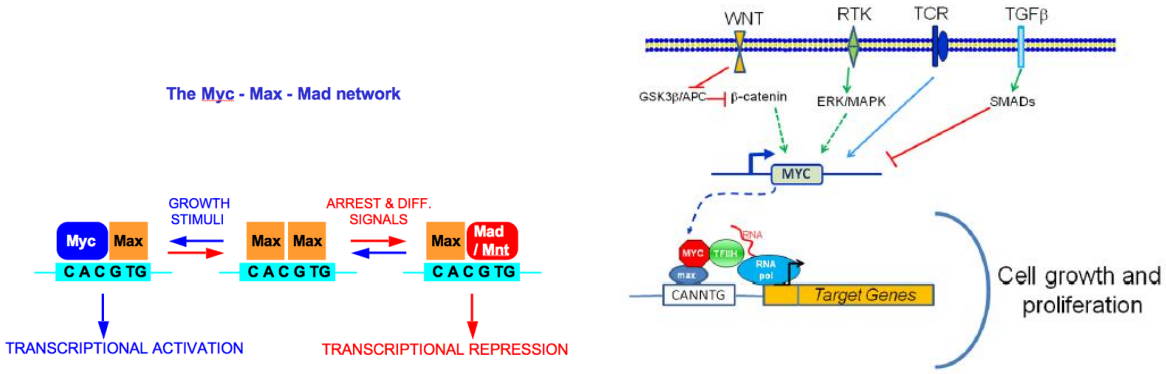

FIGURE 14. *MYC* oncogenes receives downstream growth promoting signals, elicited by many receptors, that regulate its expression. In turn, c-myc dimerizes with Max, which by binding to E-box consensus recognition elements may rule genes transcription [35].

The c-myc transcriptional activity is modulated by epigenetic modifications (defined as chromatin changes that alter its conformation and so, its transcriptional state, without modifying its genic information [36], as displayed in Figure 15) through MYC-MAX/ MYC-MAD dimerization (Figure 14). The dimer c-myc-max cooperates with histone acetylases

(HATs), that catalyze the acetylation of histones (the proteins around whose chromatin is wrapped). Their acetylation stabilize expanded chromatin conformation, promoting DNA transcription [35]. Conversely, c-MYC activity is counteracted by MAD which, after binding MAD, recruits histone deacetylases (HDACs) and promote transcriptional repression [37].

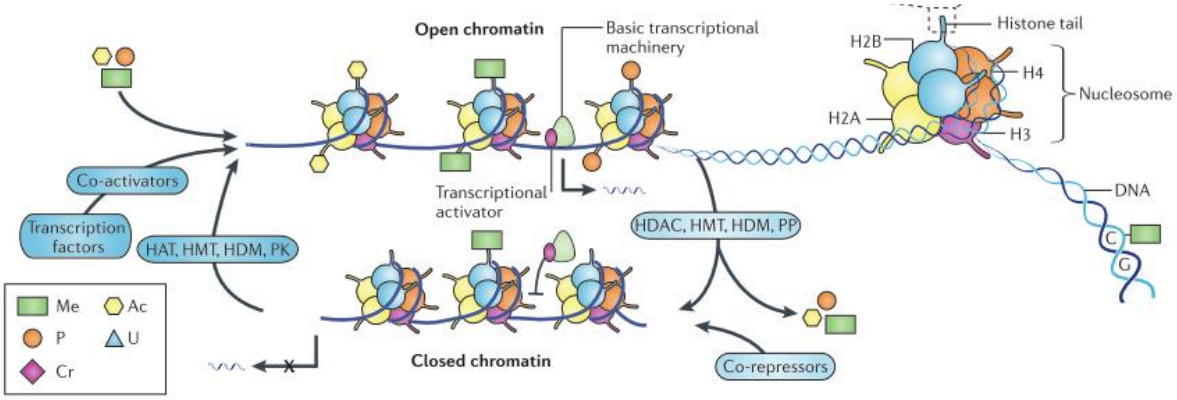

FIGURE 15. The image shows an overview of epigenetic regulation of chromatine. Epigenetic modifications include post-translational modification of histone proteins by acetylation (Ac), methylation (Me), phosphorilation (P). Lysine acetylation and DNA methylation play a key role in regulating gene expression by modulation of wrapping/unwrapping of the chromatin around protein spools called histones. Lysine acetylation is mediated by histone acetylase enzymes (HATs), that stabilize DNA in the expanse and transcriptional active state (called *euchromatin*e) rendering the DNA more accessible to the transcriptional machinery. At the contrary, histone deacetylases (HDACs) remove the acetyl groups from histones and maintain DNA into a compact state (known as *eterochromatine*) not favorable to DNA transcription (gene silencing). DNA methyltransferases (DNMT), though histone methylation, stabilize *eterochromatin*e too [36].

In addition, transcriptional regulation of c-MYC is under tight control of the transcriptional regulators FUSE-FBP-FIR system. The far upstream element (FUSE) is a DNA region that become single-strand during C-MYC transcription, while return to double-strand conformation if is not being expressed. During c-MYC transcription, the FUSE-binding protein (FBR) is bound to FUSE, whereas the interaction of FBP-interacting repressor (FIR) with FBP returns c-MYC transcription to basal levels [38].

Epigenetic regulation has a crucial role in cancer progression, since modulate genes transcription. For this reason, in the last decades it was regarded as a good target for antitumoral therapy.

Cell death

In order to eradicate tumors, antitumor drugs mainly aim to induce cell death in neoplastic cells only. Several types of cell death can be distinguished according to morphological and biochemical parameters; they co-exist within the same tumor, and are strictly interconnected, thus, it is often difficult to discriminate them [39].

However, only apoptosis and necrosis are lethal mechanisms in the strict sense of the term. As depicted in Figure 16, the others can be, in some cases, intermediate steps towards the apoptosis or necrosis.

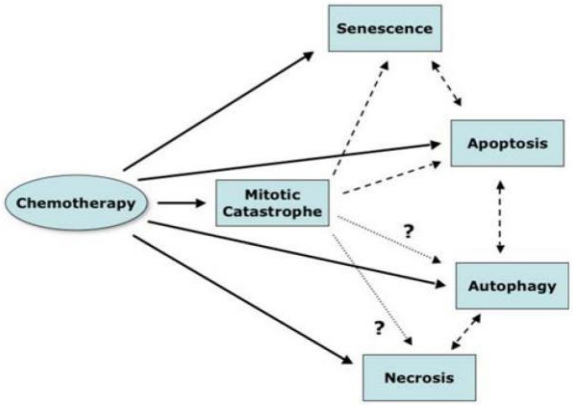

FIGURE 16. Antitumor agents lead to interconnected signals transduction cascade, that lead to different cellular fates. Understanding how these pathway crosstalk and interfere is essential for the rationale design of chemotherapeutic drugs [40].

Apoptosis is also known as programmed cell death type I (PCD). The term apoptosis comes from Greek and means *the falling off of leaves from trees*. Indeed, as this natural event, apoptosis plays a central role in several processes involved in the organism homeostasis, such as embryonic development and tissues turnover. Thus, apoptosis deregulation leads to pathogenesis: suppression of apoptosis plays a key role in cancer development.

Apoptosis can be triggered by a variety of signals, as oxidative stress, chemicals, radiation, tumor-necrosis factor-alpha (TNF-α) and it is elicited through two main pathways: the extrinsic one, mainly activated by cell-membrane receptors in the presence of extracellular stimuli, and the intrinsic one, that integrates intracellular signals such as DNA damage and involves mitochondria membrane depolarization (Figure 17). Both pathways are characterized by the activation of a particular class of cysteine-proteases, caspases, which are divided into *initiators* caspases (caspase 8 and 9, respectively, having autocatalytic activity), which activate by proteolytic cleavage the downstream effectors, the *executioners* (caspase 3 and 7). Effector caspases initiate other proteolytic cascades that lead to the DNA fragmentation and to progressively disassembling of the cell into apoptotic bodies.

Unlikely to intrinsic pathway, extrinsic circuitry does not involve mitochondria and is initiates by extracellular stimuli that activate transmembrane receptors [41].

It was suggested that extrinsic pathway is correlate to cell-membrane receptors clustering within lipid rafts, that are large and dynamic assemblies enriched in colestherol, sphingomyelins and sphingolipids that float freely within the cellular membrane bilayer [42].

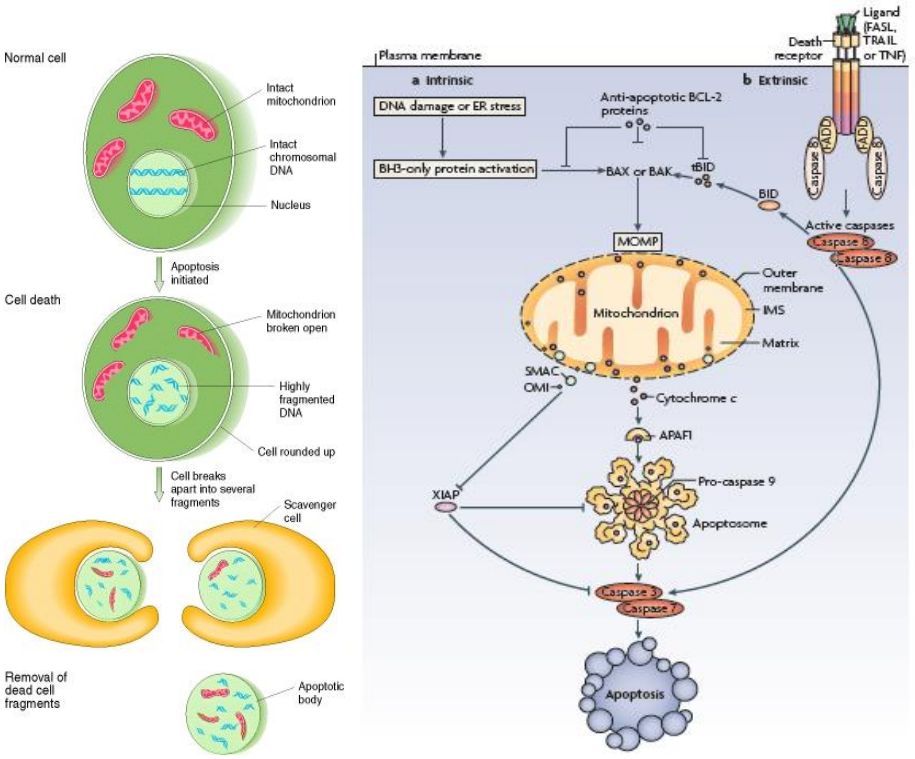

FIGURE 17. Sequence of events of apoptosis at cellular (left) and molecular (right) level. (Left) Apoptosis is characterized by a series of morphological events as cell shrinkage, disruption of membrane of organelles, nucleus condensation, chromatin cleavage and finally, cell fragmentation into apoptotic corps engulfed by macrophages (if the cells is not phagocytosed, they will undergo degradation in a process called secondary necrosis). (Right) These processes reflect the activation of molecular pathways, of whose caspases are the principal drivers. The extrinsic pathway involves the activation of death receptors (as TNF or FAS receptors) that, after binding with adapter proteins, induce activation of caspase-8. The intrinsic pathway is regulated by anti- (as Bcl-2, IAP): upon intracellular stimuli, the activation of pro-apoptotic proteins (as Bax, Bad, Bid) leads to the opening of the mitochondrial membrane transition pore (MOMP), resulting in loss of the mitochondrial transmembrane potential, and to cytocrome c release; within the cytosol, it binds and activates both apaf-1 and caspase-9, forming the *apoptosome,* with the consequent caspase 9 activation. Both the initiator caspases activate the effector caspases 3 and 7 [41].

Autophagy is another example of programmed cell death (PCD type II). It represents a physiological and adaptative response induced by cell stress as nutrient deficiency, cytokynes, damaged organelles or genomic instability. As shown in Figure 18, autophagic cells undergo auto-cannibalism to sustain viability, simply recycling some non-essential components as energy source [43].

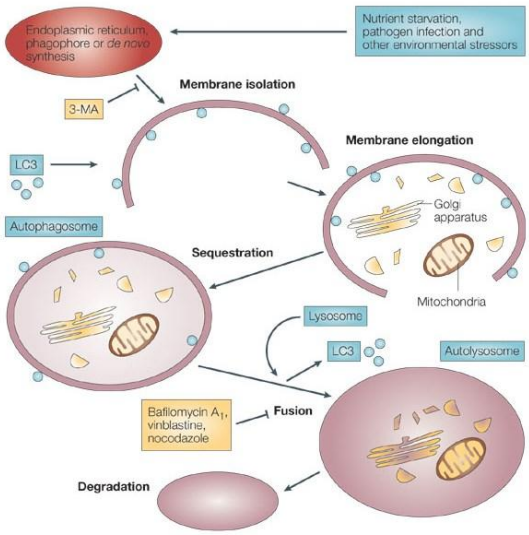

FIGURE 18. Autophagy is characterized by the formation of intracellular vesicles with double membranes, termed autophagosomes. After swallowing cellular organelles (e.g. ribosomes, mitochondria), they fuse with lysosomes. Degradation of the content occurs and the resulting metabolites are thus recycled and used for biosynthesis and energy metabolism. Beclin 1, a protein essential for autophagy, is also an oncogene [44].

Necrosis, unlike apoptosis**,** is an energy-independent process. It usually arises after a traumatic injury that perturbs cellular homeostasis. Morphological changes of necrotic cells include cell swelling, disruption of membranes and rupture of organelles. Loss of integrity of the plasmatic membrane results in the release of the cellular content into the surrounding tissue microenvironment, acting as a chemotatic signals that eventually recruit inflammatory cells [45].

The mitotic catastrophe occurs in case of failed mitosis and it is characterized by morphological alterations as multiple- and micronucleation. It mainly derives from erroneous nuclei separation during cytokinesis [46].

Cell **senescence** is a non-proliferative but viable state during which cells do not proliferate. It is a physiological destiny of normal cells that has a finite capacity for growth. As previously stated, senescence can occur following a period of cellular proliferation (*replicative senescence*) or in response to acute stress (*stress-induced premature senescence*) , such as DNA damage, telomeres shortening, excessive oncogenes signaling. As depicted in Figure 19, the senescence program is regulated by p53 and p16-pRb pathways [47].

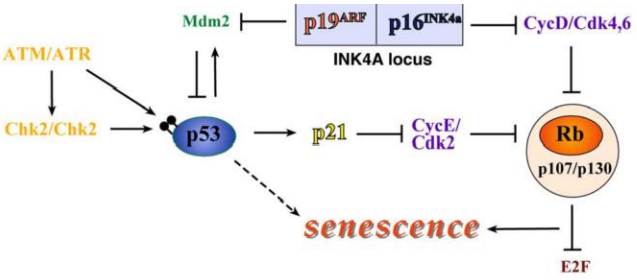

FIGURE 19. P53 and pRb are central activating pathways of senescence. The p53 protein, after activation, proceeds to activate its transcriptional target p21, which arrests the cell-cycle. p53 could be activated by several stimuli, such as DNA-lesions detected by the DNA-damage sensors ATM and ATR. P53 is inhibited by Mdm2. Senescent cells express $p16^{INK4a}$ an upstream activator of pRB. Active pRb, binds to the E2F protein family members to repress their transcriptional target required for cell-cycle progression [47].

The role of autophagy, necrosis and senescence in antitumor chemotherapy is still under debate, because they can play a dual role in tumor progression, acting both as a cancer promoters and suppressors [48]. Indeed, autophagy may either act as a defense mechanism involved in the development of a resistant phenotype either lead to cell death [49]. Also necrotic cells, albeit not viable, promote tumor progression by means of the release of pro-inflammatory signals that recruit inflammatory cells, producing growth factors and eicosanoids which can stimulate tumor growth as well. Lastly, senescence on one hand may represent a protective barrier to neoplastic expansion, counteracting aberrant cell proliferation fostered by oncogenes (Figure 20), on the other hand it might be detrimental since senescent cells cooperate with tumor progression, by means of the secretions of mitogenic factors, *i.e.* the senescence-associated secretory phenotype (SASP) [50] [51].

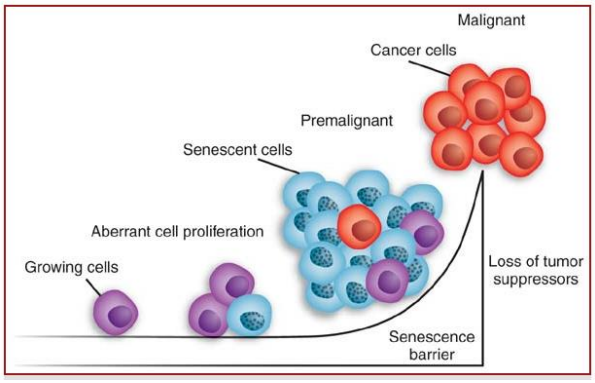

FIGURE 20. Elevated activation of oncogene signalling (as Ras, myc) *in vivo* may promote both cell proliferation and cellular senescence. However, mutations that disable cellular senescence cooperate with the initiating lesion to promote cell progression [52].

Senescent cells have large and flattened morphology , absence of proliferation markers, heterochromatic foci and expression of senescence-induced β-galactosidase enzyme. Senescent cells are displayed in blue because of X-Gal, a chemical is converted into a blue product by β-galactosidase.

DNA damage response

Most anticancer drugs are DNA-damaging agents (genotoxic agents). The efficiency of the DNA damage response have a crucial impact on cell fate; indeed, a nonfunctional repair machinery leads to genomic instability that promotes cancerogenesis and can affect the responses to DNA-damaging anticancer therapy. DNA damage activates a complex network of molecular mechanisms that involve several players (Figure 21), depending on the nature of the lesions and cell cycle checkpoint at which DNA defects is detected [53].

Lesions can affect or one DNA strand (intrastand lesions) or double strands (interstrand lesions). The former may repaired by three mechanisms: base- excision repair (BER),

nucleotide excision repair (NER) and lastly, the mismatch repair (MMR). Among them, NER has a crucial role in cancer chemotherapy. The excision repair cross-complementation group 1 (ERCC1) endonuclease is a critical component of the is a multienzimatic complex NER: bound to XPF product, the resulting heterodimer has endonuclease activity on both intrastand and interstrand cross links (ICLs). The latter ones are the most toxic lesions, since they induce a helix distortion and hinder their separation that is essential for DNA replication and transcription.

Accumulation of ICLs activate different signals, depending on the cell cycle checkpoints at which they are detected, mainly during the DNA replication, stalled replication forks. ICLs are resolved by means of a cleavage on the damaged filament and so converted into a double strand breaks (DSBs). DSB are detected by sensors as Poly (ADP-ribose) polymerase (PARP), which activate the signalling by means of ATM and/or ATR, that in turn activate p53 and other downstream signalling cascades [54] [55]. DBSs can be repaired by two mechanisms: homologous recombination (HR) or non homologous end joining (NHEJ). ICLs repair proficiency depends on the ERCC-1/XPF activity and other enzymes belonging to the MMR system. Examples of diseases associated to inefficient ability to repair ICLs are the Fanconi anemia and breast cancer associated to mutation of a critical component of HR system, the tumor suppressor BRCA1/BRCA2 [56] [57].

DNA polymerases have an important role in DNA damage repair. 15 different mammalian DNA polymerases have been identified: some of them are specialized in DNA synthesis (such as DNA Pol α and ε), others participate in repair or tolerance of DNA damage (as Pol η, Pol μ; Pol β, Pol κ, Pol θ, Pol ζ). The DNA damage tolerance process, that allow the DNA replication bypassing the damaged sites, is called translesion synthesis [58].

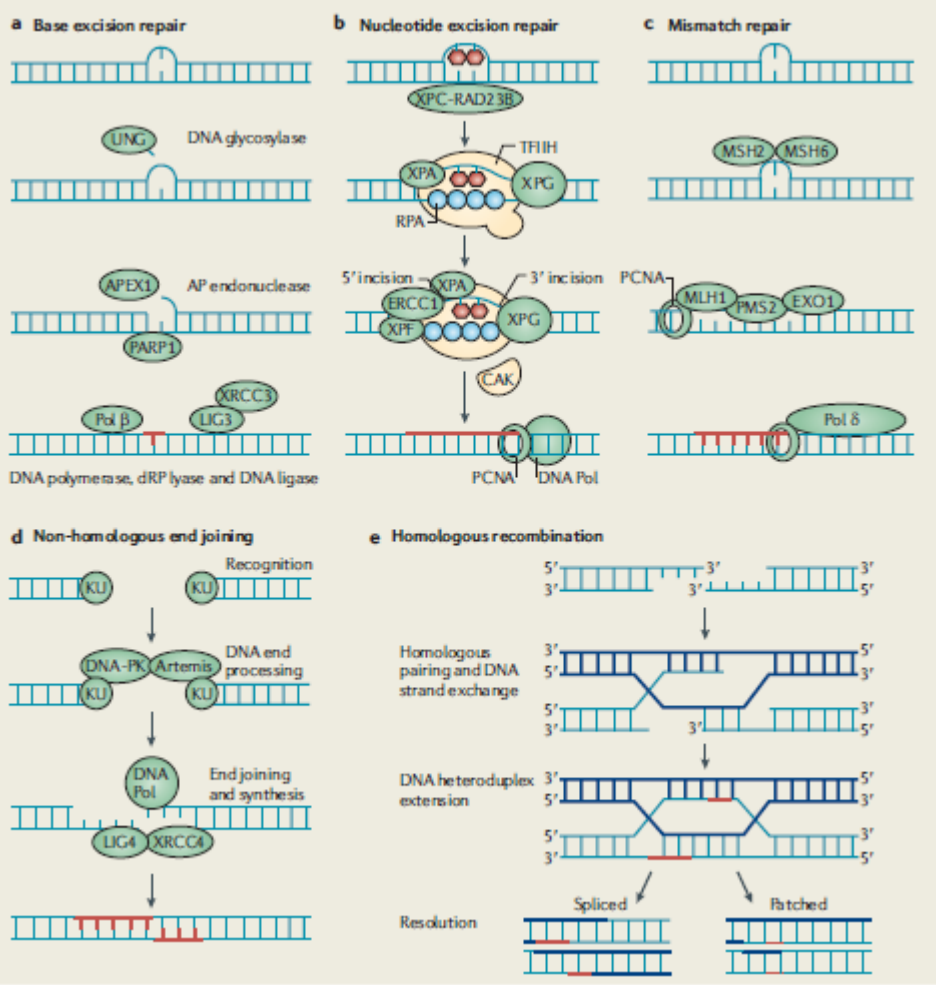

FIGURE 21. MECHANISMS OF DNA REPAIR. (**a**) Base excision repair (BER) is responsible for repair DNA adducts generated by ROS and alkylating agents. Damaged base is removed by a specific DNA glycosylase and the resulting abasic site is excised by an AP endonuclease (APEX1). The 5′-deoxyribose-phosphate is removed, leaving one nucleotide gap that is filled by DNA polymerase β and joined by a ligase. XRCC1 and Poly(ADP-ribose) (PARP) polymerase facilitate the repair. (**b**) Nucleotide excision repair (NER) removes helix-distorting adducts induced by UV radiations, polycyclic aromatic compounds and chemotherapic agents as cisplatin. It contributes to the repair of intrastrand and interstrand crosslinks (ICLs). Defects in NER components are associated with some cancer predispositions, as xeroderma pigmentous. The distorted region is removed by ERCC1-XPG and after filled by Pol δ or ε. (**c**) Mismatch repair (MMR) is a process that removes mismatched bases. If double strand breaks (DBS) arise in DNA induced by interstrand crosslinks (ICLs), (**d**) non-homologous end hoining (NHEI) or (**e**) homologous recombination (HR) processes occurs. HR operates in late S or G2 phase of the cell cycle, when as a sister chromatid operates as a template for the broken strand. Some enzymes of the NER system cooperates with HR. NHEJ introduce deletions, which can be further tumor-promoting lesions [58].

The role of extracellular microenvironment

Cancer must not be conceived as an homogeneous entity of proliferating cells. It is a complex tissue where tumor cells coexist with several normal cells, classified as stromal cells. Cancerous population is driven and sustained by both heterotypic signalling from stromal cells and by the interaction with components of extracellular matrix (ECM). ECM is a tight network of collagen, fibronectin, proteoglycans fibers and other structural proteins. ECM gives tissue their mechanical properties and help to organize communication between cells embedded within the matrix. The extracellular milieu has to be regarded as a dynamic context, because it gradually evolves supporting the malignant growth, aggressiveness and metastasis. Attachment of the cells to matrix is essential for survival and migration and lose of

contact yields to a particular type of cell death called anoikis. Anchoring is mediated by cell-surface adhesion molecules (*e.g*. cadherins and integrins) [59].

Oxygen and nutrient supply are essential for cell function and survival, obligating all cells in a tissue to reside within 100-150 μm of a capillary blood vessel. At longer distance, oxygen concentration falls to zero. So, secretion of angiogenic regulators (e.g. FGF, VEGF, PDGF) occurs promoting neovascularitation in tumor mass. Inflammatory cells help the "angiogenic switch" and in turn, cancer cells secrete chemoattracts that recuit proinvasive inflammatory cells. It should be noted that, since some tumor areas are distant to vascular supply, they are deprived of oxygen and cancer cells adapt to survive in hypoxic condition [60] [61].

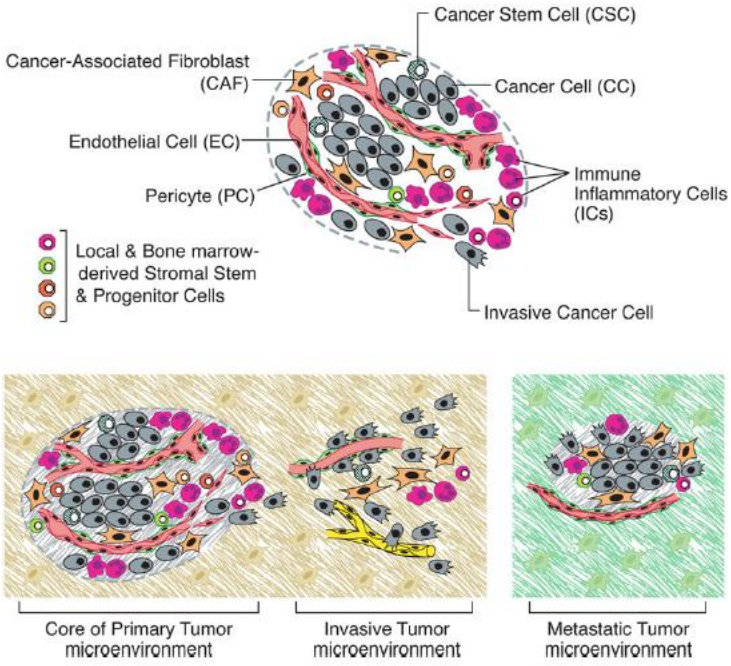

FIGURE 22. (Upper) Cancer as a complex system, sustained by cell-matrix and cell-cell communication trough autocrine and paracrine signalling. In the autocrine signalling, a cell secretes a chemical messenger that binds to a receptor located on the same cell, while in the paracrine signaling a cell produces a signal that induce changes in nearby cells. Adjacent non-malignant cells as fibroblasts, inflammatory cells, endothelial cells, cancer stem cells participate in tumor development and progression through secretion of several factors. (Lower) If altered cells remain in their original location and do not spread to other tissues, they are considered benign, otherwise if they become invasive, they are regarded as malignant. Malignant cells could penetrate the walls of lymphatic and/or boold vessels, extravase and then migrate to distants sites [24].

The anticancer chemotherapy

In the past, the term *chemotherapy* indicated the treatment used against pathogenic hosts invading the body (bacteria as well as cancer cells) by means of chemical compounds (both of natural and synthesis origin).

Conventional anticancer chemotherapy aims to arrest the proliferation of malignant cells and/or induce them to die. Thus, they mainly interfere, directly or indirectly, with the mechanism responsible for the cell duplication: the cell cycle (Figure 23).

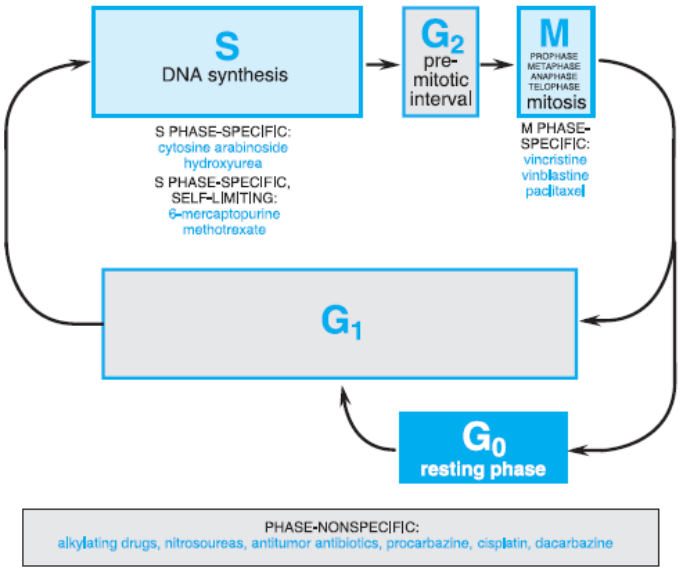

FIGURE 23. The relationship between cell cycle and tumor drugs action. Based on their mechanism of action, antitumor drugs should be divided in two main groups: specific- and non specific- cell cycle phase [62].

The words **cytostatic** and **cytotoxic** describes the way some anti cancer drugs work. The word cytotoxic means that drugs that are used to treat cancer kill the cancer cells by apoptosis induction. This is the primary mechanisms of action of many anticancer drugs, including alkylating agents, platinum compounds, topoisomerase inhibitors and the antimetabolites [63] [64]. Because in many cases the DNA synthesis machinery is involved in this cytotoxicity, some evidences indicated that S-phase cells are sensitive to these agents. Therefore, cytotoxic agents cannot distinguish between normal and malignant cells, since they act on all proliferant cells. [65].

At the contrary, cytostatic drugs work by stopping the cancer cells from multiplying; so, they stop the cancer growing. For example, hormone therapies used to treat breast cancer could also be called cytostatic therapy. They work by blocking particular receptors of the cancer cells that transmit mitogenic signals. So, by blocking them, the treatment is stopping the cancer from growing [62].

However, we would note that cytostasis or cytotoxicity often depends on the *in vitro* and *in vivo* assay conditions, such as doses, times, and schedules of exposure [66]. For example, with the topoisomerase II inhibitor daunorubicin, differential effects have been reported depending on the doses: cytostatic and G2-M arrest at low concentration and cytotoxicity and G1 and S arrest at high concentrations [67]

Similarly, cytostatic drugs could trigger cell death when damage can be resolved, as observed with microtubule-targeting agents [68]. By interfering with microtubule dynamics, these

agents arrest cells in mitosis and induce cytostasis. Since mitosis arrest is poorly tolerated, it could lead to cell death [69].

Inhibitors of Mitogenic stimuli : anti-hormones and targeted therapy

This class of drugs acts inhibiting the receptor or, in general, the pathway responsible for the proliferative stimulus.

For example, when estrogen binds to the estrogen receptor (ER) inside cells, the resulting hormone-receptor complex activates the expression of specific genes, involved in cell growth and proliferation; breast cancer cells that express these receptors (ER-positive breast cancer cells) are an effectively treated by molecules that interfere with estrogen's ability to stimulate the growth (antihormones). Several drugs have been approved by the FDA for the treatment of ER-positive breast cancer. Selective estrogen receptor modulators (SERMs), including tamoxifen, bind to the ER and prevent estrogen binding [70], while aromatase inhibitors (AIs) are another class of drugs that hinder the production of estrogen by means of blocking the activity of aromatase, and are actually used for the treatment of ER-positive breast cancer [71].

Targeted therapy, or **Molecularly targeted therapy**, aims to inhibit of the cancer *mitogenic stimuli* mainly coming from growth factors. Targeted therapy interferes with specific targets as receptors and/or enzymes specifically expressed by in a type of tumor cell and which are involved in tumor growth. Thus, targeted therapy is aimed to reduce the proliferation on a specific subset of cells (the tumor) rather than interfere with the growth of any diving cell, as the traditional chemotherapy does.

Targeted therapy drugs are small molecules, small molecule drug conjugates and monoclonal antibodies. Small-molecules are tyrosine-kynase inhibitors, such as *Imatinib mesilate (Gleveec^{TM}),* a kinase inhibitor, that has inhibitor activity against the chimeric Bcr-Abl fusion protein. In particular, Gleveec emerged as a successful drug in the treatment of chronic myelogenous leukemia, which pathogenesis is ascribed to ABL oncoprotein [72].

Nevertheless, targeted therapies have some limitations, further than the insurgence of resistance; the high selectivity limits their efficacy on cancer types specifically due to that single deregulation; for instance, *transtuzumab (Herceptin^{TM}*), a recombinant humanized monoclonal antibody direct against the HER-2 (also known as ERBB-2) protein, is only efficacy against HER-2 positive cancer. Indeed, a lack of response to *Transtuzumab* was observed when mutations on *her-2* gene occurred [73] [74]. Similarly, Gefitinib (Iressa^{TM}), a EGFR kinase inhibitor, cause tumor regression only if its target is expressed and not mutated

[75]. It is for this reason that targeted therapies may work best in combination, either with other targeted therapies or with more traditional therapies.

Antimetabolites

Antimetabolites represent a class of drugs that interferes with the synthesis of DNA and RNA, thus, these agents selectively damage cells during the S phase. They are commonly used to treat leukemias, cancers of the breast, ovary, and the intestinal tract, as well as other types of cancer.

Metotrexate is the progenitor of **folic acid antagonists** class. It is an inhibitor of dihydrofolate reductase (DHFR), the enzyme that reduces dihydrofolic to tetrahydrofolic acid. Tetrahydrofolate is essential for proliferating cells, since participates in purine and thymidylate synthesis. Another antifolate is *pemetrexed* acting not only on DHFR, but also by inhiting thymidylate synthase (TS). TS is involved in *de novo* synthesis of deoxynucleoside triphosphates (dNTPs) precursors, the substrates needed for DNA polymerase DNA strand elongation [76].

Purines *(6-mercaptopurine, 6-Tioguanine, Gemcitabine)* and **pirimidine analogues** *(5-Fluorouracil, Citosine Arabinoside),* mimic the structure of endogenous nitrogen bases (Figure 24), but with some modification on the 5' position of the sugar ring. Since DNA synthesis proceeds in a 5' to 3' direction, these nucleotide analogues are incorporated into the DNA backbone but do not allow further stand elongation.

Furthermore, they can act on other enzymes involved in nucleotide biosinthesis: for instance, *5-Fluorouracil* is a TS inhibitor.

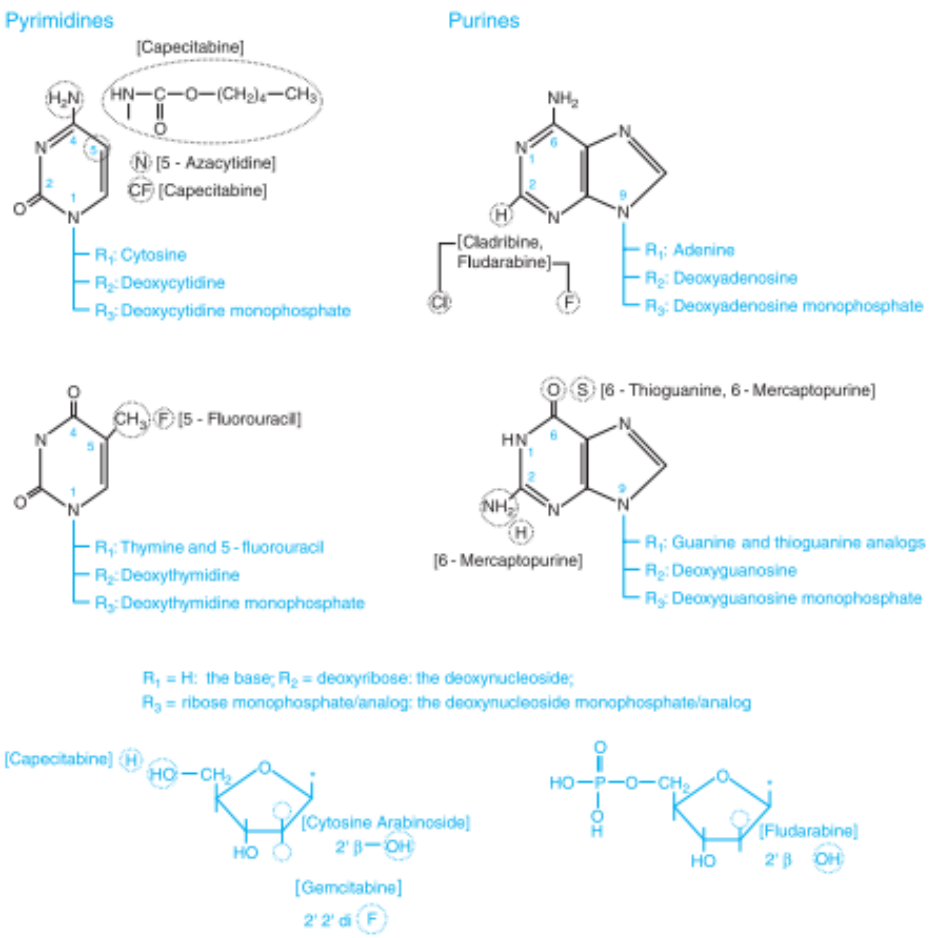

FIGURE 24. Chemical structure of the four bases that become incorporate into DNA are showed, as well as the various modification introduced in pyrimidines and purines analogs that function as cytotoxic chemoterapeutic agents [62].

Alkylating agents

The cytotoxic properties of sulfur mustard was serendipitously discovered during the World War I; later, early clinical experiments highlighted that these molecules were able to induce tumor regression trough DNA alkylation. This event started the discovery of novel antitumor agents and gave rise to the era of modern cancer chemotherapy.

Alkylating agents directly damage DNA to prevent the proliferation of cancer cells. As a class of drugs, these agents are not phase-specific; in other words, they work in all phases of the cell cycle. Their cytotoxic effect is primarily exerted on rapidly proliferating tissues, as bone narrow cells, intestinal epithelium and, hair follicles, lacking of selectivity towards malignant cells.

Alkylating agents are used to treat many different cancer type, including leukemia, lymphoma, Hodgkin disease, multiple myeloma, and sarcoma, as well as cancers of the lung, breast, and ovary [62].

They interact with the nucleophilic centers of the target forming reactive electrophilic products by means of or first-order nucleophilic substitution (SN1) or second-order nucleophilic substitution (SN2) mechanisms, that are illustrated in Figure 25. In the former case, the rate determining step is the formation of a carbocation intermediate or related transition complexes. These reactive intermediate form a covalent bond with nucleophilic sites, such as the imidazole groups of purine bases. Conversely, in SN2 the carbocation is not formed. As final result, alkyl groups are added to DNA.

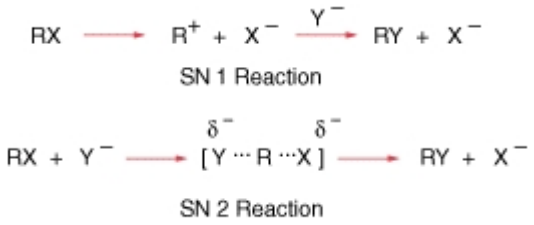

FIGURE 25. Example of first-order substitution (SN1) or second-order nucleophilic substitution (SN2) [65].

DNA-adducts induced by alkylating agents are detected by the DNA-control machinery, that triggers cell-cycle arrest at G1/S or G2/M checkpoints.

Alkylating agents are classified into five groups:

- the **nitrogen mustards,** which include *mechlorethamine, chlorambucil, cyclophosphamide,* c*iclofosfamide,* and *melphalan,* acting as shown in Figure 26;
- **aziridine**, such as *tiotepa,* form intermediates similar to those generated by nitrogen mustards;
- the **alkyl sulfonates**, as *busolfan*, alkylate DNA through the release of methyl radicals;
- **nitrosoureas**, (such as *carmustine and lomustine*) give rise to extremely reactive intermediates that could induce both intra- and inter-strands cross-links. Thanks to their lipophilicity, they can cross the blood-brain barrier, thus, they are commonly employed in the treatment of brain tumors;
- **triazenes**, which account for *dacarbazine* and *temozolomide*, are considered as pro-drugs since their metabolite methylates DNA.

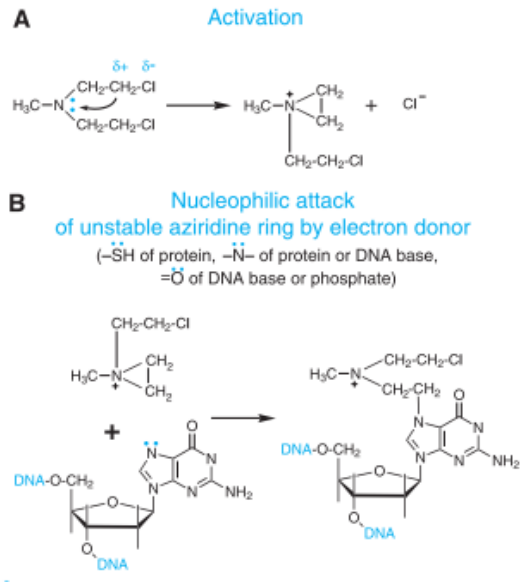

FIGURE 26. Mechanism of action of *mechlorethamine, a* nitrogen mustard (A) By a SN1 cyclization, a quaternary carbocation intermediate is formed. (B) Since it is very unstable, avidly bind N7 of guanine residues in DNA [62].

Platinating agents

Cisplatin

Cisplatin, [*cis*-diamminedichloro platinum (II)] or CDDP, is a square-planar complex of platinum composed of two ammonia as *carrier groups (*that are stable ligands that are not replaced by substitution reactions) and two chloride atoms as *leaving groups* (which are ligands that are displaced by water molecules).

Cisplatin is a Pt(II) complex, that means that metal is the oxidation state +2.

It was synthesized for the first time in 1844 by Peyrone (thus assuming the name of Peyrone'chloride), but its anticancer properties were serendipitously discovered in the 1960s, when Rosenberg studied the effect of an electric field on *Escherichia coli growth.* He observed a stop of cell division that was non ascribable to the electric field, but was attribute to platinum complexes generated by the electrolysis of platinum electrodes in contact with the NH_4Cl^- buffer in which bacteria were growing. Exactly, *cis*-[Pt(II)$(NH_3)_2Cl_2$) was identified as the bioactive species, *i.e.* cisplatin [77] [78]. This observation showed that since this compound was able to stop the cellular division of bacteria, it might also be able to stop proliferation of cancer cells. After few years of clinical trials, this hypothesis was validated and in 1979 the FDA approved cisplatin as anticancer agents. Since then, cisplatin represented the cornerstone in the treatment of a wide variety of solid tumors, such as testis and ovarian cancer (giving cancer cure in 95% cases), and bladder, head, neck, mesothelioma and small cell lung [79]. Passive diffusion was believed to be the main mechanism trough which cisplatin moves across the membrane; however, active transporter as copper transporter 1

(Ctr1) and organic cationic transporters are implicated in cisplatin cellular uptake [80] [81]. In the bloodstream, where the chloride concentration is about 100 mM, cisplatin remains intact. Once inside the cell, the chloride concentration drops to 2-10 mM, allowing cisplatin undergo aquation by means of water substitution of its chloride groups (Figure 27). The rate of aquation of cisplatin in water (or buffer, pH=7, 37 °C) was measured, and the half life for formation of monoaquo species is around 120 min [82].

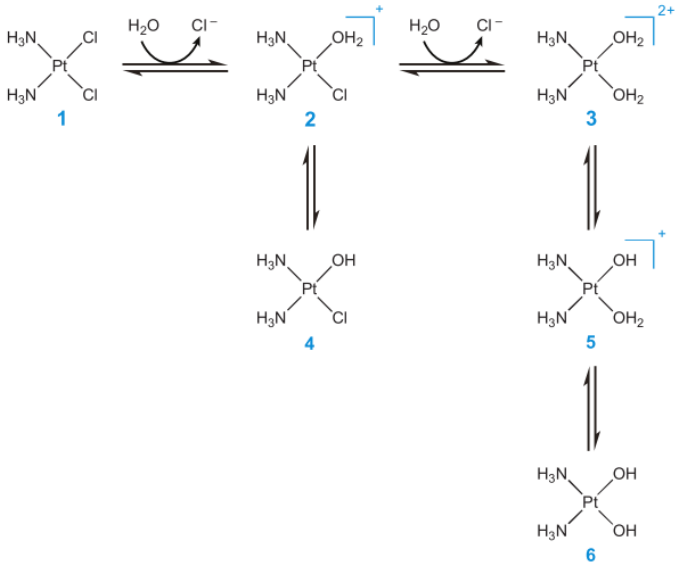

FIGURE 27. Schematic representation of cisplatin aquation. Upon entering cells, the low of chloride ion concentration causes the platinum compounds (**1**) to undergo aquation reactions, which means that water molecules replace one or both chloride leaving groups. The result is the formation of mono and diaquo species (**2** and **3**, respectively). **2** intermediates is the most reactive towards nucleophiles sites [80].

The active metabolites of cisplatin, namely the highly reactive mono-and bi-aquated species (*cis*-$[Pt(H_2O)Cl(NH_3)_2]^+$ and *cis*-$[Pt(H_2O)2(NH_3)_2]^{2+}$, avidly bind DNA, in particular, the N7 atoms of purine bases located in the major groove, inducing a double helix distortion that inhibits DNA transcription and replication. Cisplatin forms either monofunctional adducts, either bifunctional protein-DNA cross-links, intrastrand (involving adjacent bases as 1,2-d(GpG), 1,2-d(GpA) and 1,3-d(GpG) , are the most frequent lesions) and interstrand DNA cross-links. (ICLs). Although the latter ones are less frequent (5-10%), they are the most lethal lesions, since they are processed by means of DSB formation, as described above. The main mechanisms responsible for cisplatin-DNA adducts repair are NER, MMR and DSBs repair. NER is involved in repair of intrastrands Pt-DNA cross-links, while repair of Pt-DNA ICLs requires components of both NER and recombination repair machinery [83]. In the

attempt to remove Pt-adducts and restore DNA integrity , the cell cycle is arrested in G_2 phase [53] [55].

HMG-domain proteins are damage-recognition elements that identify and bind Pt-DNA adducts (especially 1,2-intrastrand crosslinks). Within this context, they have a controversial role. On one hand, they recruit the repair machinery to the damage site, on the other hand, it was postulated that they may protect Pt-adducts from recognition by DNA repair enzymes preventing NER activity and allowing the lesion to persist [84].

The persistence of DNA-adducts and the failure of DNA-repair prompt to **cell death** pathways [85]. Actually, it has been observed that high concentration of cisplatin lead to apoptosis or necrosis, while lower concentration induce cell cycle arrest/senescence [86] (Figure 28).

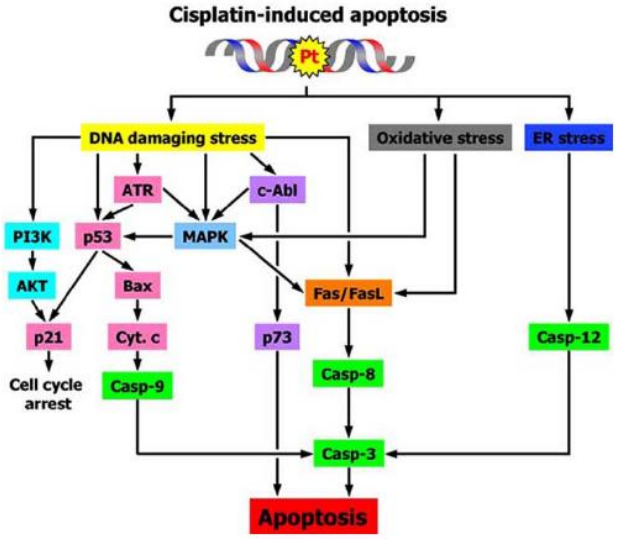

FIGURE 28. Schematic summary of cisplatin-induced damaging signalling. Initially, DNA damage activate the sensor kinases ATM and ATR. Activation of p21 an p53 prompt to cell cycle arrest, DNA repair or to intrinsic apoptosis. An extrinsic circuitry may be initiated by DNA damage. Importantly, it has been reported that cisplatin could induce apoptosis in the absence of DNA damage, through reticulum endoplasmatic (ER) stress. The fate of cancer cells following cisplatin treatment is determined both by the relative intensity of the damage and by the crosstalk between these signalling pathways [87].

In addition to genomic DNA, cisplatin could also bind mitochondrial DNA (mtDNA). These interaction drastically alter mitochondrial functionality, because mitochondria lack of mtDNA repair. Moreover, cisplatin interacts with the voltage- dependent anion channel (VDAC), inducing mitochondrial membrane permealization. It was argued that all these damages mediated cisplatin oto- and nephrotoxicity [88].Cisplatin not only reacts with DNA, but also it form covalent adducts with other many biological molecules. Obviously, it also covalently binds mRNA nucleotides [89]. Moreover, cisplatin reacts with endogenous nucleophils

containing sulphur functionalities, such as reduced glutathione (GSH), methionine, cysteine-rich proteins as metallothioneins. GSH is plays a relevant role in cisplatin detoxification. Intriguingly, it has been reported that cisplatin also interacts with membrane phospholipids, inducing changes in membrane fluidity, modification in membrane cholesterol contents and FAS receptor aggregation [90].

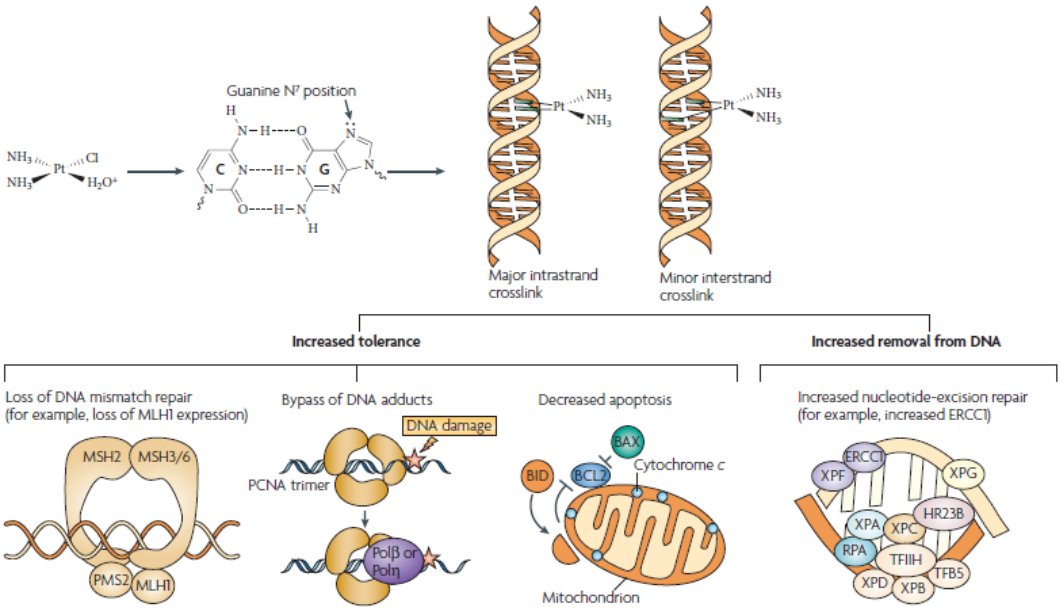

FIGURE 29. (Upper) The activated aquo platinum species covalently binds to DNA. Several types of adducts are formed, including 1,2-intrastrand cross-links and interstrand cross-links. (Lower) Basis of the insurgence of cisplatin resistance. The main removal pathway for DNA adducts is the NER system, and its increased activity can occur in tumors leading to platinum drug resistance. In addition, resistance can occurs through increased tolerance to platinum-DNA adducts, involving or loss of MMR or translesion synthesis that bypass the adducts. Lastly, downregulation of apoptotic cascade is observed [91].

Several toxicities associated with clinical treatment of cisplatin were found, with nephrotoxicity, ototoxicity and peripheral neurotoxicity being the most serious. Nephrotoxicity is primarily due to uptake of the drugs by the proximal tubule cells of the nephron; this side effect has largely been controlled by diuretics and pre-hydration of patients [79].

In addition to its toxic side effects, a major limitation of clinical use of cisplatin-based chemotherapy is **chemoresistance**. It can be inherent, if the drug is ineffective from the beginning of treatment, or acquired, when the drug is initially efficient but lose activity over time. Resistance to cisplatin is considered a multifactorial phenomenon, orchestrated by a plethora of events, as displayed in Figure 29 [92]:

1) first of all, chemoresistance processes may precede the interaction with DNA obstaculating target binding. It accounts for two main mechanisms. The first one involves reduced accumulation (low levels of CTR1) or increased efflux by means of copper-transporting P-type adenosine triphosphate (ATP7A and ATP7B) and MRP1/MRP2 isoforms [93] [94]. The second mechanisms is ascribed to sequestration by citoplasmatic scavengers containing thiols, as GSH, that prevent reaching of the target DNA. High levels of GSH, and/or GST, have been observed *in vitro* in case of cisplatin resistance [95] [96] [97] [98];

2) a second type of events is directly related to target interaction. It includes both increased repair of DNA-Pt adducts and increased tolerance to DNA lesions, as showed in Figure 29. The NER system plays a relevant role, since a correlation between NER proficiency and cisplatin resistance has been widely reported. Increased tolerance to platinum-induced DNA damage can occurs trough loss of function of MMR [99];
3) moreover, resistance mechanisms may concern defective apoptosis due to of Bcl-2, X-linked Inhibitor of apoptosis (XIAP), overexpression [100]or mutated p53. It has been reported that the p53 mutated cancer cells tolerate the formation of DNA adducts induced by cisplatin and cannot activate the apoptotic machinery [101];
4) overexpression of several factor transcription (such as TATA-binding protein (TBP), c-fos, c-myc and NF-kB) contribute to cisplatin resistance [102] [87];
5) Recently, it has been pointed out that epigenetic changes (as DNA-methylation and acetylation of histones) represent a dynamic survival strategy that contributes to cisplatin-resistant phenotype [103].

Development of new platinum anti-cancer drugs

Although cisplatin is a successful cancer treatment, it is not an ideal drug. It does not selectively act towards malignant cells, causing a plethora of side effects, it cannot be administered orally and patients can show or inherent or acquired resistance.

So, in the later decades, further platinum(II) complexes have been developed in order to improve cisplatin. These efforts led to a second-generation platinum compound, the **carboplatin**, [*cis*-diammine (cyclobutane-1,1-dycarboxilate-*O,O')*platinum(II)]. The substitution of the chloride leaving groups with a chelated carboxylate in the former one has contributed to decrease nephro- and neurotoxicity maintaining the same efficacy. Carboplatin shares the same carrier groups as cisplatin, thus, and after aquation, forms the same adducts.

Accordingly, both compounds exhibit cross-resistance. However, carboplatin aquation occurs with a slower kinetics because the dicarboxylate dianion dissociates more slowly than the chloride ligands. In fact, the half-life for aquation of carboplatin is around 100 fold higher than that of cisplatin [82].

Later, a third-generation platinum complex, **oxaliplatin,**[*(1R,2R)*-cyclohexane-1,2-diamine)(ethanedioato-*O,O'*)platinum(II)] extended Pt-based therapy to intrinsic resistant tumors, as colorectal cancer, modifying also the carrier groups. Distinct pharmacological profiles of oxaliplatin are ascribed to the different carrier groups, the bidentate ligand 1R,2R-diaminocyclohexane (1R,2R-DACH), in place of two monodentate ammine ligands of cisplatin. With respect to cisplatin-derived DNA lesions, oxaliplatin-induced DNA adducts are recognized less efficiently by MMR system [104] [105] and HMG domain proteins [106], because the bulkier and more hydrophobic carrier group distort in a different way the conformation of double helix and consequently are less efficiently repaired [107].

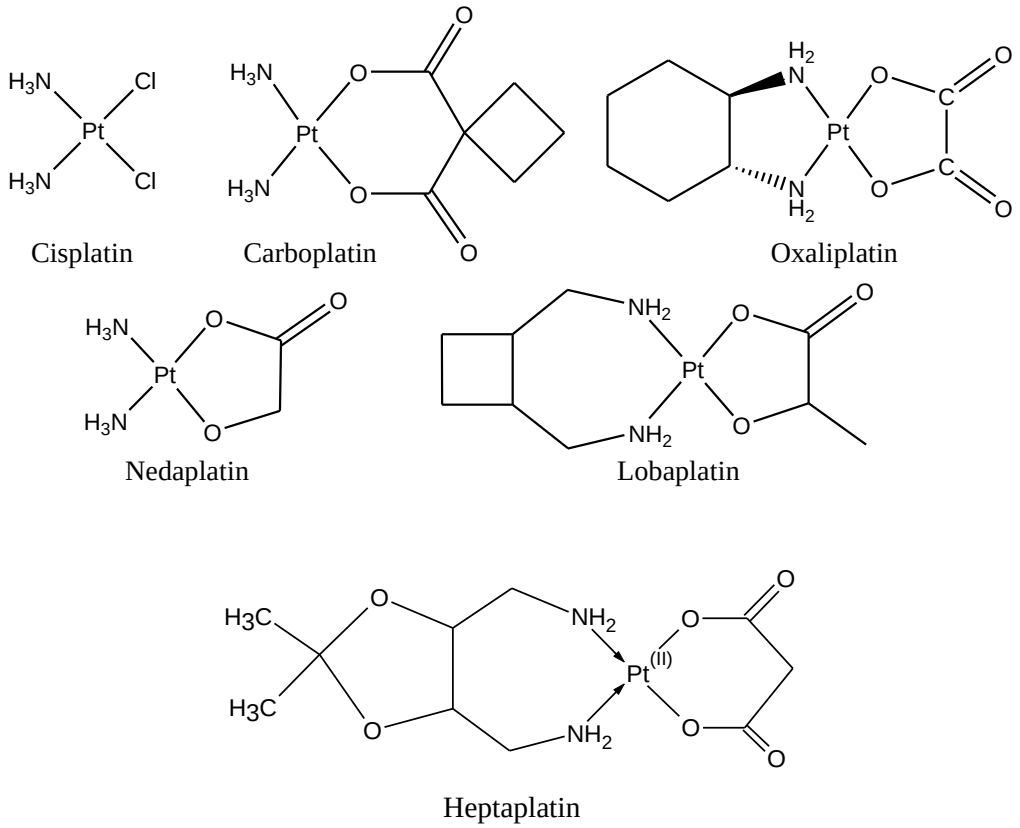

FIGURE 30. Pt(II) complex currently used in clinic

Cisplatin, carboplatin and oxaliplatin are worldwide approved drugs. Other compounds have only approved locally, like *Lobaplatin* [1,2-di(aminomethyl)cyclobutanelactatoplatinum(II)]

and *Nedaplatin* (*cis*-diamminoglycolatoplatinum(II)) and Heptaplatin [propanedioato(2-)-*0,0'*)[2-(1-methylethyl)-1,3-dioxolane-4,5-dimethanamine-*N,N'*]platinum(II), in China, Japan and Korea respectively [108] (Figure 30).

The search for new Pt(II) drugs able to overcome GSH-related cisplatin resistance led to the discovery of Picoplatin, also known as AMD473 or ZD0473 (Figure 31). It has been investigated in several clinical trials against a wide spectrum of platinum-resistant tumors as second line therapy, and it has been regarded as a promising drug candidate for the treatment of small cell lung cancer, receiving orphan drug designation in 2007, but unfortunately it seems not to be considerably effective [109].

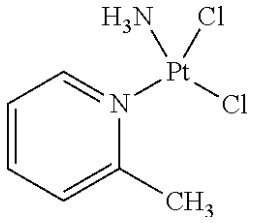

FIGURE 31. Picoplatin

As an alternative to mononuclear platinum compounds, several polynuclear platinum complexes have been synthesize by Farrell and co-workers, based on the rational that they may form a different variety of DNA adducts (mainly interstrand). Some of them entered clinical trials, but didn't go beyond the phase II because of their high toxicity [110].

Leading to Pt(IV) complexes

All Pt complexes used in clinic are administrated intravenously, by means of long and debilitating perfusion cycles. Therefore, in the last decades attention was devoted to the development of orally-administrable compounds, based on platinum at oxidation state +4, *i.e.* Pt(IV) complexes. These molecules have an octahedral coordination geometry, are inert to substitution by with biological nucleophiles. These features increase their lifetime in the bloodstream, raising their chances of reaching the tumor intact. Since their inertness, the conventional assumption is that Pt(IV) complexes are prodrugs. Pt(IV) prodrugs can be reduced by low molecular antioxidants, such as ascorbate and GSH, to their more reactive squanar-planar Pt(II) counterparts that are able to bind DNA (Figure 32). Pt(IV) reduction acts by the loss of the two axial ligands, which requires two-electron transfer process. However, ascorbate and GSH contained in the low molecular weight fraction of cell lisates inefficiently reduce Pt(IV) complexes, while the high molecular weight fraction is highly

efficient, independently on the amount of intracellular GSH; furthermore, metalloproteins can reduce Pt(IV) complexes in the presence of NADH [111].

The activation of the Pt(IV) depends on two critical parameters: the **reduction potential** (*Ep*) and **lipophilicity.** Both of them depend on the nature of the axial and equatorial ligands.
Ep determinates the ease of reduction of the complex and consequently is stability under biological conditions to reach the tumor target and exerts its biological activity. Considering complexes with the same set of equatorial ligands, the most easily reduced are those with chloride axial ligands, the most difficult to reduce are complexes with hydroxide axial ligands. The substitution of axial ligands with carboxylate chains lead to a complex with intermediate potential of reduction.[112].

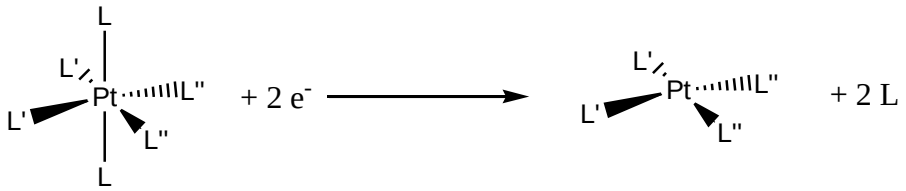

FIGURE 32. Activation of the inert Pt(IV) prodrugs. In the cell, the octahedral Pt(IV) complex undergoes a 2 electron reduction, mainly by ascorbate or GSH, yielding to their squanar-planar Pt(II) analogs.

A interesting work was performed by Hall et al. using the X-ray absorbition near edge spectroscopy (XANES), that investigated the reduction kinetics of a series of diaminedichloroplatinum(IV) complexes with different axial ligands, on A2780 human ovarian carcinoma cell line. They stated that Pt(IV) are reduced within few hours to Pt(II) after entering the cells, with a kinetics in agreement with their previous reported *Ep* calculated by means of cyclic voltammetry [113].

Moreover, axial ligands offer the opportunity to modulate the **lipophilicity** of the compounds. Lipophilicity affects the ability to enter tumor cells by passive diffusion and the propensity to be absorbed by the gastro-intestinal tract. A moderately lipophilic complex can be better absorbed and more accumulated allowing to overcome one of the main resistant mechanisms ascribed to cisplatin, the limited intracellular accumulation. Kelland and al. investigated the *in vitro* antitumor activity of a series of platinum(IV) complexes, and stated that a clear relationship exists between the number of carbons on the axial ligand and citotoxicity and that compounds with longer axial chains were significantly more cytotoxic and selective than

cisplatin [114]. In according to Kelland et al., Gramatica et al. showed that the cytotoxicity of platinum complexes is correlated with the length of axial ligands. Notably, they developed a predictive and robust quantitative structure-activity relationship (QSAR) model able to evaluate the relationship between structural features and *in vitro* citotoxicity of platinum complexes, using a lipophilic descriptor ($LogP_{o/w}$) and an electronic descriptor (E*p*) [115].

Up to now, some Pt(IV) complexes reached clinical trials but none of them has not yet obtained the approval. *Iproplatin* entered phase II clinical trials, but with limited success. The oral administrable *Satraplatin***,** (*OC*-6-43)-bis(acetato)amminedichloro(cyclohexylamine)platinum or JM216 (Figure 33), ended phase III, in combination with prednisone, for hormone refractory prostate cancer management [116].

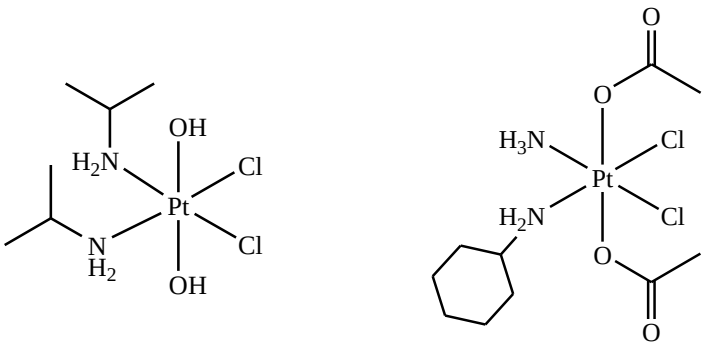

FIGURE 33. Iproplatin and Satraplatin

In recent years, drug delivery approaches have been developed to improve the selectivity of platinum complexes towards tumor cells. These efforts accounted for to several strategies, such as liposomal-based (*Lipoplatin*) or co-polymer based products (*Prolindac*) [117].

Topoisomerase inhibitors

Movement of the growing fork during DNA replication induces formation of positive supercoils; in order to extensive DNA synthesis to proceed, the supercoils must be removed. The overwinding of DNA is regulated by topoisomerases, that are enzymes that exist in two isoform, called I and II. Topoisomerase I cleaves only one strand of DNA duplex and then reseals it removing both positive and negative supercoils. Topoisomerase II enzymes have the ability to cut both strands of DNA molecule, pass another portion of the duplex through the cut, and reseal the cut [25]**.**

The former class is inhibited by campotecines (which include *irinotecan* and *topotecan*), whereas the latter class is the target of antracyclines (as doxorubicine) and antibiotics (such as Actinomycin, Mitomycin C and Bleomycin) [62].
Moreover, doxorubin acts as an intercalating agent, as far as its planar structure prompts to a distortion of the double helix.

Mitotic spindle inhibitors

These drugs block the formation of functional mitotic spindle in M phase, preventing cell division. The mitotic spindle is composed of microtubular fibers, formed by tubulin, at which duplicated DNA chromosomes are grasped. They ensure that, after cell division, each new cell gets a full set of chromosomes.
Vinca alkaloids (such as *Vincristine*, *Vinblastine*), bind tubulin, preventing its polymerization, and the formation of spindles and cell division. Conversely, **taxanes** (*Paclitaxel*, *Docetaxel*) stabilize the assembled tubulin filaments, hindering the separation of the daughter cell [118].

Epigenetic modulators

Epigenetic modifications include heritable and reversible changes modulating a variety of mechanisms such as RNA elongation, mitosis, DNA replications and repair, all of them influenced on the state of chromatin. By affecting gene activity, epigenetics also plays a major role during tumorigenesis. Therefore, the development of drugs acting as epigenetics regulators attracted considerable interest. Their general mechanism of action is simplified in Figure 34.

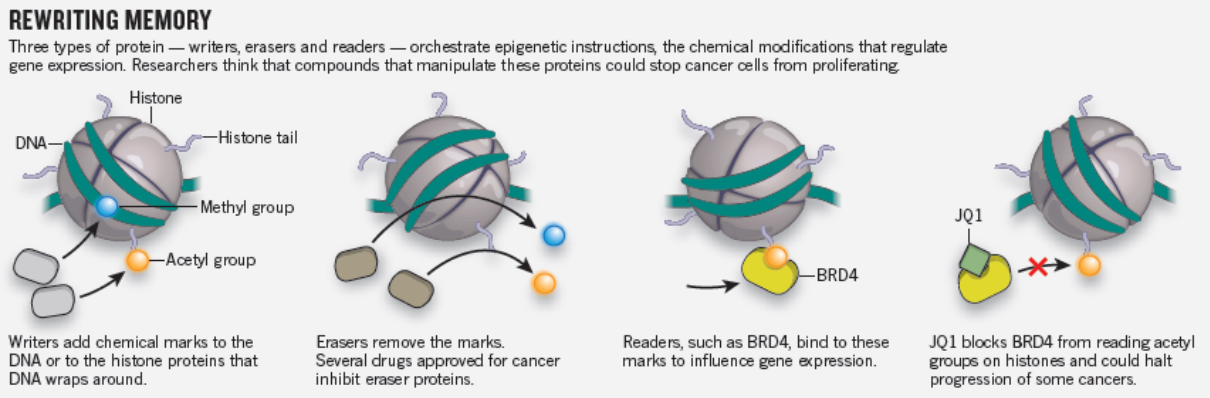

FIGURE 34. Epigenetic control systems generally involve three types of proteins: *writers* (such as *HATs)*, *erasers (*such as HDACs) and *readers* as BRD4. (+)-JQ1 prevents it from reading the acetyl-lysine residues of histones and modulating gene transcription by disruption of chromatin-dependent signal transduction [119].

Epigenetic modulators inhibit enzymes that convert chromatin to the open-active conformation, *i.e.* histone deacetylase (HDAC) and DNA methyl transferase (DNMT) inhibitors, or prevent the inactive-acetylated chromatin to be read, as BET inhibitors. Several HDACs and DNMT inhibitors have been tested *in vitro* and are currently evaluated clinically [120] [121].

HDAC inhibitors belong to different structural families that includes hydroxamates (vorinsotat and suberoylanilide hydroxamic acid, or SAHA) , cyclic peptide (trapoxin B), and short-chain fatty acids (valproic acid, sodium butyrate). HDACs inhibitors induce apoptosis by activating both extrinsic and intrinsic pathways, and prompt cells to senescence [122].

Despite promising *in vitro* observations, clinical trials using HDCA or DNMT inhibitors alone are frequently deluding, whereas given in combination show a modest antitumor effect [121] [123].

The role of BRD4 in c-myc expression and NF-kB activity

Bromodomain and extraterminal (BET) family of acetyl-lysine recognition motifs act as chromatin regulators. The BET family orchestrates the expression of genes that regulate both inflammation processes and proliferation. Notably, **BRD4,** highly expressed in a broad range of tumors, plays a key role in driving gene expression in M/G_1 mitotic chromatin and ruling, *inter alia*, c-Myc and FOS-L1 expression [124], and, indirectly, NF-kB [20] [125].

Transcriptional activation is associated with chromatin acetylation, which prompts to BRD4 recruitment. Then, BRD4 forms a complex with two transcription cofactors: the Mediator and the positive transcription elongation factor b (P-TEFb), a kinase that facilitates RNA polymerase II-dependent transcription [126]. This complex not only occupies the enhancers, but also the super-enhancers (larger complexes of transcription factors responsive elements recognized by TF and coactivator), that work through cooperative and synergistic interplay. Super-enhancers are correlated with tumor progression, since their clusters are usually generated near oncogenes in cancer cells [127] Super-enhancer activity depends on the recruitment of BRD4, thus, its inhibition leads to their disruption. In multiple myeloma, the association between super-enhancers and oncogenes transcription has been demonstrated [128]. Recently, BRD4 was proposed as good target by means modulate c-myc transcriptional function.

In the last years, the emerging drug candidate **(+)-JQ1** (Figure 35), a tieno-tiazolo-1,4-diazepine, has attracted great interest. It is a potent and high specific inhibitor of BET family.

(+)-JQ1 displaces BET proteins from chromatin by competitively binding to the acetyl-lysine recognition pocket, modulating gene transcription. (+)-JQ1 shows high binding activity for BRD4; on the contrary, the (−)-JQ1 stereoisomer has no appreciable affinity to BET bromodomains.

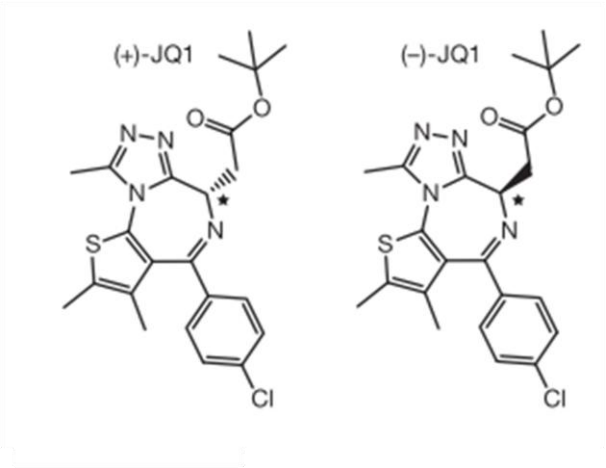

FIGURE 35. Skecth of (+)-JQ1 and (-)-JQ1

Antitumoral drug discovery *in vitro*

Hit-to-lead phase: design and screening

The process of drug discovery is a very long way. It generally follows the following path that includes the following stages:

target validation (TV) → assay development → high-throughput screening → hit to lead (H2L) → lead optimization (LO) → preclinical drug development → clinical drug development.

Hit to lead (H2L), also known as lead generation, is a stage in early drug discovery where primary active agents (namely *hit compounds*) are evaluated from a high throughtput screening (HTS), and then undergo limited optimization to identify new analogues with improved potency, called *lead compounds* [129]. Lead and hit compounds share the same *pharmacophore*, *i.e.* the set of various functional groups spatially orientated in a specific way or of features necessary for activity trough a biomolecular target, that is defined by quantitative structure-activity relationship (QSAR) studies. Further chemical modifications are introduced during *lead optimization* phase to refine flaws of each series [130].

Early screening of investigated molecules is performed in the attempt to establish the degree of their potency and selectivity and so, to identify the compounds with better pharmacological profiles that deserve to be addressed to future investigations. In a second step, drugs mechanism of action is elucidated at molecular or cellular level. In the last years, the drug discovery process has relied on *system biology* to better understand the cellular response of to bioactive agents. Its introduction has allowed to move from a "target approach" to a "system approach" and so, to connect biological activity of bioactive molecule to an increased biological space [1] [129].

In vitro processes of identification of bioactive molecules involves **high troughput screening** (HTS). HTS are assay performed by micro-plates, usually formatted of 96 or 384 wells, that allow to test simultaneously several compounds using small volumes.
Two factors are crucial: first, the choice of a reliable, rapid, sensible and reproducible HTS method; second, suitable biological model that resemble the features of the disease against which you wish intervene. For anticancer drug screening, cell lines are mainly employed. A cell line derives from a specimen of the same site of origin/tissue, thus, it composed by cells that share the same genetic and morphological characteristics. In the field of anticancer drug

discovery, tumor cell lines are employed as experimental model and the effort are focused on cytotoxic or cytostatic compounds that cause tumor regression. Cell lines of hematological tumors growth in suspension, while those of solid tumors growth attached to a solid support as monolayer. They are maintained in a growth medium that mimic bloodstream.
Unfortunately, advances in the process of anticancer drug discovery are not so fast. This drawback lie mainly on the limits harbored by *in vitro* tumor models available.

In vitro solid tumors models

Cell monolayer model

The most commonly used cell model for *in vitro* study is the monolayer of cells growing on a sterile, tissue culture treated, plastics substrate. Once the available surface is covered by cells, they reach confluence and growth stops (Figure 36). Therefore, in order to keep the cells actively growing, they have to be sub-cultured at regular intervals. However, 2-D models harbor some intrinsic limitations and are unrepresentative of solid tumor tissue and the associated microenvironment. They do not replicate the molecular patterns, gene expression and further genetic and epigenetic changes accumulated during cell replication in the body. Moreover, they do not simulate both the heterogeneity of tumor niche and cell-cell and cell-matrix interactions [131]. So, drug research based on 2-D models may not accurately predict a drug's effects in the body, leading to a high rate of false positives of promising drugs candidate.

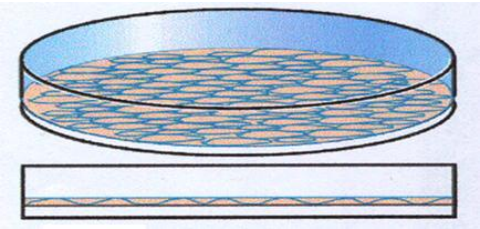

FIGURE 36. Monolayers growth of an *in vitro* cell line attached to surface of a Petri dish treated for cell culture (TC, the surface has to be hydrophilic and negatively charged). Once available surface is covered by cells, they reach confluence and growth stops.

Although the 2-D culture model offered an important contribution to drug research, a lot of efforts were done to develop *in vitro* models that resemble *in vivo* tumor tissues. In the last years, these efforts prompted to the implementation of 3-D tumor models in antitumor drug discovery.

Multicellular tumor spheroid models

3-D tumor models includes [132]:

- hollow fibers reactors: cells are seeded into hollow fiber to form solid mass; it is a discouraged procedure because fiber all both holds back cells growth;
- multicellular layer model: cells are seeded into semi-permeable support membrane; it is used to measure drug diffusion trough the membrane that stands for a barrier between extracellular environment and cells layer. The information obtained is be questionable, since it does not reflect *in vivo* cell arrangement. Also, it's not compatible with not long-term culture;
- multicellular tumor spheroids.

Multicellular tumor spheroids (MCTS) are spherical cell aggregates having diameters of around 350-400 μM . They are formed by an outer shell of proliferating cells (reflecting the *in vivo* situation of cells adjacent to blood vessels), by a inner ring of *quiescen*t cells and finally, by a necrotic/hypoxic core. Spheroids develop a concentration gradient of oxygen, nutrients, catabolites and drugs.

MCTS accurately simulate the conditions of native tumors as volume growth kinetic, cytoarchitecture and cellular communication (Figure 37); cell-cell and cell-matrix contacts are similar to those of avascular nodules, intervascular regions of large solid tumors and micrometastasis.

MCTS are less sensitive than their 2-D system counterpart to the same treatments [133]. Thus, they reproduce some physiological characteristics that are crucial for therapeutic efficacy and provide a more realistic prediction of *in vivo* drug responses. The ability to generate spontaneously MCTS is given by the presence of a peculiar sub-populations, as cancer stem cells [134]. Unfortunately, not all primary tumor cells or all established cell lines spontaneously form spheroids; it is a intrinsic ability independent of the culture technique [135]. Sometimes, cancer cells have to grow in stem cell medium, rich in growth factors, to generate MCTS [136]. Ivascu and co-worker analyzed the spontaneous generation of several cell lines, representative of different tumors, and assessed that some of them give rise to simple cellular aggregates [137].

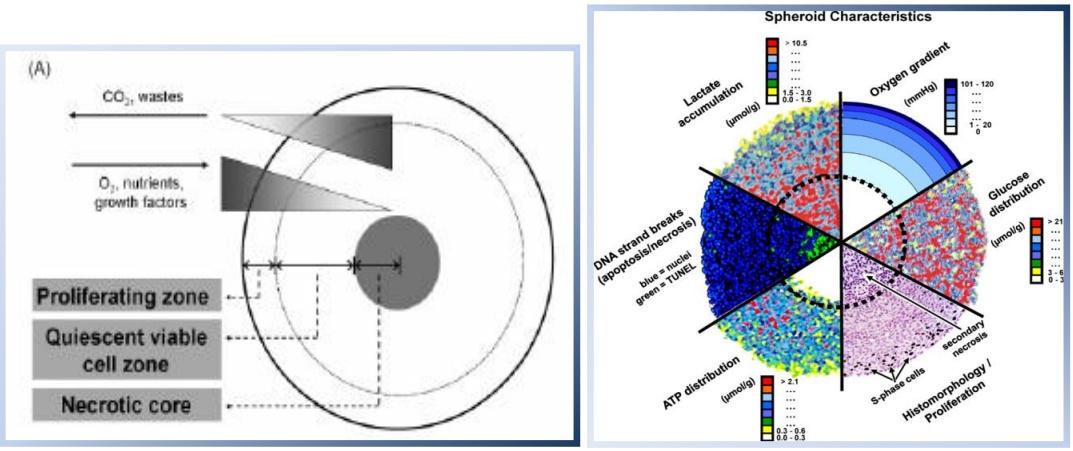

FIGURE 37. Tumor spheroids exhibit a concentric organization of proliferating, quiescent and dead cells. Moreover, they simulate the diffusion gradient of drugs, O_2 and nutrients. Molecules diffuse until a distance of 150-200 μm the outer layer [138].

Spheroids represent a useful tool since they could be used for long-term drug studies and allow to discriminate the cytostatic and cytotoxic activity of an anticancer agent. Furthermore, they could be co-cultured with different cell types, as endothelial or immune cells [138]. Lastly, MCTS allow to reduce the use of animal models (Figure 38).

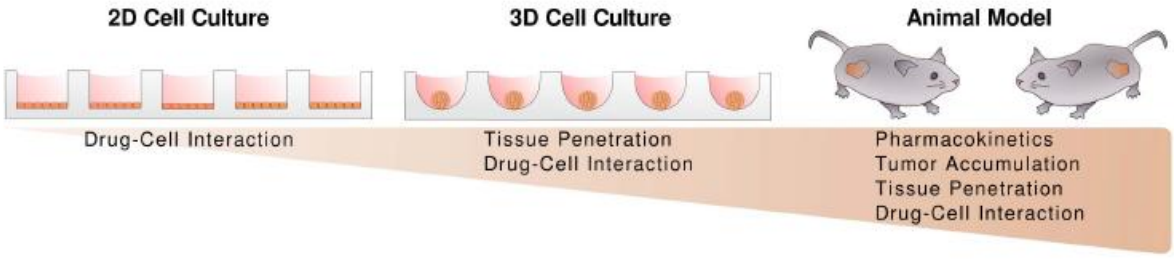

FIGURE 38. Since MCTS models approximate some features of *in vivo* tumors, they can fill the gap between conventional 2D assays and the in vivo screenings in animal models. So, they allow to reduce employment of animal test systems [139].

Several techniques have been proposed to generate MCTS, including spinning flasks, liquid overlay, microscaffolds, and the hanging drop method to shape the cell aggregation [140]. In spinner flask, cells are growth in dynamic suspension of culture medium yielding a high number of very different spheroids. In the second one, cells are seeded into culture dishes coated with agarose. The former couple of procedures are not reliable since are not able to control spheroids size, while the latter two and require specific and expensive tools.

However, in a drug screening perspective since, microplate-based methods are the best ones. In literature many methods to avoid cell adhesion have been reported, based on well surface coating, for instance by an hydrophobic polymer, *i.e.* poly (2-hydroxyethil metacrylate) or poly-HEMA, or by Matrigel® (that is a basement membrane extract that resembles ECM components) [137].

Malignant Pleural Mesothelioma

What is asbestos?

Asbestos refers to a naturally occurring family of hydrated mineral silicate fibers. It is conventionally classified in two distinct groups:

- The amphiboles, which include crocidolite ("blue asbestos"), amosite ("brown asbestos"), anthophyllite, tremolite and actinolite;
- chrysotile, or "white asbestos".

The former fibers are needle-like, while the latter fibers have a curled, "serpentine" shape.

In the 20th century, asbestos (especially crocidolite and amosite fibers) had a widespread commercial diffusion because of its ideal advantages, represented by durability, fire-resistance, and cheapness. Indeed, the term *asbestos* comes from ancient Greek and means *inextinguishable*. It was employed in building as insulation material (*e.g.* brake lining, ship building, ceiling, pool tiles), also mixed with cement, and for other disparate uses (e.g. cigarette filters, theatre curtains, tablemat, crayons).

Asbestos was regarded as the best available material for these applications until, in 1960s, many evidences highlighted its pitfall: carcinogenicity. Asbestos fibers, once inhaled, can lead to pleural plaques, to a chronic pleural and lung fibrosis (called asbestosis) and/or act as a tumor promoter or co-carcinogenic, giving rise to, broncogenic carcinoma(lung cancer) and pleural and peritoneal malignant mesotheliomas [141] [142] (Figure 39).

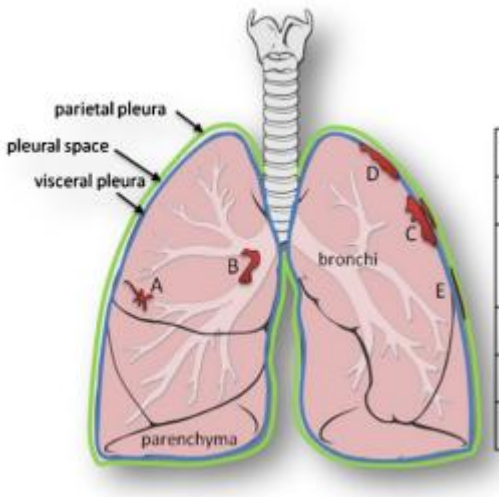

Label	Pathology	Site
A	Asbestosis	Parenchyma
B	Bronchogenic carcinoma (lung cancer)	Bronchi
C	Mesothelioma	Pleurae
D	Pleural fibrosis	Pleurae
E	Pleural plaque	Parietal pleura

FIGURE 39. Diagram showing the situation of the types of pathology caused by asbestos fibers [142].

Asbestos carcinogenicity relies on its fibrous structure: the fiber surface area, size, solubility and their chemical composition all play a role in its mechanism of action. Needle-like fibers are by far more potent than curly fibers in causing MMs because they deeply penetrate into the lower respiratory tract and they are cleared less rapidly from the lungs. This phenomenon is enhanced for longer (> 2 μm) and less soluble fibers.

Notably, among the asbestos types, crocidolite and amosite are characterized by the highest iron content, which is involved in tissue injury, since the ferrous ions integrated into asbestos fibers are oxidated by hydrogen peroxide to ferric ions (Fenton reaction) leading to the production of hydroxide anion (OH^-) and hydroxyl radicals ($HO^\bullet$). In turn, ferric ions can be reduced to ferrous ions by superoxide anion (O_2^-), as well as other biological reductants, making a chain of reactions that fuel the genesis of other damaging oxygen species (ROS), such as hydrogen peroxide (H202) and alkoxyl radicals ($RO^\bullet$) [143].

In addition crocidolite fibers has the finest fiber diameter; thus this type of asbestos is regarded as the most oncogenic one [144].

Malignant pleural mesothelioma and asbestos

Malignant mesotheliomas (MMs) are fatal tumors arising from mesothelial membranes that line the pleural, peritoneum and pericardium cavities. The primary function of mesothelial cells is to form a protective monolayer around inner organs that facilitates their movement by means of the secretion of a lubricant (consisting of glycosaminoglycans and phosphatidylcholine) that supports the lubrification of their serosal surface [145].

The association between asbestos exposure and mesothelioma was established in 1960s, when Wagner *et al.* [146] published a paper that described 33 cases of MMs, observed in African miners exposed to Caper Blue Asbestos. Two years later, Wagner confirmed this thesis producing MPM in laboratory animal models by direct exposure to asbestos dust.

Since then, a lot of extensive epidemiological data have been accumulated and the scientific community widely accepted that even a low-level exposure of asbestos is able to induce mesotheliomas [147].

MMs are considered occupational malignancies, because they mainly occured in male workers exposed to asbestos fibers. However, many cases have been observed in family members of asbestos workers and in the people living in proximity of asbestos mines and factories due to environmental pollution by asbestos mineral fibers [148].

MM most commonly occurs in the pleura: the so-called malignant pleural mesothelioma (MPM) stands for up to 80% of all cases [149].

MPM tumor cells can assume three histological subtypes, namely:

- Epithelioid, which is the most common and with better prognosis;
- Sarcomatous, with spindle-like cells;
- mixed or biphasic, with both epitheliod and sarcomatoid components.

MPM has a very poor prognosis: the median survival is less than 12 months from the diagnosis.

The malignancy develops after a long period of latency, that may be in the order of about 40 years after initial asbestos fiber inhalation [150]. In the past, MPM was considered an extremely rare tumor. However, MPM risk has been climbing more and more and its peak of incidence is coming in the next decades as a result of past widespread use of asbestos (Figure 40).

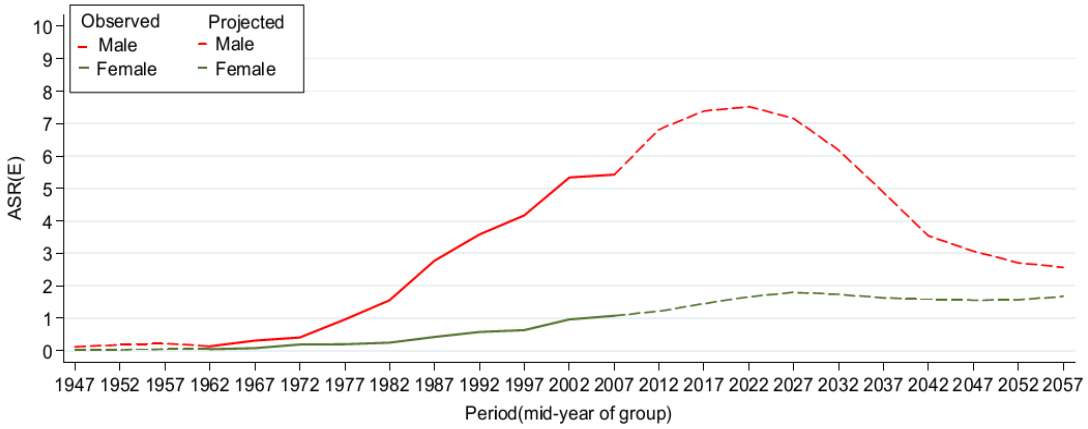

FIGURE 40. Incidence rate of MPM (age-standardized rates, ASR), observed in the past and predicted for the next decades. It mainly affect the male population arising from occupational exposure [151].

Nowadays, only few countries banned the employment of asbestos; it still can be mined and exported in Russia (which is the largest producer), Brazil, South Africa, China, India, Kazakistan and Canada, where it is often handled without adequate precautions. USA and Japan did not ban the use of asbestos but restricted its usage only. Italy banned the use of asbestos in 1992, but the hazards is still there, since huge amounts of asbestos derivates still remain in public and private buildings. Many rules to avoid the risk of accidental asbestos inhalation have been adopted and some attempts to force asbestos decontamination in industry and housing are ongoing [148].

It should be noted that asbestos represents a potential hazard in case of natural disasters or explosions, because it can become airborne from building and the air could be contaminated with its small fibers. One emblematic example is the fall of the twin towers, in 2001: the buildings was made of about 400 tons of asbestos and after their collapse to the ground, there was a release of ultra-fine asbestos fibers. Rescue workers and local population were exposed to asbestos from the air and have a high risk to develop MPM or asbestos-related diseases in the next future. [152].

In addition, in some Western countries (*i.e.* Greece, Cyprus and Turkey) there are volcanic rocks containing asbestiform minerals, that have been used by inhabitants to build houses.

So, this malignancy is not going to disappear rapidly but, on the contrary, it will represent for a long time a worldwide threat.

Analysis of mesothelioma mortality recorded in WHO database between 1994 and 2008 yielded a death rate of 6.2 cases per million population and estimated that 125 million people worldwide are currently exposed to asbestos in workplace [153].

MPM epidemiological patterns closely reflects the geography and history of asbestos exposure. Disease incidence varies between countries and the burden of MPM death cases are relevant in Australia, Belgium and Great Britain [147] (Table 2).

Table 1 Current incidence and projected future case load for malignant mesothelioma

Country	Year	Cases	Annual incidence per million†	Male-Female ratio	Predicted peak	Estimated future cases	Period of estimate
Australia (35)	2008	661	29	4:1	2014-2021	6,500§ (36)	2004-2060
United Kingdom (37)	2009	2,560	29	4.9:1	2011-2015	65,000 (38)	2002-2050
USA (39)	2009	-	10	4.6:1	2000-2005	85,000 (2)	2008-2054
Italy (40)	2004	-	24	2.6:1	2015-2024	800/year (41)	2012-2024
Japan (42)	2007	1,068	8‡	3.5:1	2027	66,000 (43,44)	2003-2050

†Age standardised; ‡Crude rate; §State of New South Wales only

TABLE 2. Disease incidence of MPM varies markedly between geographic area but the highest annual rates are reported in specific countries [154].

Italy shows one of the highest incidence rates of MPM (in the period 2003-2009, 5184 deaths per year occurred) and exhibits the highest mortality rates in Liguria, Piemonte, Friuli-Venezia Giulia and Lombardia regions, mirroring the occupational, and the cobsequentenvironmental asbestos exposure (Figure 41). The greatest mortality cluster have been observed in Casale Monferrato (AL) and its surrounding area, where, the factory Eternit was active in the production of asbestos-cement until 1986.

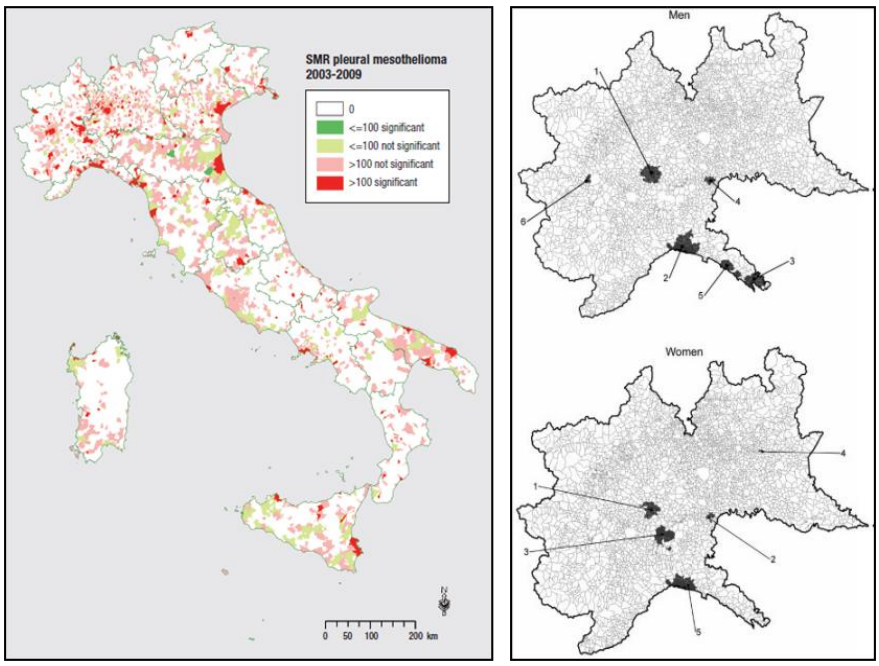

FIGURE 41. (Left): In Italy, MPM mortality has high regional variability. The acronym SMR stands for *standardized mortality relative, since* the mortality was standardized with number of resident population. MPM death cases are concentrated in specific sites (red spots), corresponding to municipalities where asbestos manufacturing and use was hugely employed in large asbestos-cement factories, in shipyards and close to quarries. (Right): Mortality cluster in North West area for men (upper) and women (lower) are depicted. Two main clusters was found in both gender, corresponding to the area with major asbestos-cement industries: Casale Monferrato (AL) and Broni (PV) [155].

Mechanisms underlying asbestos carcinogenecity

A huge number of evidences showed that asbestos is a complete carcinogen, since after its inhalation, the fibers reach the pleura and initiate a cascade of events in mesothelial and not-mesothelial cells that reshape the cellular milieu. However, hitherto it is still not completely understood the mechanism of malignant transformation. It seems that the molecular pathogenesis of MPM is a multifactorial process involving multiple phenomena (Figure 42). Three hypothesis have been reported since now [156] [142]:

1) the ***chromosome tangling theory*****:** asbestos fibers are engulfed by mesothelial cells. The uptaken fibers physically interfere with mitotic spindles during cell division, resulting in incorrect chromosomes segregation, chromosomal structural abnormalities and aneuploidy ;
2) the ***adsorbition theory*****:** *in vivo*, the positive and negative charges on mineral surface of asbestos fibers catalyze the deposition of proteins and/or hazardous chemicals;
3) the so-called ***oxidative stress theory*****:** asbestos fibers generate ROS both outside and inside the cells, triggering oxidative stress. After phagocytes (*i.e.* alveolar macrophages and leukocytes) engulf the asbestos fibers, they produce large amounts of free radicals to eliminate them, without success and (the so "frustrated phagocytosis"). The iron contained in asbestos, catalyzes the generation of reactive oxygen species on mineral fibers surface by itself and amplifies the ROS cascade.

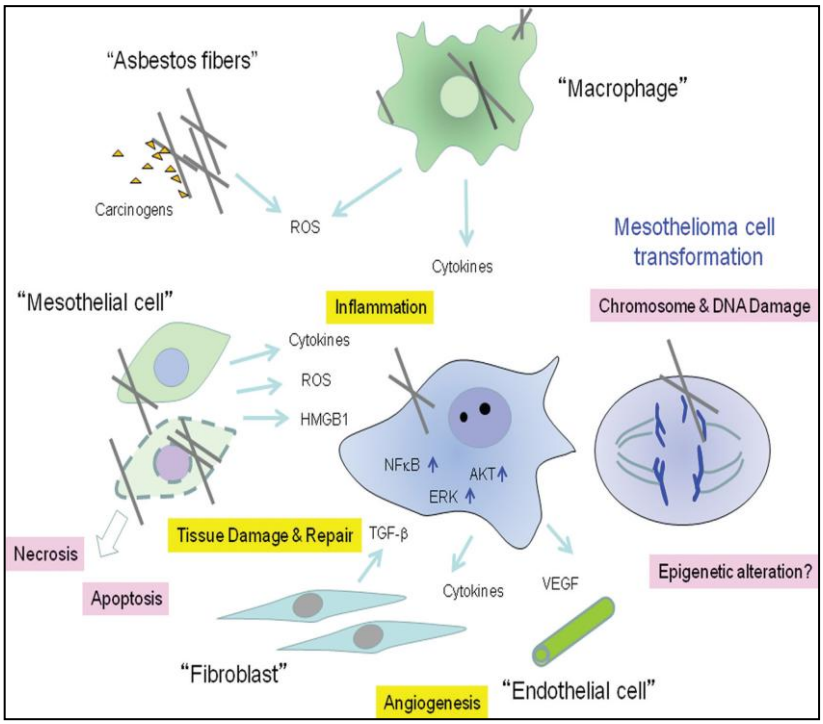

FIGURE 42. Pleural malignant transformation. Asbestos trigger ROS generation and the release of inflammation mediators. In addition, asbestos interfere with mitotic spindle during chromosomes segregation. These events allows genetic alterations to accumulate within mesothelial cells and sustain asbestos-induced DNA-damage, leading to the initiation of mesothelioma [149].

ROS generated by asbestos fibers have two main consequences that both have a crucial influence on pleural malignant transformation:

1) insurgence of **DNA damage**; since hydroxyl radicals are added to DNA bases forming DNA adducts that induces conformational changes of double helix. In particular, it was reported that 8-oxo-2' deoxyguanosine has a major role in carcinogenesis. Reduced repair of oxidized DNA bases will results in elevated genetic and epigenetic lesions and consequently, their predispose changes in expression of several genes correlated with protein metabolism, cell transformation, survival, proliferation and motility [157];
2) **chronic inflammation**; asbestos-killed cells and the frustrated phagocytosis induce the recruitment of many inflammatory cells by means of the secretion of many cytokines and growth factors, as tumor necrosis factor-alpha (TNF-α), interleukins (such as IL-1β, IL-6, IL-8); HMGB1, and VEGF. T**he prolonged state of inflammation** also enhances the expression of inducible enzymes causing, interalia, up-regulation of cyclooxigenase-2 (COX-2) [158]. It is known that prostaglandin E_2 (PGE_2), the main COX-2 metabolite, impacts several pathways involved in carcinogenesis.

Because of these signalling are persistently activated, chronic inflammation occurs. This events induce a reshaping of cellular microenvironment.

Because of the crucial role of oxidative stress in MPM pathogenesis, this malignancy is regarded as a "reactive-oxygen driven tumours".

All these perturbations induce mesothelial cells to die. However, in some of them, a compensatory mechanism is activated to inhibit asbestos-induced cytotoxicity. The high concentration of growth factors and cytokines promotes a cascade of pro-survival pathways, stimulating cell proliferation, neoplastic transformation and tumor progression. In fact, is well known that chronic inflammation promote carcinogenesis [159] (Figure 42).

It seems that genetic factors predispose specific individuals to MPM. Individual differences in genes involved in detoxification, might partly explain the difference in susceptibility to MPM. However, their role need to be further elucidated [160]. Furthermore, a possible role of the viruses has been proposed. It was hypothesized that the oncogenic Simian Virus-40 (SV-40) is a potential cancerogenic factor in MPM pathogenesis and that could increase the risk of its occurrence among people exposed to asbestos. SV-40 is a monkey virus which is thought to have infected humans via contaminated polio vaccines used in 1950s and 1960s [161]. However, the evidences are controversial and it is unlikely that SV-40 play a role in the onset of this malignancy [162].

Molecular alterations in MPM

MPM progression is a long multi-stage process, therefore, protracted oxidative stress signalling provokes persistent **DNA damages**.

Consequently, a lot of **deregulated pathways** in MPM contribute to tumor development and chemoresistance [163]. The oncogenic cascade of events include:

- activation of NF-*k*B pathway and NF-*k*B dependent genes, as *c-myc* and *c-Jun* oncogenes;
- activation of the epidermal growth factor receptor (EGFR). This event is correlated with the activation of extracellular downstream signal-regulated kinases (ERKs) (*i.e.* ERK 1/2); ERKs modulates transcriptional activity of several proto-oncogenes as c-fos and c-jun;
- promotion of antiapoptotic genes as Bcl-xl;

- upregulation of anti-oxidant enzymes, such as manganese superoxide dismutase (MnSOD) and GST [164], and increase of GSH metabolism [165] [166];
- overexpression of genes involved in each DNA repair system, especially genes related to double-strand break repair (Figure 43) [167].

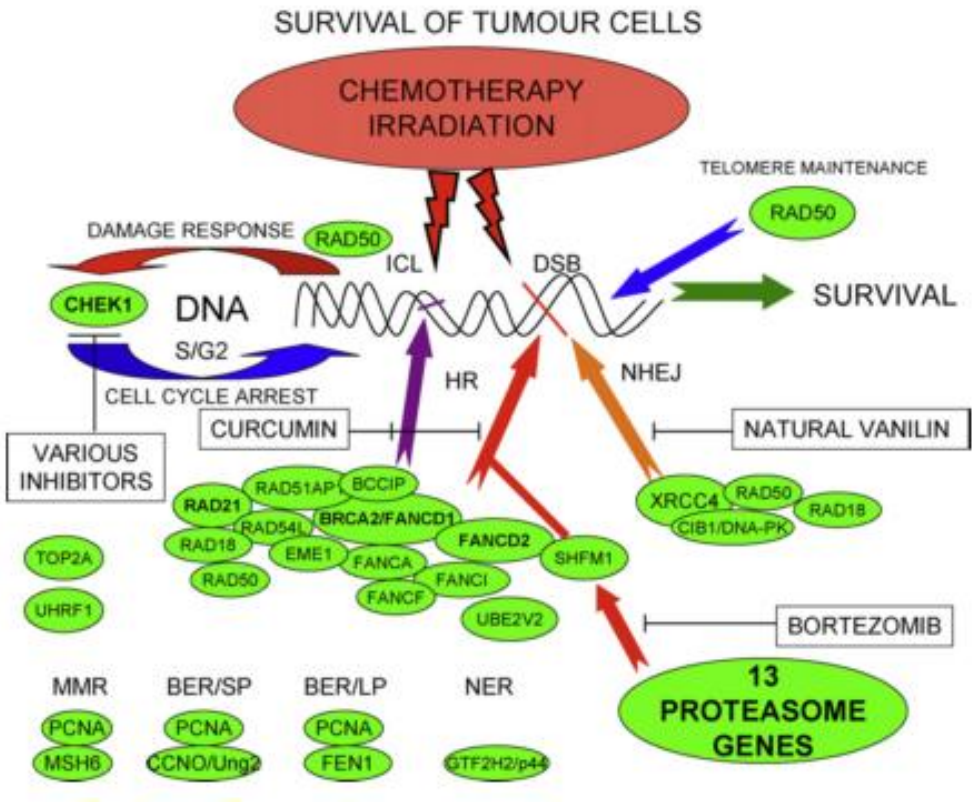

FIGURE 43. Schematic representation of genes overexpressed in malignant pleural mesothelioma related to DNA repair (green). They account for both the chemo- and radio-resistance. In particular, defects on MMR (by MSH6 overexpression) and NER (by GTF2H2/p44) confer to platinum resistance [167].

MPM Chemotherapic treatment: the state of art

MPM is highly refractory to most of the available conventional therapies. When the disease is diagnosed in advanced stage and surgical approaches are not suitable, chemotherapy is the cornerstone of the treatment and platinum-based regimens represent the gold-standard. In a meta-analysis of phase II trials conducted between 1995-2001, cisplatin was the most active single agent for the treatment of unresectable MPM [168].

First-line chemotherapic treatment combined cisplatin with gemcitabine. In 2003, a phase III randomized trial compared cisplatin alone versus cisplatin plus pemetrexed in untreated MPM. The combination gave a response rate of 41.3% compared to 16.7% for cisplatin alone and improved the median overall survival for patients of very few months (12.1 versus 9.3

months with cisplatin alone) [169] [170]. Despite association of cisplatin and gemcitabine shows similar benefits [171], gemcitabine is not still employed in clinical regimens.

A second-line therapy still lacks and need to be developed. Vinorelbine was evaluated in monotherapy for this purpose, but obtained a response rate of 16% and a median survival of 9.6 months. With the combination of vinorelbine and cisplatin, the response rate was 30%, two fold higher, and the median survival was 16.8 months [172].

The way of selectivity of **targeted therapies** was explored on the basis of markers differentially expressed by tumor cells with respect to non-malignant cells. Indeed, mesotelioma cells secrete and express several angiogenic factors (such as EGF, VEGF, PDGF) that sustain angiogenesis and increase vessel density, which is correlated with poor outcome. Consequently, a plethora of tyrosine kinase inhibitors of their receptors were investigated. They showed strong activity against *in vitro* MPM models, but were proved ineffective, both in monotherapy and in associations, in a lot of phase II/III clinical studies. Similarly, cell cycle pathway inhibitors were evaluated and failed to improve the survival. So, these evidences are damping down the enthusiasm for molecular targeted drugs as standard treatment for MPM [173].

In addition, epigenetic drugs were also evaluated, but without giving promising results [174] [175].

The failure of MPM management is due to two main reasons: first, because is often diagnosed in the late stages when the disease is too advanced for current therapies; second, because sometimes it is misdiagnosed with other malignancies (benign pleural disease, metastatic cancer, adenocarcinoma). A lot of efforts have been devoted to identify an serum biomarker, which had to guarantee selectivity, early diagnosis, and treatment outcome prediction.

Among several potential biomarkers, over-expressed in MPM cells, that have been evaluated, the most promising are the following:

- soluble mesothelin-related peptide (SMRP), a glycoprotein that plays a role in cell adhesion and cell-to-cell recognition and signaling over-expressed on mesothelioma cells;
- osteopontin, a tumor-associated glycoprotein that regulates cell-matrix interactions and cellular signaling;
- megakaryocyte potentiating factor (MPF), is a sialoprotein involved mainly in bone matrix formation and tumor invasion.

However, each biomarkers listed above have some limitations: osteopontin lacks of specificity for mesothelioma, while both SMRP and MPF show poor sensitivity for detecting non-epithelial subtypes [163]. So, further efforts are needed to discover better prognostic and detection tools for MPM.

Materials and methods

Unless specified, all reagents were purchased from Fisher Scientifics.

Unless specified, absorbance, fluorescence and luminescence values were recorded with a Tecan Infinite F200 plate reader.

Cell culture

MPM cell lines derived from pleural effusion of previously untreated patients suffering from MPM, called BR95 (epithelioid histotype), MG06 (mixed histotype, with epithelial predominance), MM98 (sarcomatoid histotype), and MM98R. The latter is a cisplatin-resistant cell line derived from wild-type MM98 by exposure to sub-lethal concentration of cisplatin for several months [176].

A human mesothelial cell (HMC) lines was employed to check the selectivity of drugs candidate investigated. HMC were isolated by gentle scraping of the peritoneum of the inner wall of uncomplicated congenital hernia sacs surgically excised from premature babies. This local environment is usually devoid of significant inflammatory stimuli in the absence of complications and therefore the peritoneum remains thin and almost transparent and the uninjured HMCs are mostly in a normal (resting) state with a pavement-like appearance. All cell lines were obtained from the bio-bank of the hospital of Alessandria (Pathology Unit). Their phenotypes are shown in Figure 44.

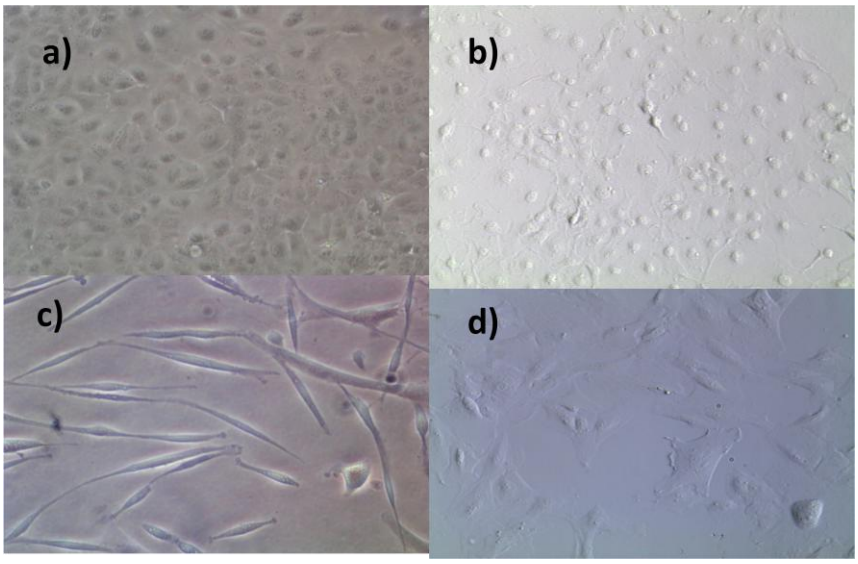

FIGURE 44. The MPM cell lines (**a)** BR95,epitheliod; **b)** MG06,mixed; **c)** MM98, sarcomatoid) and the human mesothelial cell (**d)** HMC) line were employed in this study. The epitheliod cells show a regular shape, while the sarcomatoid are spindle-shaped. MGO6 mixed phenotype cells shows a predominance of epitheliod component. HMC cells show intermediate morphological characteristics between them.

HMCs, epithelioid and mixed cells were growth in F10 Ham's medium, whereas Dulbecco's modified Eagles' s medium was used for sarcomatoid ones.

The A2780human ovarian carcinoma , the HCT-116 human colon carcinoma cell line and the MCF-7 breast cancer cell lines were purchased from ECACC (European Collection of Cell Cultures, UK) and were growth in RPMI -1640,McCoy's 5A and MEM supplemented with non-essential amino acids, respectively.

The human lung cancer cell line A549 was a kind gift of Dr. S. Bonetta (Avogadro University) and was grown in RPMI 1640.The acute leukemia HL-60 cells was a kind gift of Dr. S. Martinotti (Avogadro University) and was growth in RPMI-1640.

Media were supplemented with L-glutamine (2mM), penicillin (100 IU mL^{-1}), and 10% fetal bovine serum (FBS) to give the complete medium. FBS is commonly used as a supplement to cell culture media since it supports cell growth and product formation proving a broad spectrum of macromolecules, attachment factors, nutrients, hormones and growth factors.

Media and supplements were purchased from Sigma-Aldrich, Lonza Biosciences and Life Technologies.

Cells manipulation was performed in a laminar flow cabinet, in sterile conditions, to prevent contamination.

Cells were routinely grown in sterile polystyrene TC Petri dishes with a diameter of 10 cm at 37 °C in a 5 % CO_2 humidified chamber (Thermo Scientific, Model 370). In order to keep the cells actively growing and avoiding that they reached confluence), they were sub-cultured at around twice a week.

Briefly, medium was aspirated from the cell culture Petri dish, cells were washed once with sterile PBS (phosphate buffer saline containing 50 mM sodium phosphate, 150 mM sodium chloride, pH 7.2) and then, a trypsin-EDTA solution (0.05% and 0.2%, respectively, Hyclone) was added. Once the cells detached from the plate, serum-containing medium was added to inhibit trypsin. Harvested cells were collected into an appropriately sized centrifuge tube and centrifuged for 5 minutes at 1100 rpm. Following centrifugation, the supernatant was removed, and the cell pellet was resuspended in complete medium. Thus, cells were counted by means of an hemocytometer and an adequate cell number was re-seeded.

To perform the routine determination of the IC_{50} values, 2000-5000 cells were seeded into sterile tissue-culture-treated 96-well plates and allowed to attach 24h before drug treatment. Then, they were challenged with drugs for 72 h continuous treatment (CT) at various concentration.

For cell senescence cells (2×10^4) were seeded in 24-wells plates the day before treatment.

For clonogenic assay, 200 cells well^{-1} (BR95) or 100 cells well^{-1} (MM98) were seeded in 6-well plates the day before the treatment.

Compounds and drug candidates

Unless specified, compounds were synthesized in Osella's laboratory. Platinum complexes investigated are shown in Figure 45.

Figure 45a display cisplatin, carboplatin, ethacrynic acid and the bi-functional complexes **1** (*cis,cis,trans*-diamminodichloridobis(ethacrynato)platinum(IV)) and **2** (*cis,cis,trans*-diamminodichloridobis(ethacrynato)platinum(IV)).

In Figure 45b, picoplatin and its Pt(IV) analogues **3** (*cis,cis,trans*-[$PtCl_2$(mpy)NH_3($CH_3COO)_2$), **4** (*cis,cis,trans*-[$PtCl_2$(mpy)NH_3($CH_3CH_2COO)_2$) and **5** (*cis,cis,trans*-[$PtCl_2$(mpy)NH_3(CH_3CH_2 $CH_2COO)_2$) are reported. Platinum(IV) complexes with linear carboxilate chains as axial ligands, are **6** (*cis,cis, trans*-diaminedichlorobisacetate-platinum(IV)), **7** (*cis,cis, trans*-diaminedichlorobisbutanoate-platinum(IV)), **8** (*cis,cis, trans*-diaminedichlorobisesanoate-platinum(IV)), **9** (*cis,cis, trans*-diaminedichlorobisoctanoate-platinum(IV)), as shown in Figure 45c.

Lastly, Pt(IV) complexes with carboxylate aromatic axial ligands are reported (Figure 45d). **10** (*trans,cis,cis*-[$Pt(C_6H_5COO)_2Cl_2(NH_3)_2$]), **11 (***trans,cis,cis*-[$Pt(C_6H_5CH_2COO)_2Cl_2(NH_3)_2$]) and **12** *trans,cis,cis*-[$Pt(C_6H_5(CH_2)_2COO)_2Cl_2(NH_3)_2$]) share cisplatin as Pt(II) counterpart; while **13** (*cis,trans,cis*-(1R,2R-DACH)[$Pt(C_6H_5COO)_2Cl_2$]), **14** (*cis,trans,cis*-(1R,2R-DACH [$Pt(C_6H_5CH_2COO)_2Cl_2$]) and **15** (*cis,trans,cis*-(1R,2R-DACH) [$Pt(C_6H_5(CH_2)_2COO)_2Cl_2$]) share 1R,2R-DACH-$Cl_2$ as Pt(II) analogue.

a

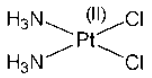

cisplatin

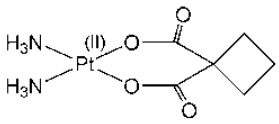

carboplatin

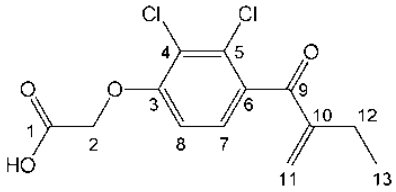

ethacrynic acid, EA

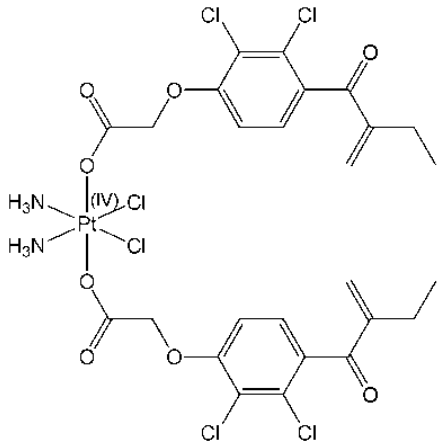

1

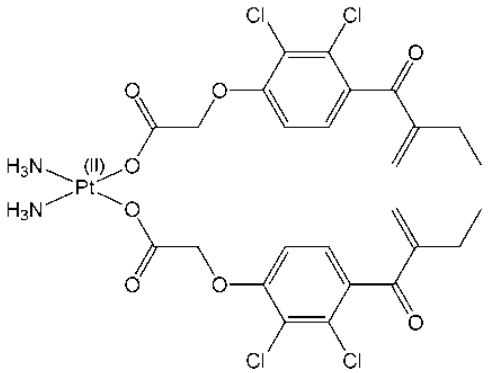

2

b

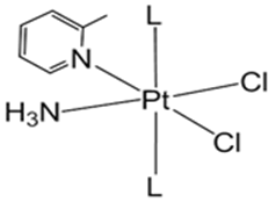

3 L = CH_3COO^-
4 L = $CH_3CH_2COO^-$
5 L = $CH_3(CH_2)_2COO^-$

c

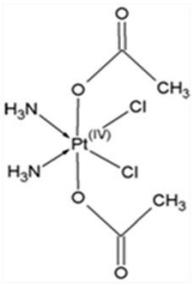

6

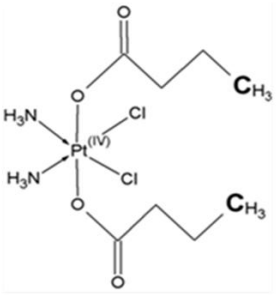

7

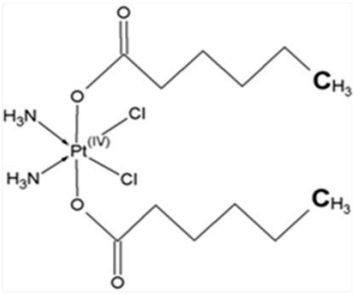

8

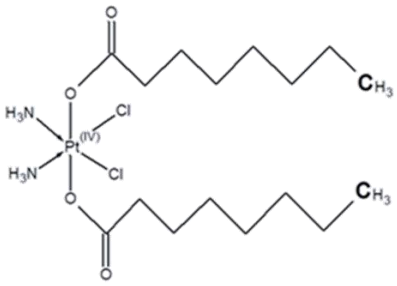

9

d

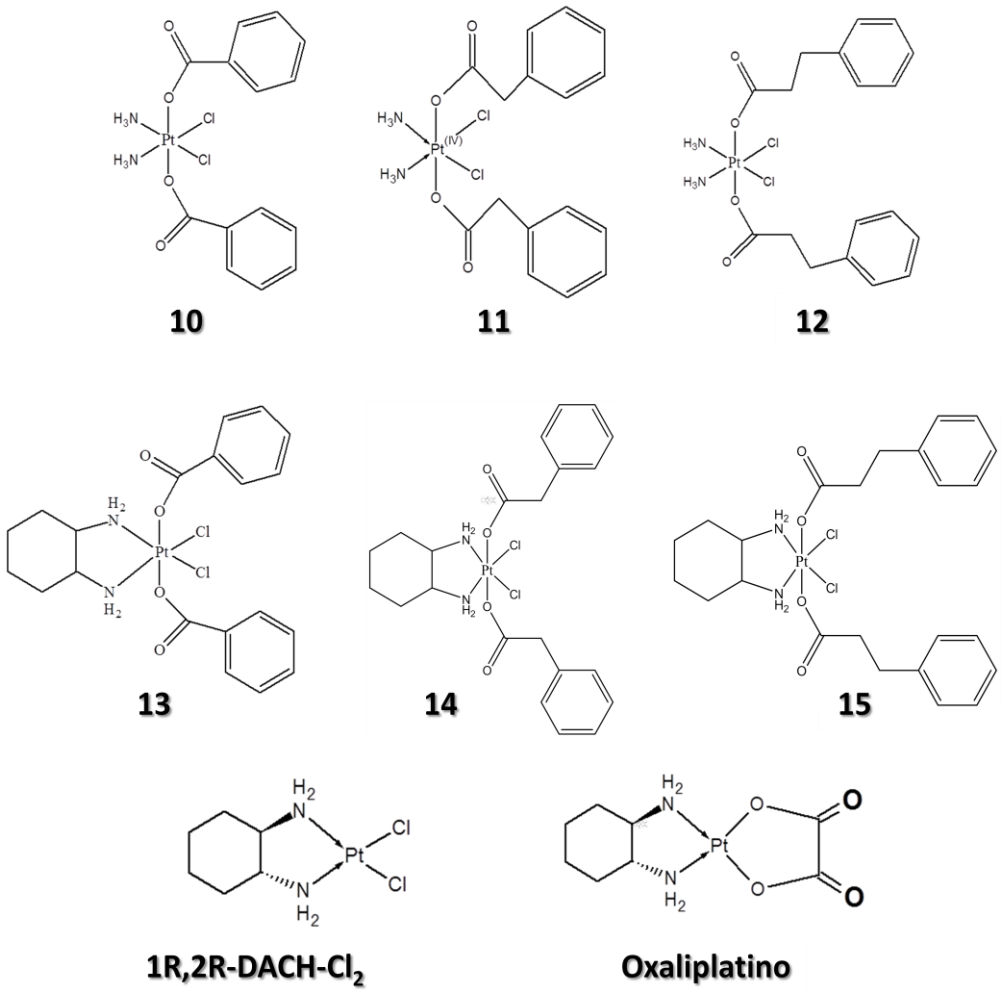

FIGURE 45. Sketch of platinum complexes investigated

Compounds preparation (solvent used, final stock concentration and storage) was summarized in Table 3.

Complex	**Final Stock concentration**	**Solvent**	**Storage**
Cisplatin (Sigma-Aldrich)	1 mM	aqueous solution of NaCl (0.9 % w/v) brought to pH 3 with HCl	–70 °C.
Carboplatin (Strem Chemicals)	25 mM	ultrapure water (Milli-Q)	Prepared immediately before the experiment.
Ethacrinic acid (EA) (Sigma-Aldrich)	0.1 M	DMSO	Prepared immediately before the experiment.
1	20 mM	DMSO	–70 °C.
2	10 mM	DMSO	Prepared immediately before the experiment.
Picoplatin	5 mM	DMSO	–20 °C.
3	5 mM	DMSO	–20 °C
4	2.5 mM	DMSO	–20 °C
5	2.5 mM	DMSO	–20 °C
6	5 mM	NaCl 0.9 %	–70 °C
7	5 mM	NaCl 0.9 %	–70 °C
8	5 mM	absolute ethanol	–70 °C
9	2.5 mM	absolute ethanol	–70 °C
10	10 mM	DMSO	–70 °C
11	10 mM	DMSO	–70 °C
12	10 mM	DMSO	–70 °C
13	10 mM	DMSO	–70 °C
14	10 mM	DMSO	–70 °C
15	10 mM	DMSO	–70 °C
1R, 2R-DACH-Cl_2	5 mM	DMSO	Prepared immediately before the experiment.
Oxaliplatin	5 mM	L-(+)-Lactic acid	dissolved over night (O.N.) the day before the treatment

TABLE 3. Solvent used, final stock concentration and storage of each platinum compound under investigation are listed.

(+)-JQ1 and **(-)-JQ1** (Figure 46) were dissolved in DMSO to final concentration 10 mM and stored at -20 °C until used. Both compounds were kindly supplied by Prof. S. Knapp (University of Oxford, UK).

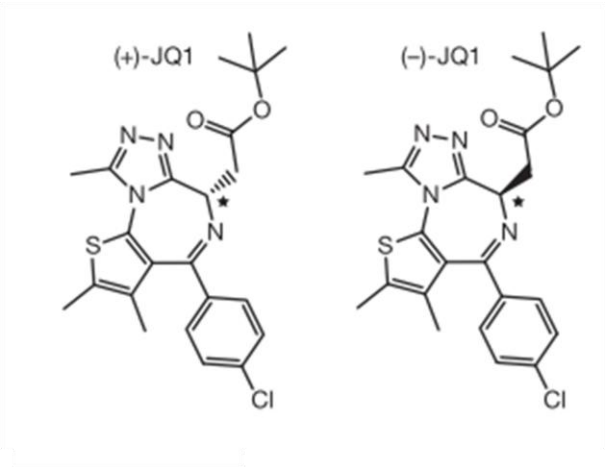

FIGURE 46. Sketch of (+)-JQ1 and (-)-JQ1

Co-ASS [2-acetoxy-(2-propynyl)benzoate]hexacarbonyldicobalt (Co-Co), **Co-EPM** hexacarbonyl[μ-(2-ethylphenyl)-methanol]dicobalt (Co-Co) and acetylsalicylic acid (**ASA)** (Sigma) were dissolved in absolute ethanol, to final concentration of 20 mM, 10 mM and 1 M, respectively (Figure 47). Cobalt complexes were stored at 4 °C, while ASA was prepared immediately before the experiment. Co-ASS was kindly supplied by Prof. R Gust (University of Innsbruck, Austria).

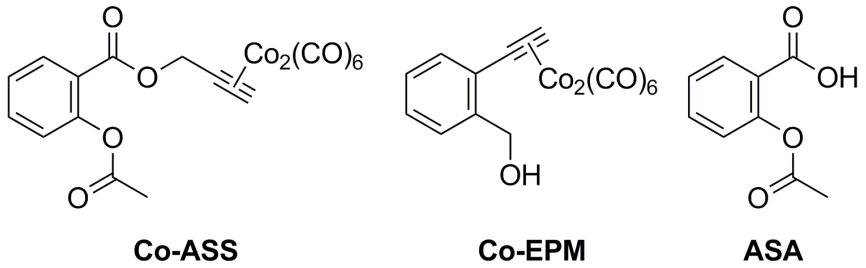

FIGURE 47. Sketch of Co-Ass, Co-EPM and ASA.

Compound stock solutions were diluted in complete medium to the required concentration ranges. In the case of co-solvent, the co-solvent concentration never exceeded 0.5 % (these concentration was found to be nontoxic to all the cells tested).

Determination of solubility and lipophilicity

Complexes 6-9

The water solubility of the Pt(IV) complexes **6**-**9** was determined preparing their saturated solutions in water, which were stirred in the dark at 25 °C. After 24 h the solid residue of each sample was filtered off (0.20 μm regenerated cellulose filters) and the Pt content of the solutions was determined by means of ICP-OES.

The lipophilicity of a molecule is usually represented by the logarithm of its n-octanol/water partition coefficient (log $P_{o/w}$). The classic method to measure log $P_{o/w}$ is the flask-shaking, based on the partition of the analyte into a mixture of n-octanol and water.

A solution ($[C]_{init.water}$) of compounds **6-8** in n-octanol-saturated water (V_{water}) was prepared and shaken with water-saturated n-octanol ($V_{oct.}$). The mixture was shaken for 30 min and centrifuged for 30 min at 4000 rpm. The platinum content of the initial and final aqueous phase ($[C]_{fin.water}$) was determinated by means of ICP-OES. This method was used to determine the log $P_{o/w}$ values of complexes **6-8** but it was not efficient in the case of the extremely lipophilic complex **9**.

In most cases the volumes of octanol and water are equal, but for compounds with extreme logP values like Pt-complexes different volumes must be used. The $logP_{o/w}$ value can be calculated with the following formula $logP_{o/w} = \log\left(\frac{[C]_{init.water} - [C]_{fin.water}}{[C]_{fin.water}} \times \frac{V_{water}}{V_{oct.}}\right)$.

Moreover, the lipophilicity of the complexes was evaluated by means of RP-HPLC.

Among the alternative experimental methods developed to measure the lipophilicity, the retention parameters in RP-HPLC (where n-octanol is ideally replaced by the C18 chains functionalizing silica as stationary phase, while the mobile phase consists of various mixtures of water and an organic co-solvent) are often used [177].

Since RP-HPLC retention is due to partitioning between (polar) mobile and (apolar) stationary phases, there is a straightforward correlation between the partition coefficient and the HPLC capacity factor *k'* (*k'* = ($t_R - t_0$) / t_0, where t_0 is the retention time for an unretained compound and t_R is the retention time of the analyte). The log k'_0 (k'_0 is the HPLC capacity factor extrapolated to 0% co-solvent) values of compounds with known log $P_{o/w}$ can be used to create a calibration curve (log $P_{o/w}$ = a log k'_0 + b) to evaluate partition coefficients of new compounds from chromatographic data.

However, owing to the very different lipophilicity of the studied complexes it was not possible to find a range of % of methanol (organic modifier of the aqueous mobile phase) to perform the logk' measurements and then the estrapolation of logk'_0. Therefore, one only chromatographic condition (90% methanol/ 10% HCOOH 15mM) was used to get logk'_{90} values for complexes **6-9.**

To determinate logk'_{90} , solutions of the platinum complexes 0.5mM were prepared. KCl was the internal reference to determine the column dead-time (t_0).

Cisplatin and complex 10

As far as chromatographic condition concerned, a solution of methanol and HCOOH 15mM was used as eluent. The lipophilicity index is derived from the log of the capacity factor *k'* (*k'* = ($t_R - t_0$) / t_0, where t_0 is the retention time for an unretained compound and t_R is the retention time of the analyte, extrapolated to 100% HCOOH (log k'_0).

To determinate log k'_0, solutions of the platinum complexes 0.25 mM were prepared.

KCl was the internal reference to determine the column dead-time (t_0).

Determination of the IC_{50} values

Unless specified, cell treatment was performed for 72h continuous treatment (CT). At the end of the period, the activity of the candidate drug or mixture was determined.

For sake of clarity, it should be pointed out that the activity of an antitumoral drug mainly resides in the inhibition of cell growth (IC_{50} value) that could be determined by means of two approaches: *i)* trough cell viability assays that reveals the amount of the remaining alive cells or *ii)* detecting the amount of dead cells by means of cytotoxic assays.

Based on their mechanisms of action, **cell viability assays** assess two main features of cell viability:

- adherence on the support: the cellular residual biomass is revealed by means of cationic dyes (such as methylene blue, BM, or Crystal Violet, CV) or anionic colorants (as sulphorodamine B), that bind to acid or basic intracellular sites (such as those of proteins and nucleic acids), respectively;
- metabolic activity: by direct detection of the adenosine tri-phosphate (ATP) amount or by means of the activity of enzymes that lye on mitochondria of living cells,

specifically the mitochondrial dehydrogenases. This group of assay includes the [3-(4,5-dimethylthiazol-2-yl)-5-(3-carboxymethoxyphenyl)-2-(4-sulfophenyl)-2-2*H*-tetrazolium] inner salt (MTS) assay, resazurin (shown in Figure 48);

- Cell proliferation: *i)* measuring incorporation of labeled DNA precursors (as ^{3}H-thimidine or bromodeoxyuridine, BrdU, a thimine analogues) that are incorporated into newly synthesized DNA strands of actively proliferating cells, or by means of *ii)* clonogenic assay, which evaluate the ability of a single cell to grow into a colony.

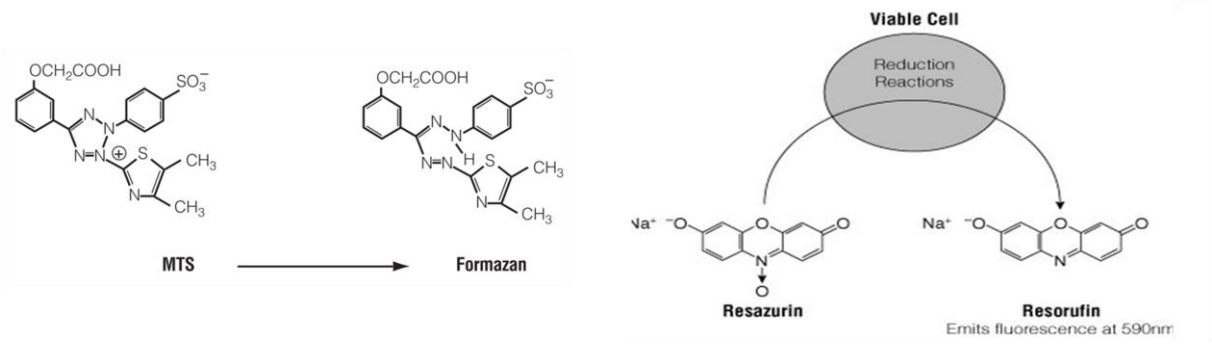

FIGURE 48. In cell metabolically active, (left) the colorless tetrazolium salt is converted to yellow formazan [178], whereas (right) resazurin is converted to resorufin, a fluorescent product, by mitochondrial enzymes [179].

Cytotoxicity tests point out dead or damaged cells (which have holes in their membrane) by means of dye exclusion, which means that live cells (due of intact membrane) will not take up any dye and will appear unstained, or by means of the detection of membrane leakage of typical intracellular markers, *i.e.* the lactate dehydrogenase.

As far as **our experimental procedure** concerned, in a first step we decided to evaluate residual cell viability by means of colorimetric tests more suitable for automation analyses: methylene blue (BM) staining or MTS assay.

Methylene blue (BM) staining

For BM staining test, cells were fixed and stained were fixed and stained at 4°C by 1 h incubation with 2 g L^{-1} methylene blue in 50% methanol-50% water, allowed to dry, washed, and eluted with 200 μL $well^{-1}$ of 50% ethanol-50% 0.1 M HCl. Absorbance was recorded at 620/405 nm [180].

MTS assay

The MTS assay was based on a commercial kit (CellTiter Aqueous Solution, Promega, Milan, Italy), according to the manufacturer's instructions. Briefly, the reagent was added to cells in complete medium, and incubated for 1-4 h. The absorbance values of the product were recorded at 490/620 nm.

Resazurin reduction assay

In a second step, viability experiments were repeated using the more sensitive resazurin reduction assay [181] to confirm the preliminary data, since resazurin method is a nontoxic, rapid and sensitive procedure. Resazurin assay is provided of a wide dynamic linear range (50-50000 cells), as shown in Figure 49, that is wider than absorbance-based methods (such as BM and MTS) but similar to luminescence-based ones (as ATP) [182].

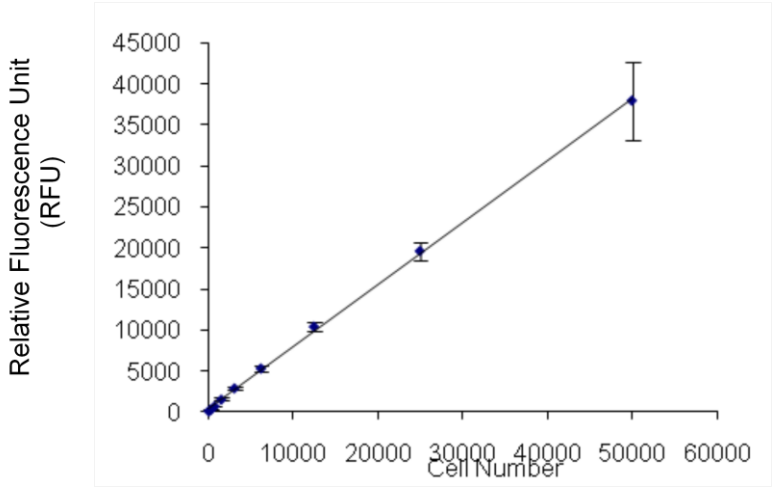

FIGURE 49. Correlation between signal-cell number is reported for resazurin assay

Resazurin (10 μg*mL^{-1}; Acros Chemicals, France) was added to cells (seeded in black plates, in order to limit cross-talk between the different well) in fresh medium for 1 h at 37 °C. The amount of reduced product, resorufin, was measured by mean of fluorescence intensity using an excitation wavelength of 550 nm and an emission wavelength of 585 nm.

The absorbance/fluorescence values of eight wells containing medium without cells were used as blank.

Clonogenic assay

In order to performed this experiment, cells are challenged with the drug, then the drug is removed and fresh medium is added (recovery), replacing it twice a week. Lastly, colonies number is evaluated. So, the clonogenic assay allows to assess the antiproliferative ability of a drug by means of clonal growth evaluation: if a drug acts as a cytostatic, its effect is lost upon its removal and cells resume proliferation; on the contrary, if a drug acts as a cytotoxic agent, triggers cell death and cells lose clonal growth ability.

Clonogenic assay method was performed as described by Franken *et al* [183]. Briefly, 200 cells well^{-1} (BR95) or 100 cells well^{-1} (MM98) were seeded in 6-well plates and allowed to attach 24h before drug treatment. Then, they were challenged by drug candidates from day 0 to day 3, and then allowed to recover in fresh medium, changed every 3 days, until day 10, when colonies were stained with methylene blue. Experiments were performed three times in triplicate. Colonies were counted manually and reported as percentage of the control.

Data analysis: IC_{50} determination

The final IC_{50} was calculated from at least three independent replicates of the same experiment each carried out in triplicate.

Data were normalized to 100 % cell viability for non-treated cells, and IC_{50} were obtained from the dose-response sigmoidal curve using Origin Pro (version 8, Microcal Software Inc., Northampton, MA, USA).

Combination experiments

Combination experiments were performed using fixed-dose-ratio concentrations. For simultaneous administration, drugs was co-diluted and the resulting stock solution was serially diluted and tested for cell viability.

Combination index (CI) values were calculated for non-mutually exclusive drugs, according to Chou and Talalay Equation (16) [184].

Other cell-based investigations

Senescent cell staining

Senescent cells remain viable, metabolically active and differ from quiescent cells that are in a temporary state of growth arrest; senescent-associated phenotype cells tend to be morphologically enlarged, flattened, and display cytoplasmatic granularity, chromatin foci and eventually, elevated activity of senescence–associated β-galactosidase (SA-β-Gal). The latter feature represent the rational of the β-galactosidase staining.

In order to carry out the assay, HMC, BR95, MG06, MM98 and MM98R cells (2×10^4) were seeded in 24-wells plates the day before treatment. At the end of the treatment, cells were washed twice with PBS, fixed in 3% formaldehyde for 30 min at 4°C, and washed again with PBS. Then, the β-galactosidase staining was performed. Cells were incubated with a chromogenic substrate for β-galactosidase, that converts it to a rich blue product [185]. Cells were washed and at least three different 10X microscopic fields were photographed with a Leica EC3 camera mounted on a Leica DMIL LED microscope. The Cell Counter plug-in of ImageJ 1.45s was used to count the total number of cells and the blue ones. The cell count was performed independently, on different experimental repetitions, by two different operators.

Treatment with cobalt complexes, cisplatin and ASA

Cells were challenged with increasing concentrations of drugs. The treatments were renewed the third day, and left until the seventh day, when β-galactosidase staining was performed as previously describes.

Treatment with cisplatin-JQ1combination

HMC, BR95 and MG06 were treated with 0.5, 1 and 2.5 μM (+)-JQ1, and/or with cisplatin at molar ratio 1:3, while MM98 and MM98R were treated with 0.05, 0.1 and 0.25 μM (+)-JQ1 and/or with cisplatin at molar ratio 1:10. After three days of incubation, a set of experiments was stopped, while drug-free fresh medium was given to a parallel set, and left until the seventh day.

Cellular accumulation: uptake

The whole cell accumulation of the platinum drug, here defined as uptake, was determined from A2780 and HCT 116 cells treated for 4 h with 10 µM cisplatin and complex **10**. Cells were washed three times with PBS, detached from the Petri dishes using 1 ml 0.25 % Trypsin-EDTAand harvested in fresh complete medium. An automatic cell counting device (Countess ®, Life Technologies), was used to measure the cell number and the mean diameter from every cell count. About 5x 10^6 cells were transferred into a glass tube and centrifuged at 1100 rpm for 5' at room temperature. The supernatant was carefully removed by aspiration; in order to limit the cellular loss, about 200 µL of the supernatant were left. Cellular pellets were stored at -80°C until mineralized. After defrosting, all tubes were weighted, in order to retrieve the actual volume from each sample by difference with the empty tube. Then, 70% HNO_3 was added and left 1 h at 60°C in an ultrasonic bath. Before the measurement, the HNO_3 is diluted to 3%. Platinum determination was performed with an ICP-MS. Instrumental settings were optimized in order to yield maximum sensitivity for platinum. For quantitative determination, the most abundant isotopes of platinum and indium (used as internal standard) were measured at *m/z* 195 and 115, respectively.

The amount of Pt found into the cells after the treatment is usually reported as ng of Pt. Thus, if the actual cell number, expressed in terms of 10^6 cells, platinum uptake is expressed by Equation 21:

$$Platinum\ uptake = \frac{ng\ Pt}{10^6\ cells} \qquad (21)$$

Spheroids treatment with drug candidates

Cells were seeded in U-shaped wells of polypropylene plates, put on an orbital mixer (Rotamax 120, Heidolph Instruments) in a CO_2 incubator. After 4 days, BR95 and HCT-116 cells gave 300-400 µm diameter spheroids from an initial seed of 10^4 cells/well and 750 cells/well, respectively.

Before drug challenging, spheroid morphology was assessed and pictures of at least three spheroids *per* conditions were taken at 4X magnification.

Treatment with Pt(IV) complexes

The spheroids (after medium removal by gentle aspiration) were challenged with drug-containing medium (200 µL/well) for 72h, then drug-free medium was replaced twice a week until the control reached the maximal growth or the experiment was stopped. At the same

time points, pictures of at least three spheroids *per* each experimental condition were taken at 4X magnification.

Sequential treatment with cisplatin and JQ1

Cisplatin was given for 24h, and then spheroids were treated with JQ1 for further three days, and re-treated with the same concentrations for further three days. Control experiments were performed in drug-free medium. The 4rd and the 7th days of treatment (corresponding to the 8th and the 11th from cell seeding), pictures of at least three spheroids *per* condition were taken at 4X magnification.

Data analysis

Dimensions of spheroids were assessed using CellProfiler^{TM} 2.0. Spheroids dimensions were confirmed using the native Leica Application Suite software (version 2.0, Leica Microsystems). Data were exported to a spreadsheet and filtered for solidity ≥0.8 and diameter ≥ 150 pixel, converted to μm by means of the microscope calibration. The spheroid volume was calculated from the mean diameter, and reported as fold change with respect to the time zero of the treatment (4th day after cell seeding).

Spheroids validation

Spheroids were fixed in 4% formaldehyde in 0.15 M phosphate buffer (pH 7.2) for 1 hr. Then they were post-fixed in tetroxide osmium for 1 hr in the same buffer. After dehydration in a graded series of ethanol solutions, specimens were embedded in Epon araldite. Semi-thin sections for light microscopy (0.5μm) were cut with an ultramicrotome (Leica Ultracut UCT), using a glass or a diamond knife, and stained with Toluidine blue. At least ten semi-thin sections per treatment were observed under a light microscope (Zeiss, Axioscop 2).

Biochemical assays

BCA

Protein concentration was determined by means of the bicinchoninic acid (BCA) colorimetric assay. This method is based on the reduction of Cu^{2+} to Cu^{1+} by protein in alkaline medium; the chelation of two molecules of BCA with one cuprous ion gives a purple-colored product. The macromolecular structure of protein, the number of peptide bonds and the presence of four particular amino acids (cysteine, cystine, tryptophan and tyrosine) are reported to be responsible for color formation with BCA [186].

Microplate protocol was performed and bovine albumin serum (BSA) was used as standard; series of dilutions of known concentration of BSA were prepared (working range of protein concentration was 20-2000µg/mL). Following manufacturer's instructions, 25µL of each standard or unknown sample were added to 175 µL of reagent in a microplate well. Plate was incubate at 37°C for 30 minutes.

The absorbance at 562 nm was measured at or near 562nm. The concentration of each unknown sample was determined based on the standard curve.

GST activity inhibition

Glutathione-S-transferase activity was recorded as the rate of conjugation of the thiol group of GSH to 1-chloro-2,4-dinitrobenzene (CDNB), that lead to an increase in the absorbance at 340 nm [187]. The assays were performed in the presence of GSH (2 mM) and CDNB (1 mM) in 100 mM phosphate buffer, pH 6.8 at 25 °C in microplate (final volume 200 µL), recording points every 30 s for a total time course of 5 min. The slope of the increase in absorbance at 340 nm ($\Delta Abs_{340}\,min^{-1}$) was determined by linear fitting. The slope of the blank was subtracted from all samples, and GST specific activity was determined by Equation 22:

$$GST\ activity = \frac{\Delta Abs_{340}/min}{0.00503\ \mu M - 1} * \frac{0.2\ mL}{0.02\ mM} * Sample\ dilution = \frac{nmol}{min * mL} \qquad (22)$$

The human GST (from placenta, Sigma-Aldrich) was used as positive control and tested for the enzyme inhibition assay. The enzyme was dissolved in 100 mM phosphate buffer pH 6.8 containing 10% glycerol to obtain a stock solution of 0.25 mg mL^{-1}, and used in final concentration of 0.5 µg mL^{-1}. The mother solutions of cisplatin, EA, **1** and **2** (see previous paragraph) were serially diluted in phosphate buffer and immediately used to test the GST activity.

Residual GST activity from cells was measured after a short treatment (4 h, 24 h) with EA, cisplatin, **1** and **2** at sub-toxic concentrations (near to the IC_{25} values of the compounds at 72h) or after a longer treatment (72h), both with low-toxic concentrations (near to the IC_{25}) and with toxic concentrations (near to the IC_{50} values of the compounds at 72h). After the treatment, cells were washed by PBS, harvested with a cell scraper in 100 mM phosphate buffer containing 2 mM EDTA (pH 7) and sonicated on ice. The cell lysate was immediately used to measure the GST activity as described above or stored at -80°C until measured. GST

activity was normalized on the protein concentration, determined by means of the BCA assay (see previous paragraph).

GSH quantification

Intracellular GSH quantification was based on a fluorometric method. · Briefly, cells were seeded in Petri dishes, and left one day before treatment. After treatment, cells were washed by PBS, trypsinized, counted with an automatic device (Countess, Invitrogen Life Science, S. Giuliano Milanese, Italy), and lysed in 0.1 M phosphate buffer pH 6.8, containing 0.1% Triton®-X-100. Lysates were immediately deproneinized by ultrafiltration (Amicon ultra®, 10 kDa cutoff, Millipore, Milan) in order to exclude endogen GST activity. Filtrates were stored at –80°C until measured. The fluorescent GST substrate monochlorobimane was used at 0.5 mM (saturating condition, K_M =74 μM) to determine sample GSH concentration using 5 μg ml^{-1} human placenta GST at 37°C in 0.1 M phosphate buffer pH 6.8. Fluorescence was read after 1h at 360/405 nm in a 96-well black plate (Nunc, Fisher Scientifics, France). A standard curve of GSH from 0.1 μM to 50 μM was used to extrapolate GSH concentration, then normalised on filtrate volume and cell number to obtain nmol GSH 10^{-6} cell. To obtain the intracellular concentration, the cell volume was calculated from cell diameters given by the cell counter (1.44 pL for MM98 and MM98R, 1.77 pL for BR95 and MG06).

PGE_2 detection

MM98 and BR95 cells were treated for 24 h with concentrations corresponding to the respective IC_{50} values of Co-ASS, Co-EPM and ASA (namely, for MM98: 2 μM Co-ASS, 25 μM Co-EPM and 5 mM ASA; for BR95: 15 μM Co-ASS, 25 μM Co-EPM and 1 mM ASA). At the end of the treatment, arachidonic acid (Cayman Chemicals, Cabru, Arcore) was added to the culture medium up to final concentration 10 μM. After 1 h, an amount of 100 μL of the supernatant was immediately assayed by means of the Human PGE_2 ELISA (Life Technologies, S. Giuliano Milanese, Italy) following manufacturer's instructions.

Apoptosis induction

Cells were treated for 24 h with increasing concentrations of Co-ASS. Caspase-3 activity was measured from the cell lysates using the Caspase-3 fluorometic kit (Cayman Chemicals, Cabru, Arcore) following manufacturer's instructions.

Mitochondrial potential gradient

The mitochondrial potential gradient ($\Delta\psi$) was assayed in living cells in black-walled, clear bottom, tissue culture treated, sterile 96 wells plates (ViewPlate 96 F, Perkin-Elmer, Milan) by means of the mitochondria staining kit (Sigma-Aldrich, Milan), following manufacturer's instructions. This method is based on a fluorescent probe, JC-1 ((5,5',6,6'-tetrachloro-1,1',3,3'-tetraethylbenzimidazolocarbocyanine iodide), that forms red fluorescent aggregates when it concentrates in the mitochondrial matrix (due to the electrochemical potential gradient), whereas it forms green fluorescent monomers dispersed throughout the entire cell after dissipation of the mitochondrial membrane potential. The red fluorescent aggregates were recorded using an excitation wavelength of 525 nm and an emission wavelength of 590 nm; the green fluorescent monomers were recorded using an excitation wavelength of 490 nm and an emission wavelength of 530 nm. Valinomycin was used as positive control.

In order to perform this experiment, cells were challenged with increasing concentration of Co-ASS (ranging from 5 μM to 50 μM and from 0.5 μM to 20 μM for BR95 and MM98, respectively) for 24 h.

Oxidative stress detection

The 2′,7′-dichlorofluorescein diacetate (H_2DCF-DA, Sigma-Aldrich) dye was used to detect reactive oxygen species (ROS) levels. After diffusion into the cell, H_2DCF-DA is deacetylated by cellular esterases to a non-fluorescent cell-impermeable compound, and later oxidized by ROS/NOS into the green fluorescent product 2', 7' –dichlorofluorescin (DCF).

Cells were seeded in white walled, clear bottom, tissue culture treated, sterile 96-well plates the day before treatment, performed in triplicate. Then, cells were treated 2 h with equitoxic concentration of the complexes under study (for MM98: 10 μM Co-ASS, 50 μM Co-EPM**,** 10 mM ASA; for BR95: 30 μM Co-ASS, 50 μM Co-EPM**,** 2 mM ASA. Moreover $CoCl_2$ 500 μM was used as positive cobalt-salt containing control). Parallel tests with 1 h pre-incubation with 1 mM N-acetylcysteine (NAC), a well known anti-oxidant were also performed. At the end of the treatment, the culture medium was replaced by 100 μM of H_2DCF-DA in medium without serum and the plates were incubated for 30 min, in the dark, at 37°C. After 2 washes by PBS, the cells were given fresh medium without serum, having 500 μM of H_2O_2 in positive control wells. Oxidized DCF fluorescence was measured at an excitation wavelength of 485 nm, and an emission wavelength of 535 nm.

NF-kB activity

2×10^6 BR95 cells were plated in Petri dishes and $4x10^6$ MM98 cells were plated in 175 cm^2 flasks 24h before treatment. Then, cells were treated with equitoxic concentration of the complexes under study (for MM98: 10 μM Co-ASS, 50 μM Co-EPM**,** 10 mM ASA; for BR95: 30 μM Co-ASS, 50 μM Co-EPM**,** 2 mM ASA. Then, cells were washed, trypsinized, and nuclear extracts were obtained following the manufacturer's instruction of a commercial kit (NE-PER®, Pierce, Thermo Fisher). Protein content was quantified by means of the BCA assay (Pierce, Thermo Fisher). NF-κB activity was tested on 5 μg of nuclear extracts using a chemiluminescent assay kit (NF kappa B p65 Transcription Factor Assay Kit, Pierce, Thermo Fisher), following manufacturer's instructions. Briefly, the kit contains two streptavidin-coated 96-well plates with the bound biotinylated-consensus sequence that can be bound only by the active forms of the target transcription factor. The captured active transcription factor is then detected with a specific primary (NF-κB p65) and a secondary HRP conjugated antibody. The nuclear extract of HeLa cells TNF- α activated was tested as positive control, while the competitor consensus DNA duplex was added in some wells as negative control (specific binding). A chemiluminescent substrate was then added to the wells, allowing quantitative measurement with the plate reader.

Statistical analysis

Statistical analysis was performed by means of the *t*-test or one-way ANOVA. The statistic significance values (*p*) are referred to control values (*****$p < 0.05$, ******$p < 0.01$, *******$p < 0.001$). Data are expressed as the means of ± standard deviation of at least 3 replicates.

Results and discussion

Generation of multicellular tumor spheroids (MCTS): optimization of microplate-based method

MCTS represent a reliable model in the prospective of screening of drug candidates against MPM, since it has been previously reported that MPM cells resist anoikis as quiescent pluricellular aggregates [188] and that tumor cells obtained from pleural fluid of MPM patient' present well-organized aggregates like spheroids [189].

MPM spheroids have been previously generated, as: *i)* tumor fragment spheroids that grew in agar-coated plates [190] and *ii)* small spheroids (d = 100 μm) that grew in poly-HEMA coated plates within and a short time of culture [191].

In order to design our microplate-based method, we combined the rational of spinner flask and rotation procedures with the prerequisite of absence of cell attachment to the substrate.
Since the hydrophobic surface of polypropylene does not allow cell adhesion and many sterile polypropylene plates are commercially available, we experimented polypropylene tubes and plates in order to develop a plastics coating free method to obtain MCTS.

We started with using sterile conical tubes made of polypropylene; 0,2 ml (PCR tube), 1,5 ml, 2 ml conical tubes and 15 ml both conical and round-bottom tubes. 500x 10^3 cell ml^{-1} were seeded in tubes of and spun 10 min at 1000 *x g* , according to Ivascu's method [137], then placed in a CO_2 humidified incubator. We obtained compact spheroids from the MM98 and MM98R sarcomatoid MPM cell lines, MG06 mixed phenotype and BR95 epithelioid cell lines.
Then, we scaled-up the procedure seeding the same number of cells in 96-wells PCR polypropylene plates sterilised under UV light, sealed with an adhesive film (BrathSela, Greiner BioOne). MM98 and MM98R gave compact spheroid within 24h, but many satellite objects could be observed, and sometimes spheroids attached to the bottom of the well, starting surface colonization. Furthermore, the small volume of medium was reduced due to massive evaporation, as any lid could not be adapted to the plate. We also tried to use Matrigel® to allow cell aggregation, according to the method reported by Ivascu et al. [137].

Unfortunately, we obtained a flat and floating dish which entrapped cells but did not evolved to a spheroid-like architecture.

After the failure of the firsts approaches, we tested a sterile low cell binding 96-wells plate, round bottomed, with lid, sold for Embryoid Body Formation. Also this attempt reveled unsuccessful, since MM98 spheroids managed to colonized the surface of the well again.

Eventually, we tried cheaper polypropylene sterile microplates, U-bottom, with lids. Apart from MPM cell lines, in this step we introduced other cell lines, previously reported to generate spheroids, as HCT-116, or cell aggregates in some conditions, as A549, MCF-7 and A2780. In addition, we introduced the non-tumor HMC cell line.
As the previous procedure, we spun cells 10 min at 1000 *x g*. The centrifugation protocol gave optimal results with MG06 and BR95 only, whereas MM98 adhered on the well's surface. We hypothesized that centrifugation was not the optimal method to allow cellular aggregation so, we moved to a milder method: thus, we put the microplates on an orbital mixer, with continuous shaking at 200 rpm in a CO_2 incubator. This method was optimal both for MG06 and BR95, while unfortunately MM98, MM98R, A549 and MCF-7 continued to colonize the well's bottom surface and A2780 formed simply aggregates, as shown in Figure 50.

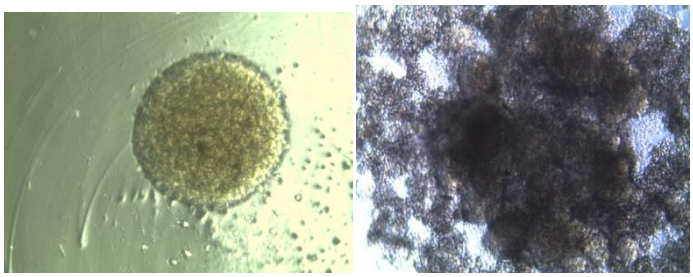

FIGURE 50. Image of MCTS of BR95 cell lines (left), and A2780 cellular aggregates (right). In BR95 spheroids, a outer translucent shell is observed, corresponding to proliferant cells.

However, orbital shaking let us obtain spheroids even from HCT-116.

Then, we performed growth kinetics to assess if spheroids able to grow in an exponential manner [192] [193].

In order to evaluate the relationship between the cell number per well and the propensity to generate spheroids, we seeded an increasing number of cells of each line. Medium was carefully replaced twice a week until compact spheroids were observed, or until the growth plateau was reached.

We toke in account only spheroids showing at least a diameter of 400 mm, that is the critical size to obtain a necrotic core and a gradient of proliferating cells had formed.
As depicted in Figure 51, only HCT-116 and BR95 cell lines gave growing spheroids.

HCT-116 cells gave 300-400 μm diameter spheroids after an initial seed of 750 cells/well, as previously reported [135], while as far as BR95 cell lines concerned it occurred after an initial seed of 10000 cells/well.
It should be noted that a minimal time lapse (at least 4-5 days) is needed to obtain mature spheroids, in order to allow cells aggregation and compaction under agitation.

MM98 and MM98R continued to compact until about 5^{th}-6^{th} day decreasing their dimension. We then tried to seed them in the presence of 20% FBS, but they were not actively growing.
A some growth was observed in MG06 cells, but too limited drug screening purposes.
The non-tumor HMC cells formed non-proliferant spheroids, according to their non-malignant nature.

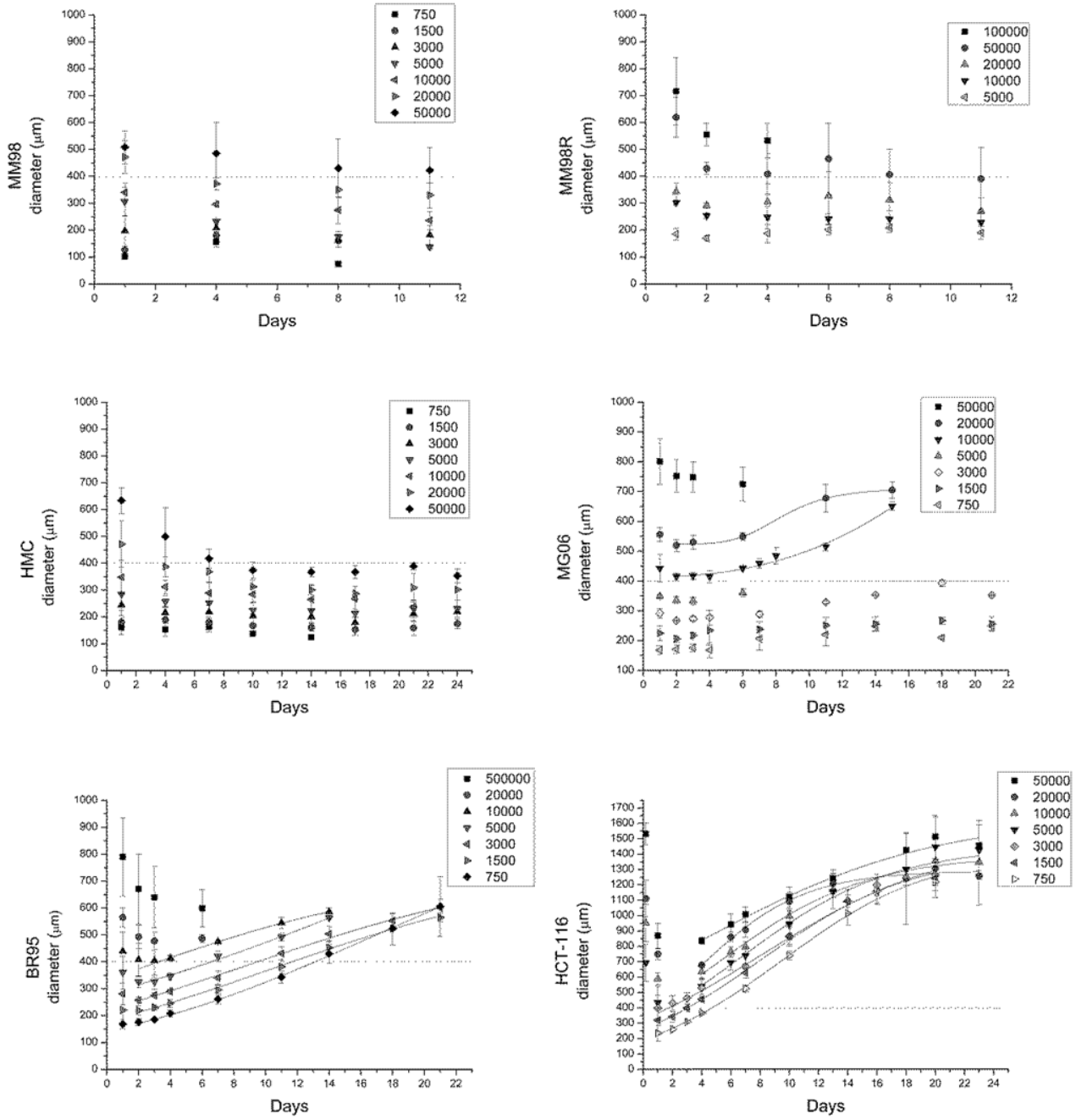

FIGURE 51. Growth kinetics of MM98, MM98R, HMC, MG06, BR95 and HCT-116 cells until until the growth plateau was reached.

For sake of clarity, Table 4 shows the overall characteristics and experimental conditions of cell lines investigated in order to generate MTCS:

Cell line	**Type**	**Spheroid Type**	**Growth**	**Medium**	**FBS (10%)**
BR95	MPM (epitheliod)	non-adherent Spheroids	exponential	Ham's F10	10
MG06	MPM (Epitheliod/Mixed)	non-adherent Spheroids	exponential	Ham's F10	10
MM98	MPM (Sarcomatoid)	plate-adherent Spheroids	stable dimensions	DMEM	20
MM98	MPM (Sarcomatoid)	plate-adherent Spheroids	decreasing dimensions	DMEM	10
MM98R	MPM (Sarcomatoid)	plate-adherent Spheroids	stable dimensions	DMEM	20
MM98R	MPM (Sarcomatoid)	plate-adherent Spheroids	decreasing dimensions	DMEM	10
HMC	Mesothelium	non-adherent Spheroids	stable dimensions	Ham's F10	10
HCT-116	Human colon carcinoma	non-adherent Spheroids	exponential	McCoy's 5A	10
MCF-7	Human breast adenocarcinoma	cell aggregates	/	EMEM+NEAA	10
A2780	Human ovarian carcinoma	cell aggregates	/	RPMI 1640	10
A549	Human lung carcinoma	cell aggregates	/	RPMI 1640	10

TABLE 4. Morphology and growth profile are listed for each cell lines investigated to assess their propensity to generate proliferant MCTS.

In the perspective to use MTCS as tools for antitumor drugs screening, we thus expressed growth kinetics of BR95 and HCT-116 MTCS as a function of the spheroid mean volume, similarly to the *in vivo* evaluation of tumor mass regression after antineoplastic treatment (Figure 52).

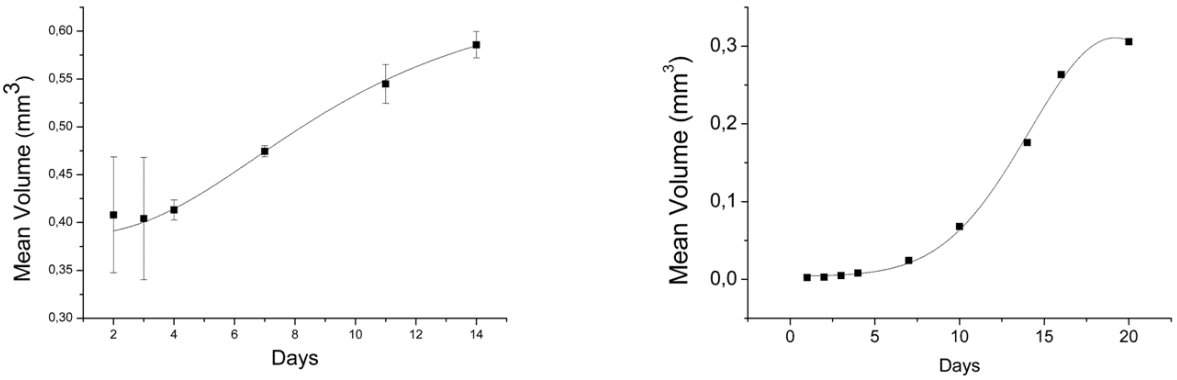

FIGURE 52. Growth kinetics of BR95 (left) and HCT-116 (right) cells, expressed as a function of volume. The growth plateau was reached after about 15 days and 20 days, respectively.

BR95 morphology was assessed by means toluidine blue staining of spheroid section, which confirm the presence of a necrotic core, as shown in Figure 53.

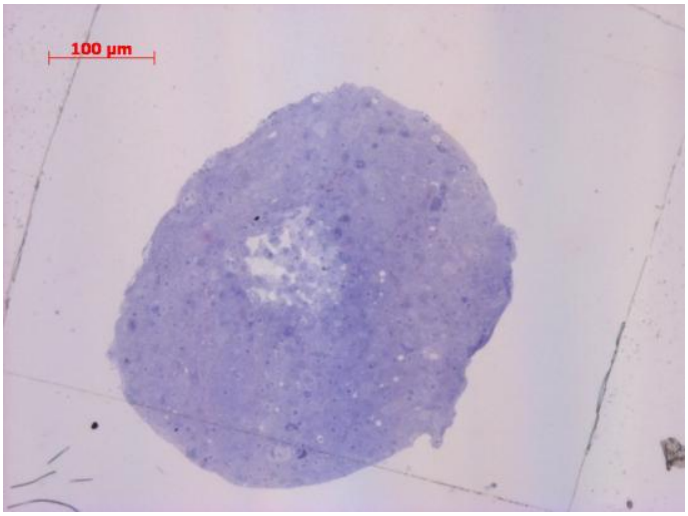

FIGURE 53. Toluidine blue staining of BR95 spheroid section after 4 days from seeding.

Pt(IV) complexes designed to circumvent cisplatin chemoresistance due to GSH/ GST system

As previously described**,** MPM is a malignancy characterized by strong intrinsic chemoresistance associated to anti-oxidant enzymes and GSH metabolism.

The conjugation between GSH and cisplatin occurs spontaneously but can also be mediated by the enzyme glutathione –S-transferase-*pi* (GST-*pi*). The conjugate $(NH_3)_2Pt\text{-}(SG)_2$ is extruded by cells via GS-X pumps, a member of the multi drug resistance-associated protein (MRP) family.

GST is also involved in the regulation of survival / cell death by interacting with the protein JNK (c-Jun N-terminal kinase) [194]. Therefore, by inhibiting GST could reduce both its detoxifying action, both pro-apoptotic signal to activate JNK.

Moreover GST enzymes, responsible for cisplatin conjugation with GSH, results in some circumstances overexpressed in MPM [195]. Therefore, we focused in the study of molecules able to bypass this chemoresistance mechanism and at the same time to exert a cytotoxic effect on tumor cells. We tried to reach this goal by means of two strategies, that will be discussed herafter.

Bi-functional platinum complexes as GST inhibitors

Interestingly, studies on human bladder cancer cells showed that the *in vitro* cisplatin resistance is partially overcome by buthionine sulfoximine (BSO) treatment, which counteracts the enzyme involved in GSH biosynthesis, as well as by ethacrynic acid (EA), a diuretic drugs, that inhibits GST [196].

So, our first study was focused on the investigation of complex **1**, *cis,cis,trans*-diamminodichloridobis(ethacrynate)platinum(IV); that is a Pt(IV) complex having cisplatin as precursor and functionalized with two molecules of (EA) in order to join cytotoxic activity of Pt-based drugs with lowered chemoresistance. Complex **1** was previously synthesized by Dyson and co-workers, called as ethacraplatin, that reported that it is strong GST inhibitor *per se* [197].

In order to better understand the role of EA on the pharmacological effects of Pt-drugs, the pharmacological properties of **1** were compared with those of a Pt(II), the *cis*-diamminobis(ethacrynate)platinum(II) or complex **2**. We assumed that both complex **1** (after

reduction and hydrolysis) and **2** (after only hydrolysis) lead to the formation of the same active molecule $[Pt(H_2O_2)_2(NH_3)_2]^{2+}$.

First of all, **1** and **2** were tested on the MPM cancer cell lines; then the antiproliferative effects of **1** and **2** bi-functional complexes were compared with the respective individual precursors. We observed that compound **1** was more active than **2** and it seemed to overcome the resistance to cisplatin and that. However, **1** and **2** complexes showed a lower activity (i.e, higher IC_{50} values) compared to the reference compound, cisplatin, that showed the best performance. In addition, cells were challenged with a combination of cisplatin and EA (given simultaneously in a molar ratio 1:2), in order to mimic the biological effect of the two bioactive constituents after their release. Interestingly, we noticed that the resistant factor (RF, i.e. IC_{50} MM98R) / (IC_{50} MM98) obtained for **2** was identical to that obtained for the co-treatment with the mixture of cisplatin and EA. These results suggest that the bi-functional molecule **2** explicates its activity merely releasing the two EA moieties and by generating the aquo complexes (Table 5).

	Cisplatin	**Carboplatin**	**1**	**2**	**EA**	**Cisplatin (+ 2 EA)**
MG06	4.1±1.5	40.0±8.0	17.6±2.3	26.9±6.3	47.5±9.6	7.3±1.6
BR95	6.2±0.9	33.1±7.6	10.9±1.2	29.4±7.6	33.6±6.6	7.6±3.3
MM98	3.2±1.0	57.5±11.5	11.8±3.5	20.7±6.5	45.8±6.5	4.8±0.1
MM98R	19.4±2.8	70.8±14.9	17.3±3.4	60.5±8.2	69.4±11.9	13.7±4.3
RF	6.1	1.2	1.5	2.9	1.5	2.9

TABLE 5. IC50 (μM) values calculated after 72 h of treatment, are listed.
Resistance factor (*RF)* = (IC_{50} MM98R) / (IC_{50} MM98).

Assuming that the Pt(IV) complex is reduced to Pt(II) within the cell and releases a molecule of cisplatin and two equivalents of EA, the pharmacological effect of **1** was compared with that of the association cisplatin + EA. On the contrary, the complex **2** was compared with the combination of carboplatin + EA, as it has been assumed that the leaving groups of **2** and carboplatin possess a similar hydrolysis kinetics. Thus, compounds **1** and **2** were considered as an intra-molecular fixed-dose-ratio combination of their building blocks: two equivalents of EA and cisplatin for **1** and two equivalents of EA and carboplatin for **2.**

Any combination did not show a synergistic effect (CI > 1), as pointed out in Figure 54. It should be noted that CI profile of the co-treatment with cisplatin and EA coincides with that

of **2**. This evidence, in according with their RF, supports our hypothesis that this bi-functional molecule exerts its activity by means of the simple release of two EA moieties, generating the active metabolite $[Pt(NH_3)_2(H_2O)_2]^{2+}$. Complex **1** gave the highest CI value. All this body of evidence indicates that compound **1** behaves differently than **2** and so, it should acts as a GST inhibitor *per se*.

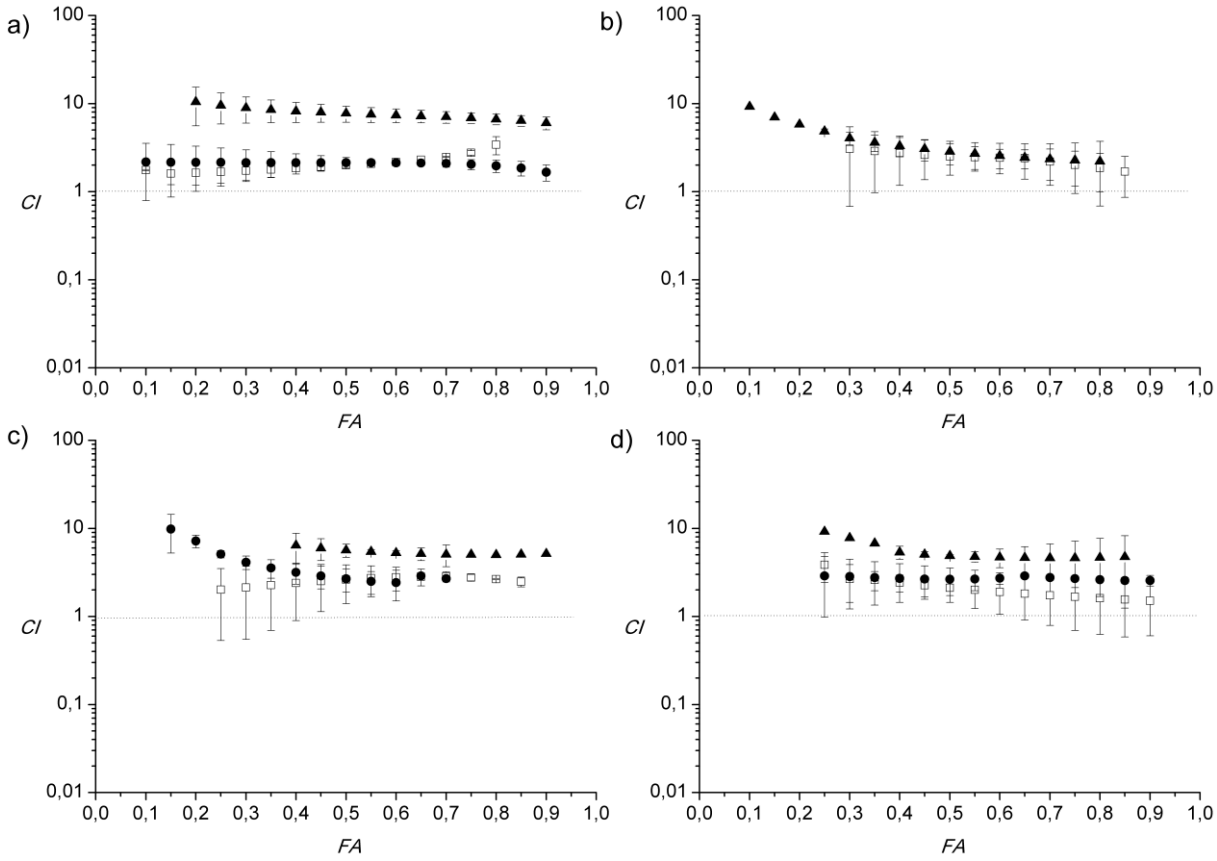

FIGURE 54. Combination Index (*CI*) vs Fraction affected (*FA*) plots for the combination of EA + cisplatin 72 h (white squares), **1** vs cisplatin and EA (black trangles), **2** vs. EA and carboplatin (black circles, except for MM98R). a) MM98; b) MM98R; c) BR95; d) MG06. The dotted line at *CI*=1 (additivity) stands for the limit between antagonism (over 1) and synergism (below 1).

Consequently, we determined the residual GST activity following candidate drugs exposure after 4, 24 and 72 h CT (drugs given at sub-lethal concentrations corresponding to their IC_{25}) and after 72 h CT of drug given at concentrations corresponding to their IC_{50}. Surprisingly, both bi-functional complexes and the cisplatin and EA combination did not result in the inhibition of cellular GST, as listed in Table 6 and Table 7. Moreover, GST activity seemed not to be related to acquired resistance since MM98 and MM98R share the same basal GST levels, which did not change after treatment.

	NT	EA	Cisplatin	1	2
4 h treatment					
MG06	120±15	111±11	124±13	104±11	106±15
BR95	98±9	91±13	98±20	107±39	83±11
MM98	40±13	37±9	46±13	44±9	44±9
MM98R	53±9	41±9	51±9	52±11	40±9
24h treatment					
MG06	107±49	110±59	130±55	115±46	129±32
BR95	119±32	135±40	119±9	146±46	114±24
MM98	80±31	65±26	74±17	53±14	51±9
MM98R	58±20	61±12	53±13	67±15	74±16
72 h treatment					
MG06	79±8	77±6	72±5	75±10	93±9
BR95	89±11	95±12	101±8	89±11	110±16
MM98	78±1	67±9	73±11	81±8	75±8
MM98R	65±11	69±7	58±10	75±14	64±6

TABLE 6. Residual specific GST activity (μmol min^{-1} g^{-1}) from from MG06, BR95, MM98 and MM98R cells treated for 4, 24 and 72 h with concentrations corresponding to their IC_{25}: 20 μM EA, 5 μM **1**, 10 μM **2**, 1 μM cisplatin (5 μM for MM98R). Data are normalized upon protein concentration and are not statistically different from the control (one-way ANOVA, $p > 0.05$).

72 h treatment	NT	EA	Cisplatin	1	2
MG06	81±10	105±31	88±30	82±11	107±34
BR95	77±18	75±1	77±4	77±13	81±7
MM98	47±6	47±6	25±2	66±21	68±18
MM98R	48±8	55±15	38±3	36±2	33±1

TABLE 7. GST specific activity (μmol min^{-1} g^{-1}) from cells after exposure to complexes. Residual specific GST activity from MG06, BR95, MM98 and MM98R cells treated for 72 h with concentrations corresponding to their IC_{50}: 20 μM EA, 5 μM **1**, 10 μM **2**, 1 μM cisplatin (5 μM for MM98R). Data are normalized upon protein concentration and are not statistically different (one-way ANOVA, $p > 0.05$), except for MM98 treated with cisplatin ($p < 0.005$).

The complexes were then tested to assess their ability to inhibit the purified enzyme. In accordance with data reported by Dyson et al., complex **1** exhibited a strong GST inhibition, much higher than that of **2**, whereas cisplatin showed no substantial GST inhibition (Figure 55). Complex **1** was as active as EA in GST inhibition , supporting our hypothesis that this bi-functional complex might be regarded as simple intracellular combination of a platinum(II) complex and EA.

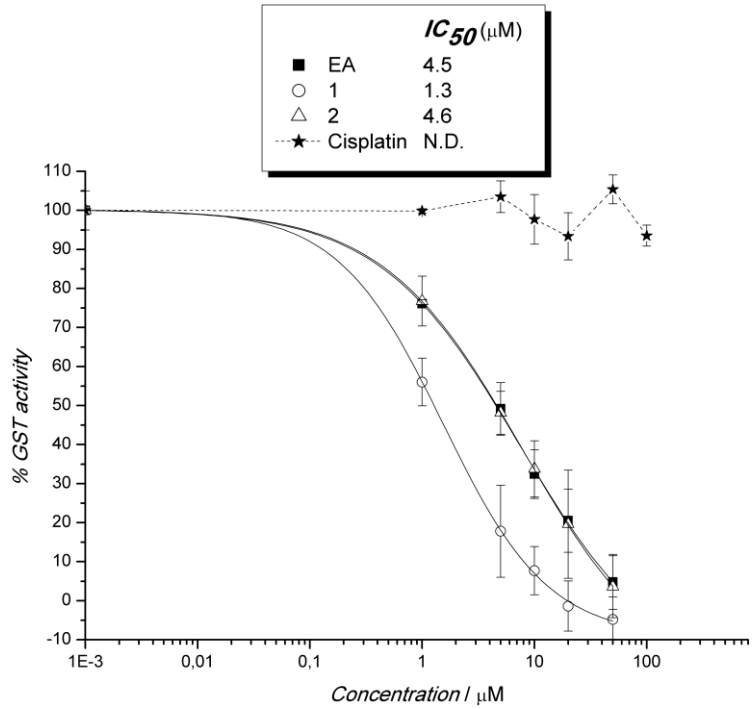

FIGURE 55. Residual % GST activity of the purified enzyme in presence of increasing concentrations of EA, **1**, **2**, and the relative sigmoidal curves (Hill equation) for the extrapolation of the IC_{50} values (in terms of enzyme inhibition). For cisplatin a dotted-line plot is reported, indicating no GST inhibition.

Previous studies showed that EA increases GSH levels in some tumor cell lines [194]. It was reported that the conjugate ethacrynic acid-GSH (EA-SG) is a sevenfold more potent GST inhibitor than free EA. Whereas EA induces GST inhibition trough a non-competitive way, EA-SG inhibits GSH by competitive mechanism [198]. In other words, the inhibition of GST induced by EA-SG should be overcome through a raise in GSH intracellular concentration. Therefore, we detected intracellular levels of GSH.

We observed a jump in intracellular levels of GSH after platinum complexes exposure, except for the epitheliod cell lines challenged with cisplatin. In addition, the cisplatin resistant cell line MM98R showed the highest raise of intracellular GSH (Figure 56).Thus, we deduced that this cellular phenomenon is responsible for the antagonist effect of platinum complexes, because counteracts their pharmacological action.

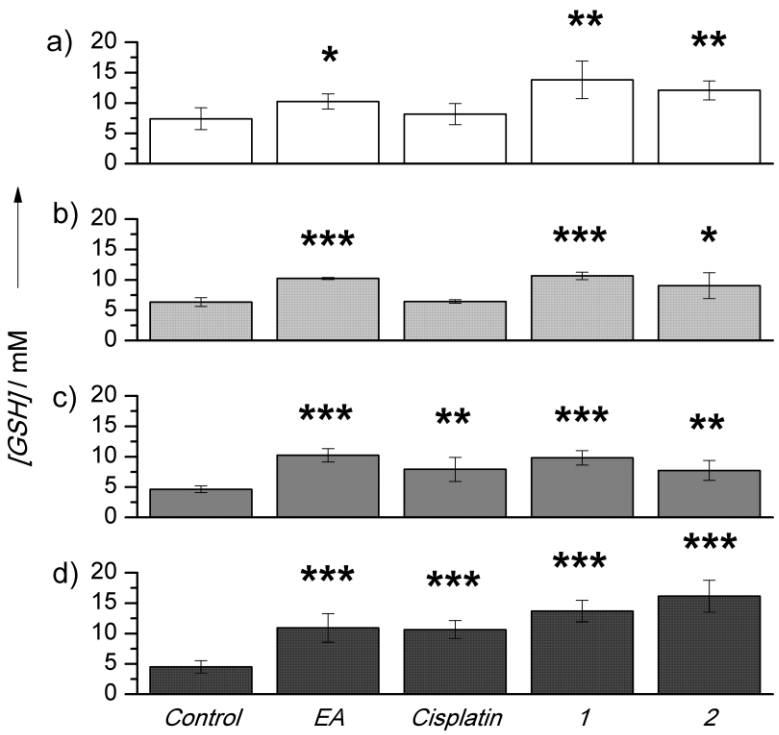

FIGURE 56. Intracellular GSH levels from a) MG06, b) BR95, c) MM98 and d) MM98R cell lines treated for 72h with 20 mM EA, 5 mM **1**, 10 mM **2**, 1 mM cisplatin (5 mM MM98R). The intracellular levels of GSH determined and normalized to cell volume, resulting in a basal value of around 5 mM. Statistical analysis was performed by unpaired *t*-test (with respect to control: **p* < 0.05, ***p* < 0.01, ****p* < 0.001.

In conclusion, the attempt to decrease MPM intrinsic resistance targeting GST with EA-bi-functional conjugates is not a useful strategy for chemotherapy [199].

Pt(IV) analogues of picoplatin

The second strategy aimed to circumvent cisplatin resistance started from a different chemical rationale.

It is well known that picoplatin, or *cis*-amminedichlorido(2-methylpyridine)platinum(II), is able to bypass GSH-related cisplatin resistance because it is composed of a bulky 2-methylpyrimidine as a carrier group: the steric hindrance created by this substituent is able to hinder the conjugation of GSH with the metal complex. On the other hand, it is generally accepted that the reduction of Pt(IV) complexes can be carried out by intracellular reductants as GSH. Pt(IV) compounds are believed to be reduced to their active Pt(II) metabolites, which, in turn, will be activated by hydrolysis and bind DNA[200] [201]. Thus, the insertion of the picoplatin square-planar structure in a Pt(IV) octahedral scaffold should give an ideal pro-drug candidate.

Furthermore, it is important to recall that picoplatin entered in a phase II trial as a second-line therapy in mesothelioma, showing a manageable tolerability profile [202].

Thus, a series of complex Pt (IV), having axial carboxilate chains of increasing length and picoplatin as common precursor, was investigated the four cell lines of MPM, on the cisplatin-sensitive ovarian A2780 cell line and on a non-malignant cell lines (HMC) and their antiproliferative activity was compared. Unfortunately, we could not challenge HMC cells with picoplatin.

As showed in Table 8, Pt(IV) congeners of picoplatin showed good activity on both ovarian and MPM cell lines. All of them were more active than picoplatin; **3** was the least potent molecule whereas **5** had similar activity than cisplatin. We observed that the longer the axial chain is, the more active and selective the Pt(IV) complex is, confirming the relationship between activity and length reported in literature. Indeed, previous studies showed a strict correlation between antiproliferative activity and length of the carbon chain was observed for other Pt(IV) complexes *in vitro* [114] [115] and *in vivo* tumor models [203].

According to our hypothesis, these compounds bypassed the resistance to cisplatin, as showed the much lower resistance factor (RF) values.

As stated above, the cisplatin-resistant cell line MM9R shows a higher increase in intracellular GSH (when treated with platinum derivatives at sub-lethal concentrations) with respect to the wild counterpart MM98, event that could partially explain the acquired resistance. For this reason, the observed low RF for compounds **3**-**5** may be related to a generally low inactivation of Pt(IV) complexes under investigation.

	Cisplatin	**Picoplatin**	**3**	**4**	**5**
A2780	1.2 ± 0.4	1.6 ± 0.3	7.4 ± 1.9	2.4 ± 1.3	0.40 ± 0.04
BR95	6.2 ± 0.9	42.9 ± 4.7	17.5 ± 4.9	15.2 ± 2.1	5.6 ± 0.2
MG06	4.1 ± 1.5	42.8 ± 2.6	13.2 ± 4	11.1 ± 0.6	7.2 ± 0.8
MM98	3.2 ± 1.0	30.2 ± 4.6	12.7 ± 3	10.1 ± 2.6	5.6 ± 0.5
MM98R	19.4 ± 2.8	34.4 ± 4.7	12.1 ± 1.9	13.2 ± 2.3	9.4 ± 0.9
HMC	6.7 ± 1.2	/	22.8 ± 2.0	21.3 ± 1.9	18.9 ± 3.1
RF[a]	6.1	/	1.0	1.3	1.7
SI[b]	1.5	/	1.6	1.8	3.1

TABLE 8. IC_{50} values calculated after 72 h continuous treatment.
[a] Resistance factor (RF)= IC50 (MM98R)/IC50 (MM98).
[b] Selectivity Index (SI)= IC50 (HMC)/ mean IC50 (BR95, MG06, MM98).

Reduction of complexes **3-5** by GSH was verified. The formation of the corresponding Pt(II) counterparts has nearly similar $t_{½}$, ranging from 25 and 32 min [204], and became almost complete after 4 h, supporting the assumption of the "activation by reduction" mechanism.

Based on these findings, we could declare that these Pt(IV) analogues of picoplatin are quite promising candidates for MPM treatment.

Pt(IV) axial dicarboxylate complexes as anticancer drug candidates

Pt(IV) complexes with linear carboxylate chains as axial ligands

We studied a series of dicarboxylate-platinum(IV) complexes, sharing the same carrier and equatorial leaving groups as cisplatin, and bearing carboxylato ligands of different length in axial position. The investigated complexes were: **6** (*cis,cis,trans*-diaminedichlorobisacetate-platinum(IV)), **7** (*cis, cis, trans*-diaminedichlorobisbutanoate-platinum(IV)), **8** (*trans,cis, cis*-diaminedichlorobisesanoate-platinum(IV)), **9** (*cis, cis, trans*-diaminedichlorobisoctanoate-platinum(IV)).

Assuming the *activation by reduction* theory, these Pt(IV) complexes series have to be regarded as pro-drugs of cisplatin, reduced by biological antioxidants in the intracellular compartments.

In order to check their anticancer activity against MPM, complexes **6-9** were tested both on the four MPM cell lines and on the healthy human mesothelial cells, as outlined in Table 9. Moreover, their antiproliferative ability exerted against MPM was compared to that observed against other cell lines, representative of most common tumoral forms, namely: A2780 (ovarian), HCT-116 (colon), A549 (lung) and MCF-7 (breast).

As expected, A2780 cells resulted the most responsive to cisplatin, whereas the MPM cell lines proved to be the less sensitive ones, confirming their intrinsic chemoresistance.

A2780 cells appeared the most sensitive cells to complexes **6-9,** in parallel with the responsiveness to their Pt(II) cognate, *i.e.* cisplatin.

Complex **6** appeared dramatically ineffective on MPM, as it was around 20 times less active than cisplatin.

At a glance, complex **7** was as nearly potent as cisplatin, except for epithelioid and mixed MPM phenotypes and mesothelial cells, that were less sensitive than sarcomatoid cells.

Complex **8** resulted more active than cisplatin on all cell lines, being the former around one and two orders of magnitude more active than the latter in non-MPM and MPM cells, respectively.

Complex **9** showed the best performance, revealing an activity around three orders of magnitude higher than cisplatin.

Interestingly, the longer the axial chain is, more the cisplatin cross-resistance is bypassed, reaching a drop of cross-resistance (RF = 1.3) for complex **9**.

Intriguingly, both **8** and **9** acted in a selective way against malignant cells, as pointed out by selective index (SI, *i.e.*, the ratio between IC50 (HMC) and the IC50 on the tumor MPM cell line) value, ranging between 3-6.

	Cisplatin	**6**	**7**	**8**	**9**
A2780	$0.5\pm0.1\times10^{-6}$	$12.1\pm5.2\times10^{-6}$	$0.5\pm0.1\times10^{-6}$	$1.5\pm0.7\times10^{-8}$	$2.3\pm0.6\times10^{-9}$
HCT-116	$2.3\pm0.3\times10^{-6}$	$55.3\pm1.7\times10^{-6}$	$1.8\pm0.3\times10^{-6}$	$4.2\pm1.0\times10^{-8}$	$9.0\pm0.5\times10^{-9}$
A549	$3.8\pm0.7\times10^{-6}$	$78.0\pm17.7\times10^{-6}$	$5.6\pm3.2\times10^{-6}$	$20.7\pm0.8\times10^{-8}$	$14.7\pm3.2\times10^{-9}$
MCF-7	$6.5\pm0.9\times10^{-6}$	$>100\times10^{-6}$	$8.0\pm1.9\times10^{-6}$	$33.5\pm16.3\times10^{-8}$	$16.5\pm4.8\times10^{-9}$
HMC	$6.7\pm1.2\times10^{-6}$	$>100\times10^{-6}$	$38.6\pm8.8\times10^{-6}$	$2.7\pm0.4\times10^{-6}$	$91.7\pm2.8\times10^{-9}$
BR95	$6.2\pm0.9\times10^{-6}$ (1.1)	$>100\times10^{-6}$ (-)	$34.1\pm6.0\times10^{-6}$ (1.1)	$0.9\pm0.1\times10^{-6}$ (2.9)	$64.3\pm19.2\times10^{-9}$ (2.0)
MG06	$4.1\pm1.5\times10^{-6}$ (1.6)	$>100\times10^{-6}$ (-)	$23.1\pm6.2\times10^{-6}$ (1.7)	$0.9\pm0.2\times10^{-6}$ (3.1)	$41.3\pm11.0\times10^{-9}$ (2.6)
MM98	$3.2\pm1.0\times10^{-6}$ (2.1)	$>100\times10^{-6}$ (-)	$7.4\pm2.3\times10^{-6}$ (5.2)	$0.3\pm0.1\times10^{-6}$ (11.0)	$17.0\pm3.9\times10^{-9}$ (5.9)
MM98R	$19.4\pm2.8\times10^{-6}$ (-)	$>100\times10^{-6}$ (-)	$18.7\pm0.5\times10^{-6}$ (2.1)	$0.8\pm0.1\times10^{-6}$ (3.5)	$22.0\pm3.3\times10^{-9}$ (5.7)
[a]RF	6.1	-	2.5	3.2	1.3

TABLE 9. IC_{50} values (M) obtained after 72 h CT.
Data in brackets reports the selectivity index, SI, *i.e.*, the ratio between IC50 (HMC) and the IC50 on the tumor MPM cell line.
[a] Resistance Factor, RF = IC50 MM98R / IC50 MM98.

The prolonged antitumoral effects of complexes **6-9**, compared with that of cisplatin, the reference compound, was investigated. Since the microplate-based (2D) methods are limited by cellular confluence to 3 days of treatment, we employed *in vitro* MCTS (obtained with the method described in the previous section) of BR95 and HCT-116 cells.

Spheroids were challenged for 72 h (3 days), the drug was removed and fresh medium was added (recovery), replacing it twice a week. We adopted this procedure for two reason: *i*) first, by monitoring the changes in their volume it is possible to discriminate more accurately if the compounds act as cytostatic (stabilizing spheroids volume) or cytotoxic (leading to volume decrease); *ii)* second, drug removal mimics the *in vivo* blood clearance and so, the recovery period allow to establish whether the spheroids resume proliferation. It should be noted that a similarity exists between the *in vitro* experimental approach that we carried out and the *in vivo* procedure that assess tumor regression, which measure the change in the tumor mass volume for prolonged times.

First of all, we challenged MCTS with cisplatin. Spheroids were followed *in vitro* up to one month for BR95 (Figure 57a), whereas up to 10 days for HCT-116 cells (Figure 57b).

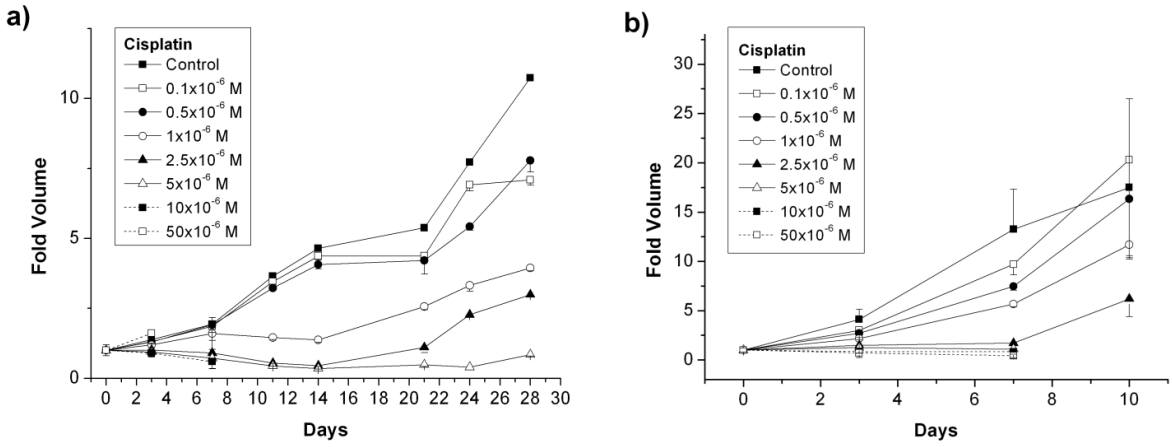

FIGURE 57. a) BR95 spheroids; b) HCT 116 spheroids. Spheroids were treated with increasing concentrations of cisplatin (reported in the legends) from day 0 to day 3, then the recovery lasted to the maximal control growth. The time zero volume was used for normalization of the fold increase.

In the initial phase of recovery (from 3 to 7 days), we observed that low concentration was initially stopped the growth, which restarted after 14 days and 7 days for BR95 and HCT 116 spheroids, respectively. The growth was arrested suggesting that cisplatin elicited a cytostatic effect, with concentration similar to the IC_{50} values. Higher concentrations exerted a cytotoxic effect, leading to the loss of spheroids.

Then, platinum(IV) complexes were tested on BR95 spheroids only in order to check their activity in MPM.

Complexes **6** and **7** showed a behavior comparable to that of cisplatin, since the growth was curbed at low concentration (Figure 58a, 58b) . Lastly, both **8** and **9** showed the most promising results, since also at low concentration cytotoxic effect was observed (leading to a drop of spheroid volume) (Figure 58c, 58d). Moreover, high concentration sometimes induced an initial swelling (due to loss of intracellular contacts and consequently, spheroids integrity), followed by the spheroid disintegration.

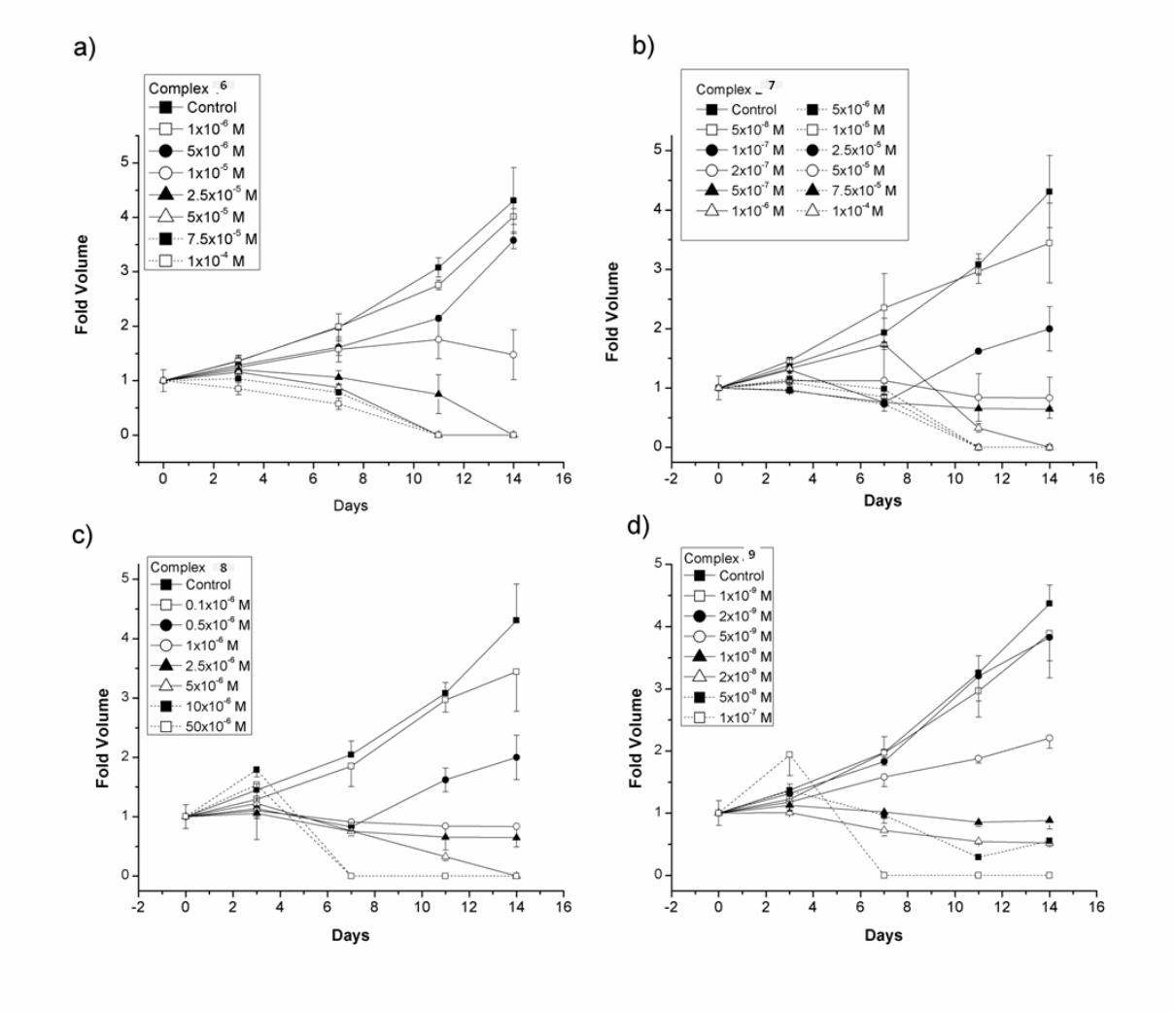

FIGURE 58. BR95 spheroids treated with increasing concentrations (reported in the legends)of complexes **6**, **7**, **8** and **9** from day 0 to day 3, then the recovery lasted to the maximal control growth. The time zero volume was used for normalization of the fold increase.

Since the lipophilicity of the compounds increased in the following order: cisplatin < **6** < **7** < **8** < **9** (Table 9) the antiproliferative activity of Pt(IV) complexes correlates with their lipophilicity.

Compound	**t_R (min)**	**LogK'$_{90}$**	**LogP$_{o/w}$**	**Solubility (mM)**
6	2.598	-0.404	-1.922	0.598 ± 0.008
7	2.732	-0.331	0.388	0.138 ± 0.048
8	3.044	0.198	1.142	0.002 ± 0.001
9	3.744	0.004	4.1425 (from LogK'$_{90}$)	< 0.00008

TABLE 9. Lipophilicity and water solubility. Data are means ± standard deviation of at least 3 replicates. The logP$_{o/w}$ values and logK'$_{90}$ values of complexes **6**-**8** were correlated with a linear equation that was used to calculated the logP$_{o/w}$ values of compound 9 starting from its logK'$_{90}$.

Pt(IV) complexes with aromatic carboxylate as axial ligands

It was reported that the introduction of aryl groups as axial ligands can improve the intracellular uptake of the compounds, since they confer higher lipophilicity and facilitate the transport across the cell membrane [200].

Based of this rationale, we studied two series of Pt(IV) complexes, with different carrier groups. Both series had aromatic carboxylate ligands of increasing length (benzoate, phenyl-acetate and dihydrocinnamate).

The first series included Pt(IV) complexes sharing cisplatin as Pt(II) common precursor, namely complex **10** (*trans,cis,cis*-[$Pt(C_6H_5COO)_2Cl_2(NH_3)_2$]), **11** (*trans,cis,cis*-[$Pt(C_6H_5CH_2COO)_2Cl_2(NH_3)_2$]) and **12 (***trans,cis,cis*-[$Pt(C_6H_5(CH_2)_2COO)_2Cl_2(NH_3)_2$])

On the contrary, the second series consists of Pt(IV) complexes bearing 1R,2R-diaminecyclohexane (1R,2R-DACH) as carrier group, that is exactly the same of oxaliplatin, namely **13** (*cis, trans, cis*-(1R,2R-DACH)[$Pt(C_6H_5COO)_2Cl_2$]), **14** (*cis, trans, cis*-(1R,2R-DACH [$Pt(C_6H_5CH_2COO)_2Cl_2$]) and **15** (*cis, trans, cis*-(1R,2R-DACH) [$Pt(C_6H_5(CH_2)_2COO)_2Cl_2$]).

In order to check if they retained anticancer activity against MPM, Pt(IV)complexes **10**-**15** were tested both on the four MPM cell lines and on the healthy human mesothelial cells.

Moreover, their antiproliferative ability exerted against MPM was compared to that observed against other ovarian cancer (A2780 cell line), known to be high responsive to platinum-based chemotherapy, and against colon tumor (HCT-116 cell lines), regarded chemoresistance to cisplatin but sensitive to oxaliplatin.

As expected, A2780 cells resulted the most responsive ones to both series whereas the MPM cell lines proved to be the less sensitive, confirming again their intrinsic chemoresistance. Pt(IV) complexes showed activity around three orders of magnitude higher than that of cisplatin,.

On MPM, complexes **10**-**12** were around ten times more active than their Pt(II) analogues. However, complexes belonging to the same series showed a similar biological activity. This implies that the activity of the Pt(IV)complexes provided with aryl axial ligands does not considerably raise with increasing axial chain length (Table 10).

However, it should be noted that the increase of the length of axial chain lead to a gain on selectivity against malignant cells. Moreover, these complexes are able to circumvent cisplatin resistance, showing a resistance factor three times lower than cisplatin (Table 10).

	Cisplatin	10	11	12
A2780	$0.5 \pm 0.1 \times 10^{-6}$	$4 \pm 1 \times 10^{-9}$	$60 \pm 3 \times 10^{-9}$	$5 \pm 1 \times 10^{-9}$
HCT-116	$2.3 \pm 0.3 \times 10^{-6}$	$5 \pm 10 \times 10^{-9}$	$0.21 \pm 0.05 \times 10^{-6}$	$50 \pm 0.6 \times 10^{-8}$
HMC	$6.7 \pm 1.2 \times 10^{-6}$	$0.32 \pm 0.05 \times 10^{-6}$	$4.16 \pm 0.8 \times 10^{-6}$	$0.9 \pm 0.42 \times 10^{-6}$
BR95	$6.2 \pm 0.9 \times 10^{-6}$ (1.1)	$0.33 \pm 0.09 \times 10^{-6}$ (0.97)	$1.97 \pm 0.64 \times 10^{-6}$ (2.1)	$0.53 \pm 0.006 \times 10^{-6}$ (1.7)
MG06	$4.1 \pm 1.5 \times 10^{-6}$ (1.6)	$0.48 \pm 0.09 \times 10^{-6}$ (0.73)	$1.24 \pm 0.57 \times 10^{-6}$ (3.35)	$0.71 \pm 0.57 \times 10^{-6}$ (1.27)
MM98	$3.2 \pm 1.0 \times 10^{-6}$ (2.1)	$0.12 \pm 0.032 \times 10^{-6}$ (2.7)	$0.64 \pm 0.028 \times 10^{-6}$ (6.5)	$0.2 \pm 0.073 \times 10^{-6}$ (4.5)
MM98R	$19.4 \pm 2.8 \times 10^{-6}$ (-)	$0.47 \pm 0.085 \times 10^{-6}$ (0.68)	$1.23 \pm 0.33 \times 10^{-6}$ (3.38)	$0.44 \pm 0.12 \times 10^{-6}$ (2)
RF	6.1	3.9	1.9	2.2

TABLE 10. IC_{50} values (M) obtained after 72 h CT.
Data in brackets reports the selectivity index, SI, *i.e.*, the ratio between IC50 (HMC) and the IC50 on the tumor MPM cell line.
[a] Resistance Factor, RF = IC50 MM98R / IC50 MM98.

A similar biological behavior was observed for the **13-15,** belonging to the other series, corroborating previous observations: these complexes showed a similar biological activity, in spite of the increasing length of the axial aromatic chains.

Further investigations of these complexes are in progress, in order to dissect the molecular basis of biological effect observed.

Complexes **13-15** appeared more effective than oxaliplatin, *i.e* their Pt(II) counterparts used in clinic, and hugely by-passed cisplatin resistance, since showed a better RF than cisplatin (Table 11).

	1R,2R-DACH-Cl_2	Oxaliplatin	13	14	15
A2780	$0.12 \pm 0.04 \times 10^{-6}$	$0.17 \pm 0.01 \times 10^{-6}$	$2.2 \pm 3 \times 10^{-9}$	$3.6 \pm 0.9 \times 10^{-9}$	$1.3 \pm 1 \times 10^{-9}$
HCT-116	$0.275 \pm 0.028 \times 10^{-6}$	$0.33 \pm 0.015 \times 10^{-6}$	$2.6 \pm 0.4 \times 10^{-9}$	$11 \pm 0.1 \times 10^{-8}$	$5 \pm 0.1 \times 10^{-9}$
HMC	$0.8 \pm 0.1 \times 10^{-6}$	$4.9 \pm 0.5 \times 10^{-6}$	$0.13 \pm 0.08 \times 10^{-6}$	$0.23 \pm 0.07 \times 10^{-6}$	$0.15 \pm 0.08 \times 10^{-6}$
BR95	$1 \pm 0.2 \times 10^{-6}$ (0.8)	$2.4 \pm 0.7 \times 10^{-6}$ (2)	$21 \pm 0.5 \times 10^{-8}$ (6.2)	$20 \pm 0.5 \times 10^{-8}$ (11.5)	$14 \pm 0.7 \times 10^{-8}$ (10.7)
MG06	$0.8 \pm 0.2 \times 10^{-6}$ (1)	$3 \pm 0.9 \times 10^{-6}$ (1.6)	$40 \pm 0.2 \times 10^{-8}$ (3.2)	$0.9 \pm 0.08 \times 10^{-6}$ (0.2)	$80 \pm 20 \times 10^{-8}$ (1.9)
MM98	$2.2 \pm 0.4 \times 10^{-6}$ (0.36)	$4.4 \pm 0.8 \times 10^{-6}$ (1.1)	$15 \pm 3 \times 10^{-8}$ (8.6)	$60 \pm 0.2 \times 10^{-8}$ (3.8)	$60 \pm 20 \times 10^{-8}$ (2.5)
MM98R	$2.5 \pm 0.6 \times 10^{-6}$ (0.32)	$3.8 \pm 0.9 \times 10^{-6}$ (1.29)	$20 \pm 0.3 \times 10^{-8}$ (6.5)	$30 \pm 0.1 \times 10^{-8}$ (7.6)	$70 \pm 30 \times 10^{-8}$ (2.1)
[a]RF	1.1	0.9	1.3	0.5	1.7

TABLE 11. IC_{50} values (M) obtained after 72 h CT.

Data in brackets reports the selectivity index, SI, *i.e.*, the ratio between IC50 (HMC) and the IC50 on the tumor MPM cell line. [a] Resistance Factor, RF = IC50 MM98R / IC50 MM98.

In order to verify whether the different cytotoxicity observed for complex **10** is affected by a different cell accumulation, the cellular uptake of complex **10** was determined on A2780 HCT116 cell lines. The results support the activity data: the very lipophilic complex **10** (Table 12) enters cell in a superior extent than cisplatin. Indeed, as shown in Table 13, **10** intracellular uptake is 30 and 120 times higher than that observed with cisplatin on A2780 and HCT-116 cell lines, respectively.

Compound	**log k'_0**
cisplatin	-0.567
10	3.022

TABLE 12. logK'_0 values of cisplatin and **10**

	Control	**Cisplatin**	**10**
A2780	0.09 ± 0.09	1.78 ± 0.57	54.71 ± 12.07
HCT-116	0.05 ± 0.01	1.83 ± 0.5	214.65 ± 37.28

TABLE 13**.** Uptake (ng Pt/10^6 cells) after 4h of treatment con 10 μM with each compound

C-Myc inhibition to enhance cisplatin-based MPM chemotherapy

It has been reported that (+)-JQ1 reduce expression of *c-MYC* and its target genes, prompting to cell-cycle arrest and cell senescence in many tumoral models, with encouraging *in vivo* results [124][205]. Furthermore, JQ1 has been shown to act on solid tumour cells through FOS-Like antigen 1 (FOSL1) modulation, in a cell-line dependent manner [206]. c-*MYC* suppression enhanced the effectiveness of cisplatin in osteosarcoma and melanoma [207] and recently, it has been reported that a virus vector encoding the c-Myc repressor FIR showed synergistic antitumor effects in combination with cisplatin *in vitro* e *in vivo* in the treatment of MPM [207].

Thus, we hypothesized that JQ1 could enhance cisplatin-based chemotherapy in MPM.

In accordance with the *in vitro* previous results, As shown in Table 14, (+)-JQ1 resulted far more active than is enantiomer (-)-JQ1. So, in the following investigations we considered only the more potent enatiomer (hereafter (+)-JQ1 was simply defined as JQ1).

The MM98 and MM98R sarcomatous cell lines resulted more responsive to JQ1 than epitheliod an mixed phenotypes; in addition, it exerted a cytotoxic activity tenfold more high than cisplatin. On the contrary, JQ1 was threefold more potent than cisplatin in BR95 and MG06 cell lines. Notably, JQ1 overcame cisplatin resistance lowering the resistance factor value (RF = 2).

It should be noted that JQ1 acts in a quite selective way against malignant cells. The selectivity is ascribed to expression of its target, c-myc, that is low in normal cells but it is elevated in a broad range of human cancers, including MPM [208].

	(-)-JQ1	(+)-JQ1	Cisplatin
HMC	5.3 ± 0.9	3.1 ± 0.9	6.7 ± 1.2
BR95	3.9 ± 1.0 (1.4)	2.2 ± 0.6 (1.4)	6.2 ± 0.9 (1.2)
MG06	3.0 ± 0.4 (1.8)	1.0 ± 0.3 (3.1)	4.1 ± 1.5 (1.8)
MM98	3.8 ± 0.6 (1.4)	0.089 ± 0.6 (31.6)	3.2 ± 1.0 (2.3)
MM98R	2.8 ± 0.2 (1.9)	0.18 ± 0.08 (17.2)	19.4 ± 2.8 (0.4)
RF[a]	0.7	2.0	6.1

TABLE 14. IC50 values (intended as μM concentrations) obtained after 72h of treatment. Data in brackets reports the selectivity index, SI, *i.e.*, the ratio between IC50 (HMC) and the IC50 on the tumor MPM cell line.
[a] Resistance Factor, RF = IC50 MM98R / IC50 MM98.

Based on these encouraging data, a drug combination study was performed, in order to: *i)* reduce cisplatin dosage, *ii)* minimize its side effects and so, *iii)* improve therapeutic *compliance* (term that refers to the match between medical prescriptions and their applications by the patient in order to obtain the cure of an illness).

We employed cisplatin and JQ1 given simultaneously at fixed molar ratio (10:1 on sarcomatous cells and 3:1 on epithelial, mixed and healthy cells, chosen according to the ratio of IC_{50} values found for cisplatin and JQ1).

For the sake of clarity, in Table 15 only the Combination Index (CI) values obtained for the combination that gave 50 % growth inhibition (FA=0.5) are reported. The combination resulted additive on both sarcomatous and epitheliod cell lines, whereas it resulted synergistic on MG06 cells only. Interestingly, the pharmacological association induced a little antagonistic effect on non-tumoral HMC cell lines, indicating selectivity.

	HMC	BR95	MG06	MM98	MM98R
Cisplatin + (+)-JQ1	1.20 ± 0.07	1.08 ± 0.19	0.38 ± 0.04	0.79 ± 0.18	1.06 ± 0.24

TABLE 15. combination Index (CI) was obtained for the drug combination that gave 50% growth inhibition (FA=0.5). CI < 1: synergism; CI around 1: additive; CI> 1: antagonism.

These data correlate with the activation of caspase-3. MG06, BR95 and HMC cells were treated with 7.5 μM CDDP, 2.5 μM JQ1, or both, while MM98 and MM98R cells were treated with 2.5 μM CDDP, 0.25 μM JQ1, or both. As shown in Table 16, caspase-3 activity was almost undetectable in HMC and MM98. In MM98R, JQ1 induced a slight activation, which increased in the combination with CDDP. A similar behavior was observed in BR95, but with higher caspase-3 activities. In MG06, both CDDP and JQ1 induced caspase-3 activation, with the latter giving similar values as in the combination. CDDP alone induced a strong caspase-3 activation in the positive control (A2780).

Cells	Control	CDDP	JQ1	JQ1+CDDP
HMC	8.4±3.1	3.0±0.7	24.3±4.4	23.1±18.4
BR95	48.9±18.0	55.5±1.4	194.2±5.0	336.4±50.3
MG06	40.0±5.9	172.0±40.2	358.7±52.7	384.0±27.3
MM98	0.8±0.3	10.6±3.4	14.4±10.4	32.7±20.7
MM98R	3.6±2.5	10.0±9.1	48.3±1.8	60.0±9.0
A2780	24.2±8.9	709.5±51.4	-	-

TABLE 16. Caspase-3 activity (arbitrary units/min) ± standard deviation after 24h of treatment. The human ovaric carcinoma cell line A2780, treated with 10 μM cisplatin, was used as positive control. After cell lysis, the caspase-3 fluorescent substrate Ac-DEVD-AFC was followed for 1 h, normalized over the blank and fitted with a linear kinetic. The slope, standing for the caspase-3 activity is the average from duplicate experiments. The caspase-3 inhibitor Ac-DEVD-CHO suppressed every signal (for the sake of clarity, data are not shown).

Since JQ1 is known to exert its cytostatic effect by means of senescence induction [205], which could be also initiated by cisplatin [209], the analysis of senescent cells after the same combination protocol was performed. It should be recall that an increasing number of reports indicate that senescence could be a potential therapeutic treatment to overcome drug resistance in solid tumors [210] [211].

Interestingly, cisplatin did not trigger senescence on HMC cells (within this experimental range of concentrations) and slightly decreased senescence induction due to JQ1 (Figure 59a). Thus, the antagonistic effect between JQ1 and cisplatin in antiproliferative activity on these healthy cells could be ascribed to an antagonistic effect in senescence induction. Accordingly, high concentrations of cisplatin, exerted a cytostatic effect on this cell line.

In MG06 (Figure 59b), a bumpy fall in the number of remaining cells was observed in the same experimental conditions, thus confirming the strong synergistic effect. On BR95 (Figure 59c), MM98 (Figure 59d) and MM98R cells (Figure 59e), the combination seemed to be the orthogonal sum of the effects observed for cisplatin and JQ1 in single treatments (higher level of senescent cells, top right corner of each plot). Thus, the additive effect correlated once again with senescence induction.

These data indicate that senescence is the main mechanism of action underlying the effectiveness of the combination between cisplatin and JQ1.

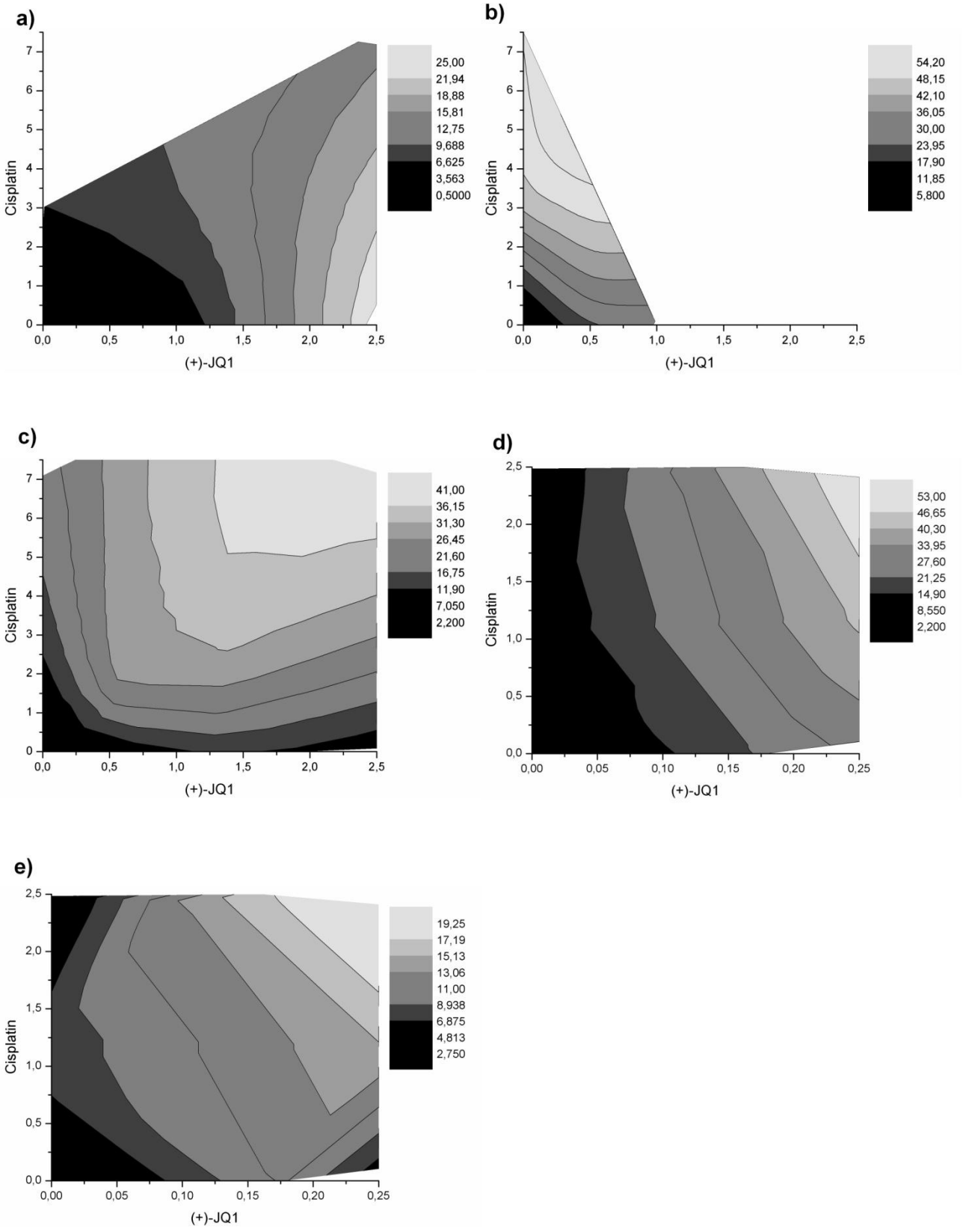

FIGURE 59. Contour plots of % of SA-β-gal positive (senescent) cells after 3 days of treatment, indicated by the legend located on the right of each graph. From top to bottom: a)HMC; b) MG06; c)BR95; d) MM98 and e)MM98R.

We further investigated the trend of senescence after three days of continuous treatment (3CT) and four more days of recovery (4R) in drug-free medium, to check if cells are able to revert their quiescence to a proliferant/viable state after drugs removal.

Once again, a cell line-specific behaviour was observed: senescence level remained stable only in the non-tumor cell line (HMC, Figure 60a), while on MG06 cells (Figure 60b) high levels of senescence were observed as far as the recovery partially restored cellular viability. The percentage of senescent cells clearly decreased in BR95 (Figure 60c), MM98 (Figure 60d), and MM8R (Figure 60e) cell lines, which means that the additive effect in senescence induction is maintained until cells are challenged with the drugs.

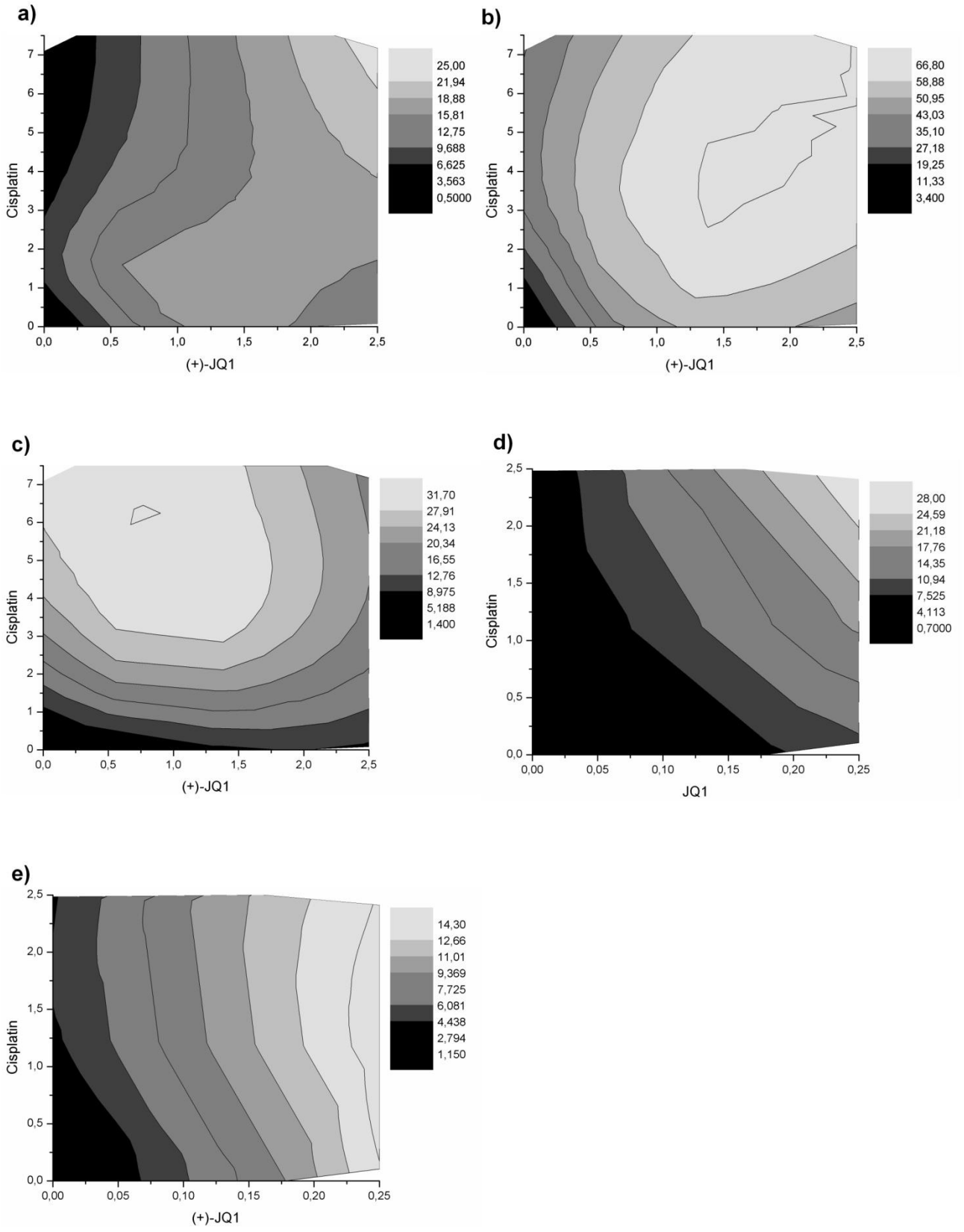

FIGURE 60. Contour plots of % of SA-β-gal positive (senescent) cells after 3 days of treatment+ 4 days of recovery. From top to bottom: a)HMC; b) MG06; c)BR95; d) MM98 and e)MM98R.

Based on these observations, we checked if a sequential treatment of cisplatin, followed by repeated treatments with JQ1 should be beneficial. We explored if the combination would be effective after prolonged exposure, the multicellular tumor spheroids (MCTS) of BR95 were employed.

We treated BR95 spheroids with cisplatin (for 1 day) at the same concentrations as for the senescence experiments, followed by 3+3 days of treatment with JQ1 given at 1/3 concentration in according to the dose ratio. As shown in Figure 60, while cisplatin alone (1 CT + 3R+3R) induced the reduction of the spheroid volume with the higher concentration (3 μM and 7.5 μM) (Figure 61a), JQ1 (1R+ 3 CT+ 3 CT) simply counteracted the tumor growth (Figure 61b). Thus, cisplatin exerted cytostatic effect, while JQ1 resulted in cytostatic effect.

The combination of the two drugs (1 CT + 3 CT JQ1 + 3 CT JQ1) gave better outcomes, showing the strongest volume decrease even at lower cisplatin concentration (Figure 61c). Thus, the sequential order of treatment give the better therapeutic outcomes and allows to reduce cisplatin concentration.

Mannava et al. reported that myc- depleted melanoma cells undergo extensive DNA damage that is caused by the unexpression of thymidylate synthase (TS) and ribonucleotide reductase (RR) and subsequent depletion of deoxyribonucleoside triphosphate (dNTPs) pools, leading to senescent phenotype [212]. These evidence might explain the strong cytotoxic effect induced by cisplatin-JQ1 sequential treatment: it is likely that DNA-damage induced by cisplatin couldn’t be efficiently repaired because of JQ1 ability to counteract TS and RR activity by means of c-myc inhibition.

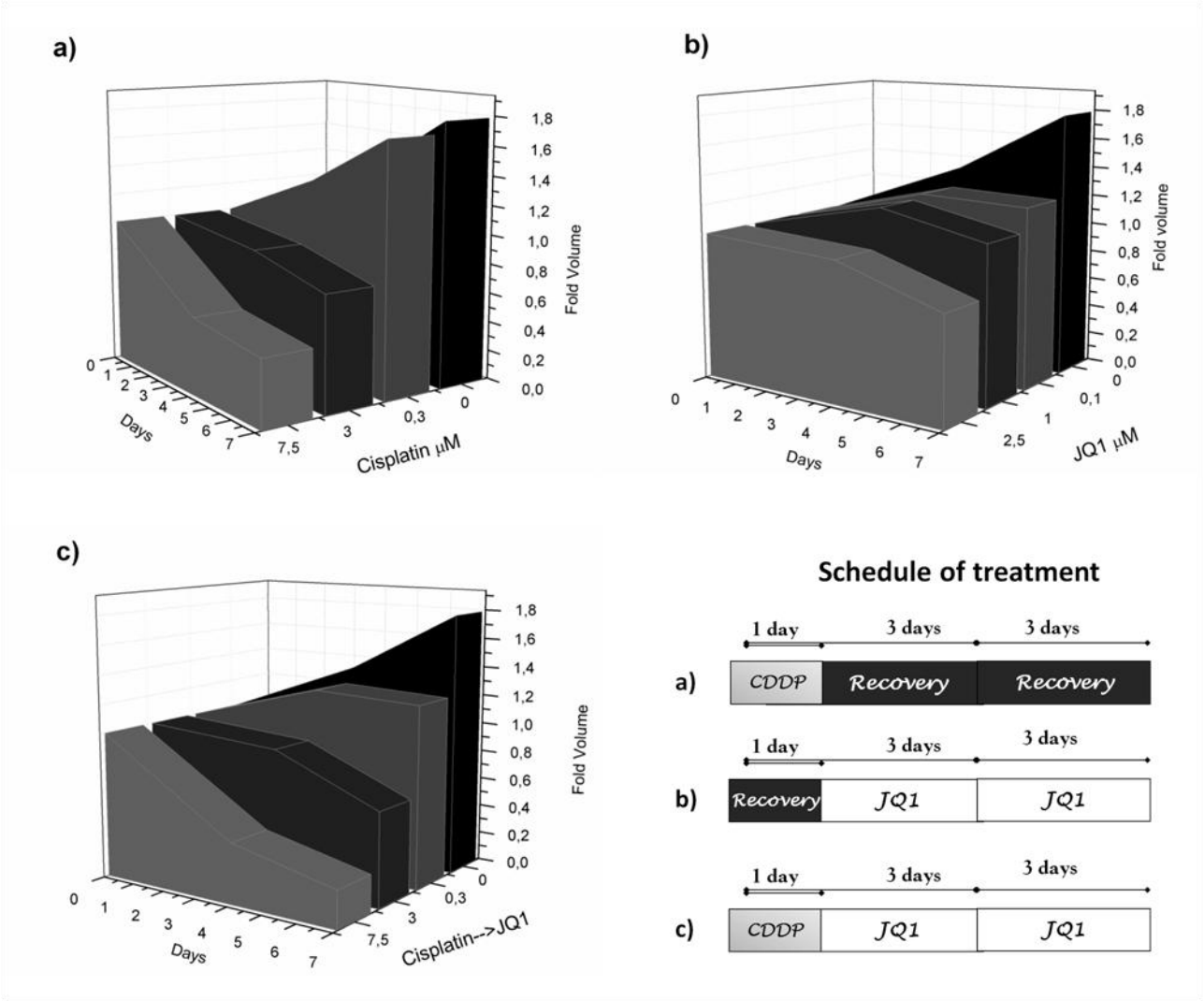

Figure 61. BR95 spheroids fold volume. a) treatment with cisplatin for 1 day, followed by drug-free medium for 3 days, and drug-free medium again for further 3 days; b) treatment with cisplatin for 1 day, followed by JQ1 for 3 days, and JQ1 again for further 3 days; c) treatment with drug-free medium for 1 day, followed by JQ1 for 3 days, and J JQ1 again for further 3 days.

Evaluation of a Cobalt-based complex as candidate drug for MPM treatment

Malignant pleural mesothelioma (MPM) is a fatal malignancy related to previous asbestos exposure. Asbestos generates a prolonged state of inflammation that enhances the expression of inducible enzymes causing, *inter alia*, up-regulation of cyclooxigenase-2 (COX-2) [158]. It is known that prostaglandin E_2 (PGE_2), the main COX-2 metabolite, impacts several pathways involved in carcinogenesis. Celecoxib, a COX-2 inhibitors, showed to have antineoplastic efficacy against MPM both *in vitro* and *in vivo* [213].

Therefore, The aspirin derivative Co-Ass, [2-acetoxy-(2-propynyl)benzoate]hexacarbonyldicobalt (Co-Co), was investigated as potential drug against MPM, and its biological properties was compared to those of both its analogue Co-EPM, hexacarbonyl[μ-(2-ethylphenyl)-methanol]dicobalt (Co-Co) and acetyl salicilic acid (aspirin or ASA). Co-EPM is deprived of its COX inhibition ability (that lie in acetyl group), whereas ASA is a well-know COX-2 inhibitor.

First of all the antitumoral activity of the investigated compounds was explored on the MPM cell lines. As expected, ASA showed IC_{50} values 2-3 orders of magnitude higher than Co-ASS in all cell lines (Table 17).

We found that Co-ASS was more active than the metal-reference drug cisplatin on cells having sarcomatous phenotype, whereas it was 10 fold less potent on cells having epitheliod phenotype that showed equal sensitivity to both Co-Ass and Co-EPM. Moreover, both cobalt-complexes were able to circumvent-cisplatin chemoresistance in MM98R cell lines, as proved by low RF values.

Thus, Co-ASS acted in a selective way against the responsive sarcomatous phenotype MM98, while the opposite is true for the less sensitive BR95 and MG06 cell lines. Our data are in line with previous results, which highlighted that Co-Ass antiproliferative activity is highly dependent on the peculiarities of each tumoral cell line [214]. In order to examine the weight of COX-2 inhibition on the different antiproliferative ability, Co-ASS and Co-EPM were also tested on two other tumor model cell lines: the human colon carcinoma HCT-116 (non-expressing COX-2), and human lung cancer A549 (expressing COX-2). As predicted, the HCT-116 cells were less sensitive to Co-ASS than A549, but this difference in activity (IC_{50} ratio = 1.9) was lower than that observed between BR95 and MM98 (IC_{50} ratio = 8.9) and MG06 and MM98 (IC_{50} ratio = 7.7). Moreover, Co-EPM showed a similar IC_{50} ratio in HCT-

116 and A549 of (1.4). These data suggested that COX-2 inhibition might not the only mechanisms involved in the antiproliferative of Co-Ass on MPM (Table 17).

	Co-ASS (μM) (SI)	Co-EPM (μM) (SI)	ASA (mM) (SI)	Cisplatin (μM) (SI)
HCT-116	7.5 ± 0.5	43 ± 5	3.8 ± 0.2	2.3 ± 0.3
A549	4.8 ± 2.2	30.2 ± 2.7	2.01 ± 0.9	3.7 ± 0.8
BR95	15.1 ± 2.6 (0.4)	25.7 ± 5.6 (2.1)	0.6 ± 0.3 (4.5)	6.2 ± 0.9 (1.2)
MG06	24.7 ± 4.8 (0.3)	19.7 ± 3.2 (2.7)	1.5 ± 0.4 (1.8)	4.1 ± 1.5 (1.8)
MM98	1.7 ± 0.7 (3.6)	25.2 ± 5.2 (2.1)	4.6 ± 0.4 (0.6)	3.2 ± 1.0 (2.3)
MM98R	3.2 ± 0.8 (1.9)	25.1 ± 7.4 (2.1)	2.8 ± 0.2 (1)	19.4 ± 2.8 (0.4)
HMC	6.2 ± 1.3	53.4 ± 3.4	2.7 ± 0.7	6.7 ± 1.2
RF[a]	1.9	1	0.6	6.1

TABLE 17. IC_{50} values calculated after 72 h continuous treatment.

[a] Resistance factor (RF)= IC50 (MM98R)/IC50 (MM98)
[b] Selectivity Index (SI)= IC50 (HMC)/ IC50 malignant cell line

These observations correlated with PGE_2 levels, the main metabolite of COX-2, that pointed out that there wasn't a reduction of enzyme activity (Figure 62). In particular, we observed a huge increase of PGE_2 levels in BR95 cells after exposure to both cobalt-complexes and ASA; this event should be conceived as a defense response operated by the cells to abrogate pro-death mechanisms. On the contrary, PGE_2 levels remained stable on the more responsive MM98 cell lines, except after ASA treatment, that reduced them.

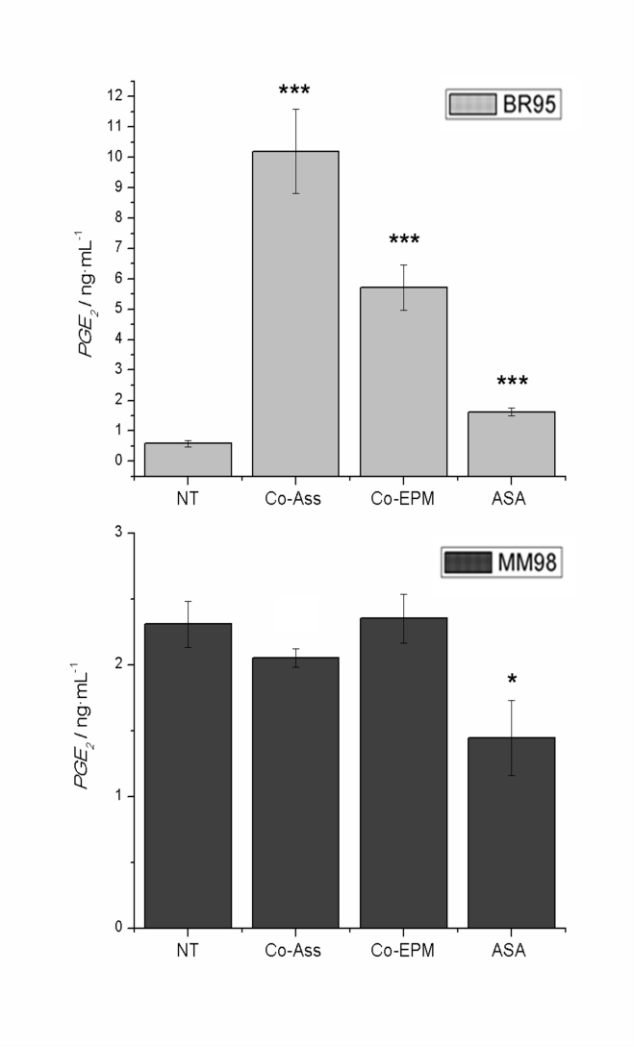

FIGURE 62. PGE_2 levels in extracellular medium of BR95 and MM98 detected after 24h of CT with Co-ASS, Co-EPM, ASA at concentration around IC_{50}.

In order to explain if the cobalt-based complexes have a cytotoxic or cytostatic effect, their antiproliferative activity was compared by means of clonogenic assay employing the BR95 and MM98 cell lines. As shown in Table 18,Co-ASS and Co-EPM gave more or less the same IC_{50} value as that obtained from the viability assay on both cell lines, indicating that its growth inhibition corresponds to a cytostatic effect on both phenotypes. On the contrary, Co-Ass was far more active than Co-EPM in MM98 cells, standing for a strong cytotoxic activity.

	Co-ASS (μM)	**Co-EPM (μM)**
BR95	28.0 ± 2.3	28.6 ± 0.9
MM98	0.050 ± 0.001	19.7 ± 4.6

TABLE 18. IC_{50} values obtained by clonogenic assay of BR95 and MM98 cell lines, challenged with 3 days CT and then 1 week recovery.

As previously reported, Co-ASS exert its cytotoxic effect inducing apoptosis: indeed, activated caspase-3, the main effector caspase, was detected in MM98 cells only (Figure 63). The opposite is true for BR95, for which we didn't reveal caspase-3 activation, confirming the results of clonogenic assay.

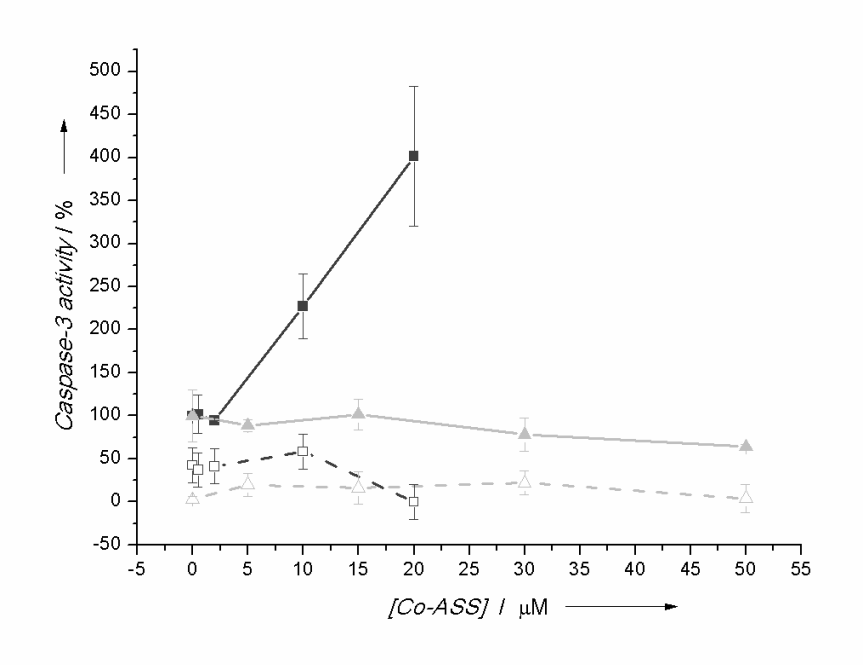

FIGURE 63. Percentage of caspase-3 activity in MM98 (dark grey) and BR95 (light grey) after 24h CT with increasing concentration of Co-Ass. The corresponding data in the presence of the specific inhibitor Ac-DEVD-CHO are reported (empty symbols, dashed lines).

Co-Ass induced apoptosis in MM98 through the intrinsic pathway, mitochondrial potential gradient ($\Delta\psi$) was affected by the treatment, as reported in Figure 64. Absence of $\Delta\psi$ dissipation in BR95 confirm again the reluctance of this cell lines to undergo cell death.

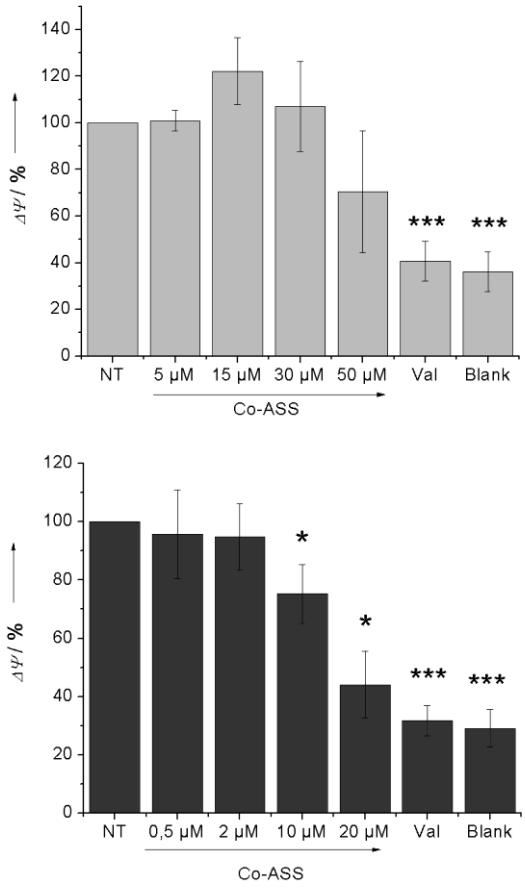

FIGURE 64. Mitochondrial potential gradient (ΔΨ) of BR95 (top, grey bars) and MM98 (bottom, dark bars), reported as percentage of the signal. Cells were treated for 24 h with increasing concentration of Co-ASS.

The only common effect to both cell lines following a short treatment (2 h) with equitoxic cobalt-complexes was the reduction of ROS/NOS levels (for sake of clarity, it must be pointed out that the fluorophore probe used, the dichlorofluoresceine-diacetate, H2DCF-DA, is able to detect both species), as shown in Figure 65. ROS levels were assessed in order to verify if apoptosis induction was mediated by ROS/NOS generation, in a similar manner as the cobalt-salt $CoCl_2$ [215]. Surprisingly, $CoCl_2$ induced a significant ROS increase in in MM98 cells only that could be stopped by pre-treatment with N-acetylcysteine (NAC, an amino-acid derivative with antioxidant properties), but no change in ROS levels were observed in BR95 cells, showing that also the response to $CoCl_2$ was cell-type specific.

ASA induced a ROS increase in both cell lines, while the pre-treatment with NAC was not able to abrogate its ROS generation (Figure 65). Therefore, the ASA-moiety could not be responsible for the observed of antioxidant effect of Co-ASS, shared with Co-EPM. Thus, the

dicobalthexacarbonyl moiety and its decomposition products were the only remaining candidates responsible for such an antioxidant behavior. While the Co salts are excluded since they produce the opposite effect, while the released gaseous CO is the candidate for such a biochemical pathway. Interestingly, ROS decrease was also observed in chondrocytes treated with CO-releasing molecules (CO-RMs), leading to an overall inflammation decrease by decreasing oxidative stress and NO_2 levels [216]. CO-RMs is a family of transition metal-carbonyl complexes designed to release CO on decomposition in a controlled fashion, that includes the alkynehexacarbonyldicobalt (Co-Co) complexes. Thus, we be supposed that both the hexacarbonyldicobalt (Co-Co) derivatives, namely Co-ASS and Co-EPM, deliver CO into the cells exerting anti-inflammatory activity and causing ROS level drop [217].

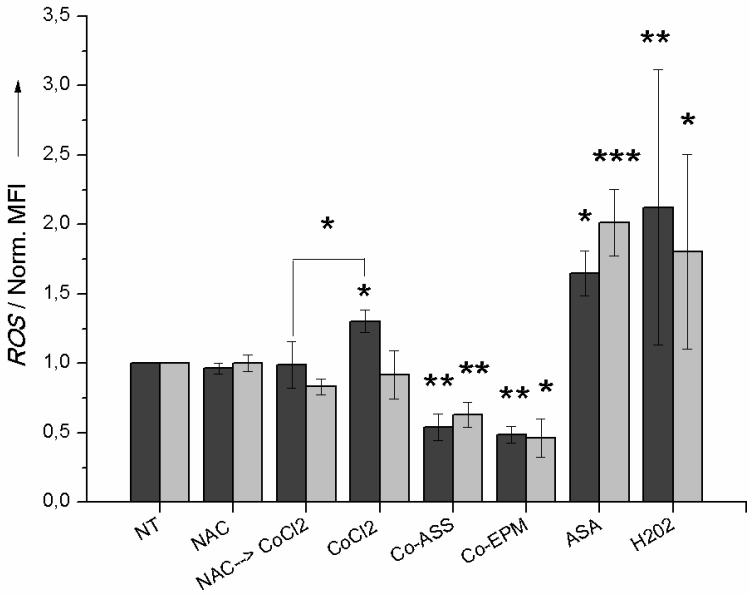

FIGURE 65. ROS levels of BR95 (light grey) and MM98 (dark grey); % DCF fluorescence was normalized upon % viability after 2 h of treatment at equitoxic concentration, and reported as normalized mean fluorescence intensity (MFI). H_2O_2 was used as positive control.

The released CO inhibits with heme proteins, such as NOS, the enzyme that produces NO along with citrulline from arginine. NO and CO are two gaseous mediators that interplay in a intricate way, since NO counteracts CO generation and in turn, CO inhibits NOS activity, as simplified in Figure 66 [218].

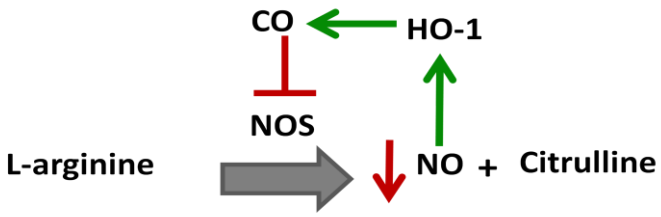

FIGURE 66. CO is produced physiologically through the degradation of heme catalyzed by heme oxygenase (HO). The inducible isoform of the enzyme, HO-1, is activated in stressing conditions, as in various inflammatory diseases. Gaseous CO inhibits NOS by binding to the NOS-heme moiety, leading to a fall of NO levels.

Thus, CO would lead to reduced RNS, the more stable derivatives of NO .Therefore, the nitrite levels have been measured.

HL-60 cells were stimulated byinterleukin-1β (IL-β) to increase the production of NO and then treated with increasing concentration of Co-Ass and Co-EPM.

As show in Figure 67, both cobalt-complexes prompted to nitrite levels fall to a similar extent (20 % and 25 % with Co-EPM and Co-ASS, respectively), confirming their CO-RM activity.

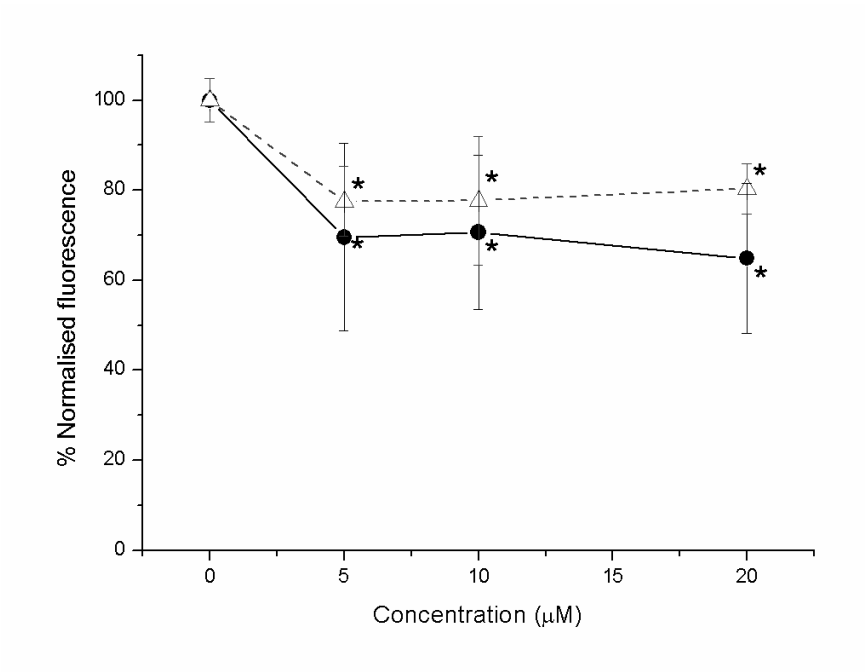

FIGURE 67. Nitrite levels of HL-60 cells after 24 h of treatment with 5 mM, 10 mM and 20 mM of Co-EPM (white triangles) and Co-ASS (black filled circles).

COX-2 is a heme proteins too. It explain how complexes with $Co_2(CO)_6$ cluster could inhibit COX activity, as it was previously reported [219].

ROS, COX-2 and NOS-dependent signaling converge in the nuclear transcription factor NF-κB, which has a central role in both inflammation and cancer, regulating the expression of proteins involved in cell survival and proliferation. The levels of NF-κB activity are ruled by ROS [220]. Therefore, the activity of NF-κB was analyzed by means of its nuclear translocation. On BR95 cells, Co-ASS induced a huge jump of NF-κB activity, while Co-EPM and ASA did not affect its nuclear translocation. We supposed that NF-κB is responsible for the PGE_2 increase, since it rules COX-2 expression [221].

On the contrary, all drug treatments in the Co-ASS-sensitive MM98 decreased the NF-κB activity, with the strongest inhibition exerted by Co-ASS. The decrease of NF-κB activity induced by Co-ASS on MM98 explains its strong cytotoxic effect (Figure 68).

Thus, Co-ASS modulates NF-κB positively or negatively in cell-specific way.

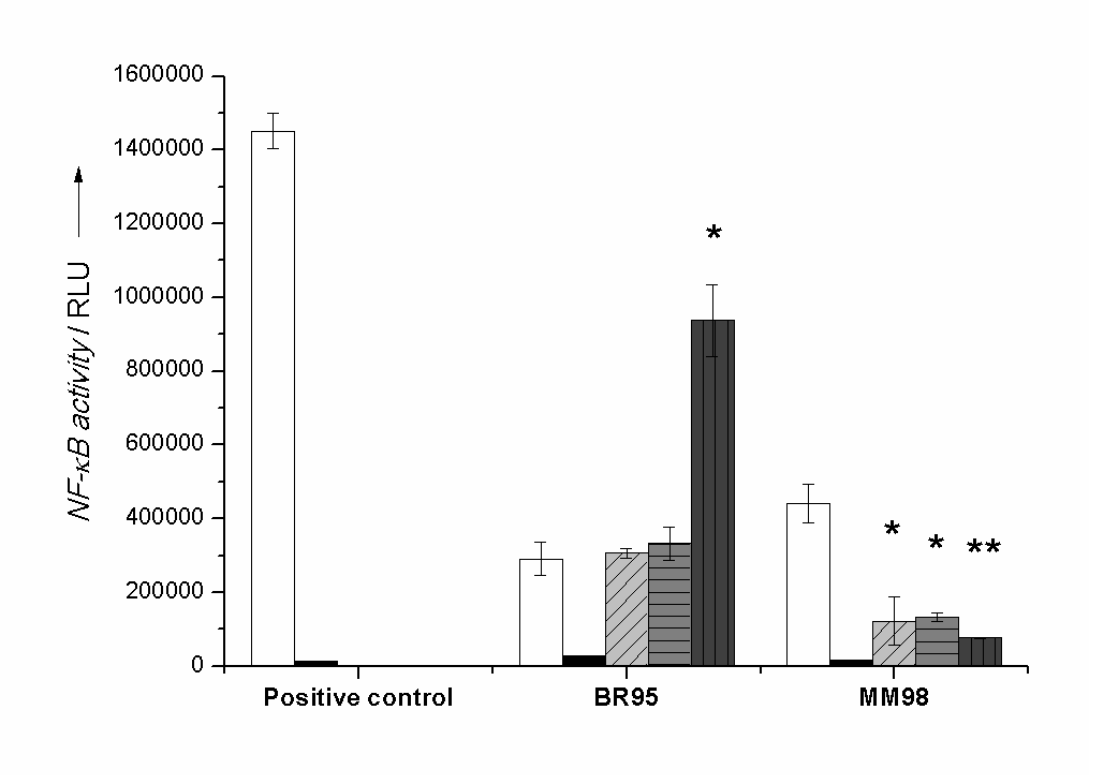

Figure 68. activity of NF-κB was analyzed by means of its nuclear translocation after 24 h CT with the tested compounds ASA (light grey bars, upright lines), Co-EPM (grey bars, horizontal lines) and Co-ASS (dark grey bars, vertical lines).

While the cytotoxic effect of Co-ASS on MM98 corresponds to apoptotic cell death, its cytostatic effect on BR95 had to be still explained. Cancer cells treated with chemotherapeutics can trigger senescence as a survival strategy or as an intermediate step towards cell death by means of a permanent growth inhibition. Senescence limits the propagation of cells with damaged DNA. Indeed, as NF-kB is activated, many cellular fates

occur ranging from cell survival to cell death or senescence [33]. Therefore, we supposed that senescence induction in BR95 cell lines should be responsible of biological responses triggered by alkynehexacarbonyldicobalt (Co-Co) complexes. Indeed, NOS inhibition can trigger cell senescence [222]. So, we checked the activity of the marker senescence-associated (SA) β-galactosidase, after a prolonged treatment (one week), as shown in Figure 69. BR95 cells resulted more prone to senescence, when challenged with each compound under study with respect to MM98. It should be noted that concentrations of Co-ASS above 10 μM killed all MM98 cells, in accordance with its cytotoxic property. Cisplatin caused the highest level of senescent cells, followed by Co-EPM, Co-ASS, and ASA. The prolonged treatment with Co-EPM gave a significant amount of positive cells, as expected from its CO-RM, and consequent NOS-inhibiting activity (Figure 69). On the contrary, in both cell lines Co-ASS produced only few senescent cells. Therefore we hypothesized that the lack of senescence caused by Co-ASS should be rather ascribed to its ASA-portion. Indeed, it has been previously reported that ASA reduces cell senescence, even a low concentration (within the μM range, as in the case of Co-ASS), triggering lipoxin synthesis by means of acetylation of COX-2 active site, which induce the restoration of the basal NOS activity [223].

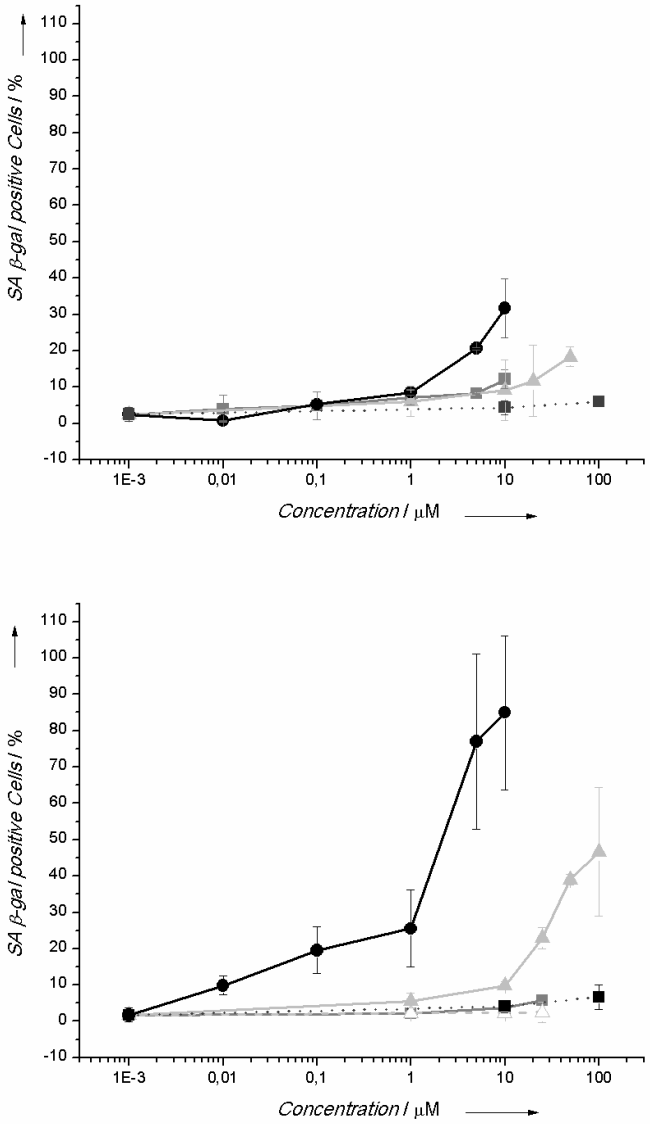

FIGURE 69. SA β-galactosidase percentage of positive cells after one week of treatment with increasing concentrations of cisplatin (black filled circles), Co-EPM (light grey filled triangles), Co-EPM+ASA (light grey empty triangles, dashed line), Co-ASS (grey filled squares) and ASA (black filled squares). Top: MM98, bottom: BR95.

In order to verify if the ASA-like portion of Co-ASS counteracted the CORM-induced senescence, BR95 cells were challenged simultaneously with equimolar concentration of Co-EPM and ASA. As shown in Figure 69, we observed a net reduction of senescent cells. Thus, the reduced senescence rate observed for Co-ASS treatment could be ascribed to the action of its ASA-like portion, counteracting the initial NO-inhibiting activity.

In perspective, Co-ASS would be better considered as aCO-NSAID agent (a CO-releasing molecule retaining the NSAID properties similar to NO [224] and H2S-NSAIDs [225]) than as an antitumor drug candidate.

Conclusions

A microplate-based coating-free method to generate multicellular spheroids (MCTS) *in vitro* was optimized for drug screening purposes. The spheroid growth was easily obtained by simple seeding in round-bottomed polypropylene plates placed on orbital mixer within a CO_2 incubator. Spheroids allowed to discriminate between the cytostatic and cytotoxic effect of the drugs that we investigated.

We realized that targeting the GSH system for therapeutic purposes could be both a boon and a curse. Bi-functional complexes targeted to GST were an unsuccessful attempt, since GST inhibition by EA is not synergistic with cisplatin *per se*.
On the contrary, picoplatin-based Pt(IV)complexes represented a more successful strategy. On one hand, GSH promotes the reduction of Pt(IV) to Pt(II), activating the pro-drugs in the cells, and on the other hand the presence of a bulky moiety hinders the GSH inactivation of the reduced Pt(II) metabolite.

Good results were obtained from a series of dicarboxylateplatinum(IV) complexes, sharing the same carrier and equatorial leaving groups as cisplatin (*i.e.* the same equatorial structure), and bearing carboxylate ligands of different length in axial position. On the contrary, Pt(IV) complexes provided of aromatic carboxylate chains as axial ligands did not show a vastly gain of antitumor activity compared to that of cisplatin. Analogues Pt(IV)complexes series, that differ for the presence of (1R,2R-DACH) moiety as carrier group, showed better performance. So, platinum(IV) complexes represent a quite promising strategy for malignant pleural mesothelioma and although we observed a correlation between the antiproliferative activity of Pt(IV) complexes *in vitro* and their lipophilicity, a rational choice of the axial carboxylate ligands is needed.

Furthermore, an innovative approach for MPM was explored, based on the hypothesis that targeting c-myc expression with JQ1 could enhance cisplatin activity. The combination resulted additive to synergistic on all MPM cell lines, and antagonistic on the healthy cells, showing selectivity towards the tumor. Although the mechanism of action underlying the effectiveness of the combination deserves for further investigations, our data showed that apoptosis and senescence are the main cell death pathways involved in the antitumor activity.

Acknowledgements

In questa sezione, ho preferito adottare la mia lingua madre per poter esprimere al meglio la mia gratitudine nei confronti delle persone che mi hanno affiancato lungo questo cammino.

Desidero innanzitutto ringraziare il Prof. Domenico Osella, relatore di questa tesi, per la sua guida sapiente, per la grande cortesia e disponibilità dimostratemi, e per avermi offerto l'opportunità di intraprendere questo percorso di ricerca.

Un sentito ringraziamento alla mia collega, la Dott.ssa Ilaria Zanellato, per il suo prezioso aiuto nella progettazione degli esperimenti, nell'analisi critica dei dati e nella stesura della tesi.

Ringrazio il Dott. Simone Cantamessa per l'analisi delle sezioni degli sferoidi, la Dott.ssa Manuela Alessio e la Dott.ssa Sabrina Bianco per la sintesi dei complessi a base di platino, la Dott.ssa Elisabetta Gabano e il Dott. Mauro Ravera per la disponibilità.

Desidero ringraziare il CIRCMSB per le borse di studio che hanno reso possibile lo sviluppo di questo lavoro, la regione Piemonte e la CRT per il supporto economico ai progetti.

Ringrazio Jon, Frenz, Giuly, Maria, Fabio il "Cuciu", Fabio "il Satiro", Albe e Lorenzo che hanno reso questo 3 anni splendidi. Non dimenticherò mai le cene a base di pesto, i memorabili dopocena al Ribaldo e le lezioni di francese. E' grazie loro che, quando ripenserò al mio dottorato, lo farò con un sorriso.

Daniele merita un ringraziamento particolare, perché in questi anni è stato molto più che un semplice coinquilino: per me ha rappresentato un solido punto di riferimento.

Un grazie di cuore a Rachele e a Tommy, per essere arrivati al momento giusto e per la loro presenza "illuminante".

La mia gratitudine spetta anche ad un'amica speciale, Sara, che ho sentito vicina anche quando la distanza ci ha diviso.

Infine, un grazie di cuore a Laura e Ramona per il loro impareggiabile sostegno.

References

[1] K. TP, *A Pharmacology Primer*. .

[2] Langmuir I, “THE ADSORPTION OF GASES ON PLANE SURFACES OF GLASS, MICA AND PLATINUM..pdf.” J. Am. Chem. Soc, pp. 1361–1403, 1918.

[3] Scatchard G, “The attractions of proteins fro small molecules and ions.pdf.” Annals of the New York Academy of Sciences, pp. 660–672, 1949.

[4] Z. Yan, X. Zheng, E. Wang, and J. Wang, “Thermodynamic and kinetic specificities of ligand binding,” *Chem. Sci.*, vol. 4, no. 6, p. 2387, 2013.

[5] D. Wootten, A. Christopoulos, and P. M. Sexton, “Emerging paradigms in GPCR allostery: implications for drug discovery.,” *Nat. Rev. Drug Discov.*, vol. 12, no. 8, pp. 630–44, Aug. 2013.

[6] C. Aj, “The mode of action of drugs on cells,” p. 1933, 1933.

[7] R. P. Stephenson, “A modification of receptor theory,” 1956.

[8] T. Kenakin, “Principles: receptor theory in pharmacology.,” *Trends Pharmacol. Sci.*, vol. 25, no. 4, pp. 186–92, Apr. 2004.

[9] V. Hill, “THE COMBINATIONS OF HAEMOGLOBIN WITH OXYGEN AND WITH CARBON MON-,” no. 1, 1913.

[10] S. Goutelle, M. Maurin, F. Rougier, X. Barbaut, L. Bourguignon, M. Ducher, and P. Maire, “The Hill equation: a review of its capabilities in pharmacological modelling.,” *Fundam. Clin. Pharmacol.*, vol. 22, no. 6, pp. 633–48, Dec. 2008.

[11] T. Chou and P. Talalayi, “QUANTITATIVE ANALYSIS OF DOSE-EFFECT RELATIONSHIPS : THE COMBINED EFFECTS OF MULTIPLE DRUGS OR ENZYME INHIBITORS,” *Adv. Enzym. Regul.*, vol. 22, pp. 27–55, 1984.

[12] Binslev, “Drug-acceptor interactions,” 2008.

[13] “http.www.tutorvista.comcontentbiologybiology-ivplant-growth-movementsgrowth-curve.php.” .

[14] J. Webb, “Enzyme and metabolic inhibitors.pdf.” 1963.

[15] V. J. Feron, “Toxicology of simple and complex,” vol. 22, no. 6, pp. 316–322, 2001.

[16] M. Goldoni and C. Johansson, “A mathematical approach to study combined effects of toxicants in vitro: evaluation of the Bliss independence criterion and the Loewe additivity model.,” *Toxicol. In Vitro*, vol. 21, no. 5, pp. 759–69, Aug. 2007.

[17] R. J. Tallarida, “An Overview of Drug Combination Analysis with Isobolograms,” vol. 319, no. 1, pp. 1–7, 2006.

[18] R. J. Tallarida, “Drug synergism: its detection and applications.,” *J. Pharmacol. Exp. Ther.*, vol. 298, no. 3, pp. 865–72, Sep. 2001.

[19] T. Chou, “Theoretical Basis , Experimental Design , and Computerized Simulation of Synergism and Antagonism in Drug Combination Studies □,” *Pharmacol. Rev.*, vol. 58, no. 3, pp. 621–681, 2006.

[20] M. J. Napolitano AP, Chai P, Dean DM, “Dynamics of the self-assembly of complex cellular aggregates on micromolded nonadhesive hydrogels.,” *American journal of physiology. Endocrinology and metabolism*, vol. 304, no. 3. Oncogene, pp. 2087–94, 01-Feb-2007.

[21] S.-I. Lee, “Drug interaction: focusing on response surface models.,” *Korean J. Anesthesiol.*, vol. 58, no. 5, pp. 421–34, May 2010.

[22] J. E. Visvader, “Cells of origin in cancer,” 2011.

[23] D. Hanahan, R. A. Weinberg, and S. Francisco, “The Hallmarks of Cancer Review University of California at San Francisco,” vol. 100, pp. 57–70, 2000.

[24] D. Hanahan and R. a Weinberg, “Hallmarks of cancer: the next generation.,” *Cell*, vol. 144, no. 5, pp. 646–74, Mar. 2011.

[25] and J. D. W. Bruce Alberts, Dennis Bray, Julian Lewis, Martin Raff, Keith Roberts, “Molecular Biology Of The Cell 4th Ed,” 2005.

[26] and J. D. W. Bruce Alberts, Dennis Bray, Julian Lewis, Martin Raff, Keith Roberts, “Molecular Biology Of The Cell 3th Ed.pdf.” 1994.

[27] J. T. Zilfou and S. W. Lowe, “Tumor suppressive functions of p53.,” *Cold Spring Harb. Perspect. Biol.*, vol. 1, no. 5, p. a001883, Nov. 2009.

[28] M. a Lemmon and J. Schlessinger, “Cell signaling by receptor tyrosine kinases.,” *Cell*, vol. 141, no. 7, pp. 1117–34, Jun. 2010.

[29] S. R. Hubbard and W. T. Miller, “NIH Public Access,” vol. 19, no. 2, pp. 117–123, 2008.

[30] R. Ren, “Mechanisms of BCR-ABL in the pathogenesis of chronic myelogenous leukaemia.,” *Nat. Rev. Cancer*, vol. 5, no. 3, pp. 172–83, Mar. 2005.

[31] T. Bowman, R. Garcia, J. Turkson, and R. Jove, “STATs in oncogenesis.,” *Oncogene*, vol. 19, no. 21, pp. 2474–88, May 2000.

[32] G. TD, “The Re1NF-kappa BI kappa B signal transduction pathway and cancer.pdf.” 2003.

[33] N. D. Perkins, “The diverse and complex roles of NF-κB subunits in cancer,” *Nat. Rev. Cancer*, vol. 12, no. 2, pp. 121–132, Feb. 2012.

[34] B. Lüscher and J. Vervoorts, “Regulation of gene transcription by the oncoprotein MYC,” *Gene*, vol. 494, no. 2, pp. 145–160, 2012.

[35] D. CV, “MYC on the Path to Cancer,” vol. 149, no. 1, pp. 22–35, 2013.

[36] J. Gräff and L. Tsai, “Histone acetylation : molecular mnemonics on the chromatin,” *Nat. Rev. Neurosci.*, vol. 14, no. 2, pp. 97–111, 2013.

[37] R. N. Eisenman, “Deconstructing Myc,” pp. 2023–2030, 2001.

[38] L. H. Hurley, “The c- MYC NHE III 1 : Function and Regulation,” 2010.

[39] G. Kroemer, L. Galluzzi, P. Vandenabeele, J. Abrams, E. S. Alnemri, E. H. Baehrecke, M. V Blagosklonny, and W. S. El-deiry, “Classification of cell death : recommendations of the Nomenclature Committee on Cell Death 2009,” *Cell Death Differ.*, pp. 3–11, 2009.

[40] A. Manuscript, “Chemotherapeutic Approaches for Targeting Cell Death Pathways,” vol. 11, no. 4, pp. 342–357, 2011.

[41] S. W. G. Tait and D. R. Green, “Mitochondria and cell death: outer membrane permeabilization and beyond.,” *Nat. Rev. Mol. Cell Biol.*, vol. 11, no. 9, pp. 621–632, Aug. 2010.

[42] K. S. George and S. Wu, “Lipid raft : A floating island of death or survival,” *Toxicol. Appl. Pharmacol.*, vol. 259, no. 3, pp. 311–319, 2012.

[43] J. Van Limbergen, C. Stevens, E. R. Nimmo, D. C. Wilson, and J. Satsangi, “Autophagy: from basic science to clinical application.,” *Mucosal Immunol.*, vol. 2, no. 4, pp. 315–30, Jul. 2009.

[44] Y. Kondo, T. Kanzawa, R. Sawaya, and S. Kondo, “The role of autophagy in cancer development and response to therapy.,” *Nat. Rev. Cancer*, vol. 5, no. 9, pp. 726–34, Sep. 2005.

[45] S. L. Fink and B. T. Cookson, “Apoptosis , Pyroptosis , and Necrosis : Mechanistic Description of Dead and Dying Eukaryotic Cells,” vol. 73, no. 4, 2005.

[46] M. Castedo, J.-L. Perfettini, T. Roumier, K. Andreau, R. Medema, and G. Kroemer, “Cell death by mitotic catastrophe: a molecular definition.,” *Oncogene*, vol. 23, no. 16, pp. 2825–37, Apr. 2004.

[47] I. Ben-Porath and R. a Weinberg, “The signals and pathways activating cellular senescence.,” *Int. J. Biochem. Cell Biol.*, vol. 37, no. 5, pp. 961–76, May 2005.

[48] X. Sui, R. Chen, Z. Wang, Z. Huang, N. Kong, M. Zhang, W. Han, F. Lou, J. Yang, Q. Zhang, X. Wang, C. He, and H. Pan, “Autophagy and chemotherapy resistance: a

promising therapeutic target for cancer treatment.," *Cell Death Dis.*, vol. 4, p. e838, Jan. 2013.

[49] A. Eisenberg-Lerner and A. Kimchi, "The paradox of autophagy and its implication in cancer etiology and therapy.," *Apoptosis*, vol. 14, no. 4, pp. 376–91, Apr. 2009.

[50] R. R. Gordon and P. S. Nelson, "Cellular senescence and cancer chemotherapy resistance.," *Drug Resist. Updat.*, vol. 15, no. 1–2, pp. 123–31, 2012.

[51] Y. Chien, C. Scuoppo, X. Wang, X. Fang, B. Balgley, J. E. Bolden, P. Premsrirut, W. Luo, A. Chicas, C. S. Lee, S. C. Kogan, and S. W. Lowe, "Control of the senescence-associated secretory phenotype by NF-κB promotes senescence and enhances chemosensitivity.," *Genes Dev.*, vol. 25, no. 20, pp. 2125–36, Oct. 2011.

[52] M. Narita and S. W. Lowe, "Senescence comes of age.," *Nat. Med.*, vol. 11, no. 9, pp. 920–2, Sep. 2005.

[53] N. J. Curtin, "DNA repair dysregulation from cancer driver to therapeutic target.," *Nat. Rev. Cancer*, vol. 12, no. 12, pp. 801–17, Dec. 2012.

[54] J. Bartek, C. Lukas, and J. Lukas, "CHECKING ON DNA DAMAGE IN S PHASE," *Group*, vol. 5, no. October, pp. 792–804, 2004.

[55] J. Yang, Z. Xu, Y. Huang, H. E. Hamrick, P. J. Duerksen-hughes, and Y. Yu, "ATM and ATR : Sensing DNA damage," *J. Gastroenterol.*, vol. 10, no. 2, pp. 155–160, 2004.

[56] A. J. Deans and S. C. West, "DNA interstrand crosslink repair and cancer.," *Nat. Rev. Cancer*, vol. 11, no. 7, pp. 467–80, Jul. 2011.

[57] M. L. Dronkert and R. Kanaar, *Repair of DNA interstrand cross-links.*, vol. 486, no. 4. 2001, pp. 217–47.

[58] S. S. Lange, K. Takata, and R. D. Wood, "DNA polymerases and cancer," vol. 11, no. FEBRUARy, 2011.

[59] a P. Gilmore, "Anoikis.," *Cell Death Differ.*, vol. 12 Suppl 2, pp. 1473–7, Nov. 2005.

[60] H. Ungefroren, S. Sebens, D. Seidl, H. Lehnert, and R. Hass, "Interaction of tumor cells with the microenvironment.," *Cell Commun. Signal.*, vol. 9, no. 1, p. 18, Jan. 2011.

[61] C. E. Weber and P. C. Kuo, "The tumor microenvironment.," *Surg. Oncol.*, vol. 21, no. 3, pp. 172–7, Sep. 2012.

[62] G. Gilman, *The Pharmacological Basis of Therapeutics*. .

[63] V. Cepeda, M. a Fuertes, J. Castilla, C. Alonso, C. Quevedo, and J. M. Pérez, "Biochemical mechanisms of cisplatin cytotoxicity.," *Anti-cancer agents in medicinal chemistry*, vol. 7, no. 1. pp. 3–18, Jan-2007.

[64] A. Montecucco and G. Biamonti, “Cellular response to etoposide treatment.,” *Cancer Lett.*, vol. 252, no. 1, pp. 9–18, Jul. 2007.

[65] C. M, “Holland-Frei Cancer Medicine 6th edition.pdf.” .

[66] O. Rixe and T. Fojo, “Is cell death a critical end point for anticancer therapies or is cytostasis sufficient?,” *Clin. Cancer Res.*, vol. 13, no. 24, pp. 7280–7, Dec. 2007.

[67] N. Cells, W. D. Stein, R. Robey, C. Cardarelli, M. M. Gottesman, and S. E. Bates, “Low and High Concentrations of the Topo II Inhibitor Daunorubicin in NIH3T3 cells .,” no. April, pp. 134–142, 2003.

[68] I. S. Johnson, J. G. Armstrong, and M. Gorman, “The Vinca Alkaloids : A New Class of Oncolytic Agents The Vinca Alkaloids : A New Class of Oncolytic Agents,” pp. 1390–1427, 1963.

[69] M. V Blagosklonny and T. Fojo, “Molecular effects of paclitaxel: myths and reality (a critical review).,” *Int. J. Cancer*, vol. 83, no. 2, pp. 151–6, Oct. 1999.

[70] K. L. Bradley, S. Tyldesley, C. H. Speers, R. Woods, and D. Villa, “Contemporary Systemic Therapy for Male Breast Cancer.,” *Clin. Breast Cancer*, pp. 1–9, Oct. 2013.

[71] I. E. Smith and M. Dowsett, “Aromatase Inhibitors in Breast Cancer,” pp. 2431–2442, 2005.

[72] B. J. Druker, “STI571 (Gleevec) as a paradigm for cancer therapy.,” *Trends Mol. Med.*, vol. 8, no. 4 Suppl, pp. S14–8, Jan. 2002.

[73] K. Tomizawa, K. Suda, R. Onozato, T. Kosaka, H. Endoh, Y. Sekido, H. Shigematsu, H. Kuwano, Y. Yatabe, and T. Mitsudomi, “Prognostic and predictive implications of HER2/ERBB2/neu gene mutations in lung cancers.,” *Lung Cancer*, vol. 74, no. 1, pp. 139–44, Oct. 2011.

[74] T. Vu and F. X. Claret, “Trastuzumab: updated mechanisms of action and resistance in breast cancer.,” *Front. Oncol.*, vol. 2, no. June, p. 62, Jan. 2012.

[75] J. G. Paez, P. a Jänne, J. C. Lee, S. Tracy, H. Greulich, S. Gabriel, P. Herman, F. J. Kaye, N. Lindeman, T. J. Boggon, K. Naoki, H. Sasaki, Y. Fujii, M. J. Eck, W. R. Sellers, B. E. Johnson, and M. Meyerson, “EGFR mutations in lung cancer: correlation with clinical response to gefitinib therapy.,” *Science*, vol. 304, no. 5676, pp. 1497–500, Jun. 2004.

[76] A. a Adjei, “Pemetrexed (ALIMTA), a novel multitargeted antineoplastic agent.,” *Clinical cancer research : an official journal of the American Association for Cancer Research*, vol. 10, no. 12 Pt 2. p. 4276s–4280s, 15-Jun-2004.

[77] B. Rosenberg, L. Vancamp, and T. Krigas, “Inhibition of Cell Division in Escherichia Coli By Electrolysis Products From a Platinum Electrode.,” *Nature*, vol. 205. pp. 698–9, 13-Feb-1965.

[78] B. Rosenberg, L. Van Camp, E. B. Grimley, and A. J. Thomson, “The Inhibition of Growth or Cell Division in Escherichia coli by Different Ionic Species of Platinum (IV) Complexes The Inhibition of Growth or Cell Division in Escherichia by Different Ionic Species of Platinum (IV) Complexes *,” no. Iv, 1967.

[79] D. Resistance and I. S. Effects, “Cisplatin as an Anti-Tumor Drug: Cellular Mechanisms of Activity, Drug Resistance and Induced Side Effects,” *Rev. Lit. Arts Am.*, pp. 1351–1371, 2011.

[80] M. D. Hall, M. Okabe, D.-W. Shen, X.-J. Liang, and M. M. Gottesman, “The role of cellular accumulation in determining sensitivity to platinum-based chemotherapy.,” *Annu. Rev. Pharmacol. Toxicol.*, vol. 48, pp. 495–535, Jan. 2008.

[81] A. K. Holzer and S. B. Howell, “The internalization and degradation of human copper transporter 1 following cisplatin exposure.,” *Cancer Res.*, vol. 66, no. 22, pp. 10944–52, Nov. 2006.

[82] R. J. Knox, F. Friedlos, D. A. Lydall, T. Ii, and J. J. Roberts, “Mechanism of Cytotoxicity of Anticancer Platinum Drugs : Evidence That cis - Diamminedichloroplatinum (II) and cis Only in the Kinetics of Their Interaction with DNA Mechanism of Cytotoxicity of Anticancer Platinum Drugs : Evidence Differ Only in the Kin,” no. Ii, 1986.

[83] C. A. Rabik and M. E. Dolan, “Molecular mechanisms of resistance and toxicity associated with platinating agents,” vol. 33, no. 1, pp. 9–23, 2007.

[84] T. B. S. October, D. B. Zamble, and S. J. Lippard, “Cisplatin and DNA repair in cancer chemotherapy,” no. Iv, 1995.

[85] S. Cohen, SM Lippard, “Cisplatin from DNA damage to cancer chemotherapy.pdf.” Prog Nucleic Acid Res Mol Biol., 2001.

[86] M. Berndtsson, M. Hägg, T. Panaretakis, A. M. Havelka, M. C. Shoshan, and S. Linder, “Acute apoptosis by cisplatin requires induction of reactive oxygen species but is not associated with damage to nuclear DNA.,” *Int. J. Cancer*, vol. 120, no. 1, pp. 175–80, Jan. 2007.

[87] T. Torigoe, H. Izumi, H. Ishiguchi, Y. Yoshida, M. Tanabe, T. Igarashi, I. Niina, T. Wakasugi, T. Imaizumi, M. Kuwano, and K. Kohno, “Cisplatin Resistance and Transcription Factors,” pp. 15–27, 2005.

[88] Z. Yang, L. M. Schumaker, M. J. Egorin, E. G. Zuhowski, Z. Guo, and K. J. Cullen, “Cisplatin preferentially binds mitochondrial DNA and voltage-dependent anion channel protein in the mitochondrial membrane of head and neck squamous cell carcinoma: possible role in apoptosis.,” *Clin. Cancer Res.*, vol. 12, no. 19, pp. 5817–25, Oct. 2006.

[89] O. M. F. and D. V. Hostetter A.A, “Characterization of RNA-Pt Adducts from Cisplatin Treatment of Saccharomyces cerevisiae,” vol. 7, no. 1, pp. 218–225, 2013.

[90] S. Lacour, A. Hammann, S. Grazide, D. Lagadic-gossmann, A. Athias, O. Sergent, G. Laurent, P. Gambert, and E. Solary, “Cisplatin-Induced CD95 Redistribution into Membrane Lipid Rafts of HT29 Human Colon Cancer Cells Cisplatin-Induced CD95 Redistribution into Membrane Lipid Rafts of HT29,” pp. 3593–3598, 2004.

[91] L. Kelland, “The resurgence of platinum-based cancer chemotherapy.,” *Nat. Rev. Cancer*, vol. 7, no. 8, pp. 573–84, Aug. 2007.

[92] L. Galluzzi, L. Senovilla, I. Vitale, J. Michels, I. Martins, O. Kepp, M. Castedo, and G. Kroemer, “Molecular mechanisms of cisplatin resistance.,” *Oncogene*, vol. 31, no. 15, pp. 1869–1883, Sep. 2011.

[93] P. Borst, R. Evers, M. Kool, and J. Wijnholds, “REVIEW A Family of Drug Transporters : the Multidrug Resistance-Associated Proteins OF THE M EMBERS OF THE D RUGS OF A,” vol. 92, no. 16, pp. 1295–1302, 2000.

[94] D. Keppler, “Export pumps for glutathione S-conjugates,” vol. 27, no. 99, pp. 985–991, 1999.

[95] K. J. Cullen, K. A. Newkirk, L. M. Schumaker, and B. R. Haddad, “Glutathione S - Transferase π Amplification is Associated with Cisplatin Resistance in Head and Neck Squamous Cell Carcinoma Cell Lines and Primary Tumors Advances in Brief in Head and Neck Squamous Cell Carcinoma Cell Lines and Primary Tumors,” pp. 8097–8102, 2003.

[96] A. K. Godwin, A. Meistert, P. J. O. Dwyer, C. S. Huangt, T. C. Hamilton, and M. E. Andersont, “High resistance to cisplatin in human ovarian cancer cell lines is associated with marked increase of glutathione synthesis,” vol. 89, no. April, pp. 3070–3074, 1992.

[97] C. Meijer, N. H. Mulder, and H. Timmer-bosscha, “Relationship of Cellular Glutathione to the Cytotoxicity and Resistance of Seven Platinum Compounds Relationship of Cellular Glutathione to the Cytotoxicity and Resistance of Seven Platinum Compounds 1,” pp. 6885–6889, 1992.

[98] H. H. W. Chen and M. T. Kuo, “Role of glutathione in the regulation of Cisplatin resistance in cancer chemotherapy.,” *Met. Based. Drugs*, vol. 2010, Jan. 2010.

[99] S. Shamsuddin, I. Takahashi, Z. H. Siddik, and A. R. Khokhar, “Activity of a Series of Novel Cisplatin Analogs with cis-1 , 4 = Diaminocyclohexane as Nonleaving Amine Group,” vol. 10010, pp. 291–301, 1996.

[100] D. J. Stewart, “Mechanisms of resistance to cisplatin and carboplatin,” *Crit. Rev. Oncol. Hematol.*, vol. 63, pp. 12–31, 2007.

[101] Z. H. Siddik, “Cisplatin : mode of cytotoxic action and molecular basis of resistance,” *Oncogene*, pp. 7265–7279, 2003.

[102] S. Pyndiah, S. Tanida, K. M. Ahmed, E. K. Cassimere, C. Choe, and D. Sakamuro, “c-MYC suppresses BIN1 to release poly(ADP-ribose) polymerase 1: a mechanism by

which cancer cells acquire cisplatin resistance.," *Sci. Signal.*, vol. 4, no. 166, p. ra19, Jan. 2011.

[103] D.-W. Shen, L. M. Pouliot, M. D. Hall, and M. M. Gottesman, "Cisplatin resistance: a cellular self-defense mechanism resulting from multiple epigenetic and genetic changes.," *Pharmacol. Rev.*, vol. 64, no. 3, pp. 706–21, Jul. 2012.

[104] S. G. Chaney, S. L. Campbell, E. Bassett, and Y. Wu, "Recognition and processing of cisplatin- and oxaliplatin-DNA adducts.," *Crit. Rev. Oncol. Hematol.*, vol. 53, no. 1, pp. 3–11, Jan. 2005.

[105] D. Fink, S. Nebel, S. Aebi, H. Zheng, B. Cenm, A. Nehmã, D. Christen, and S. B. Howell, "The Role of DNA Mismatch Repair in Platinum Drug Resistance Advances in Brief The Role of DNA Mismatch Repair in Platinum Drug Resistance1," pp. 4881–4886, 1996.

[106] S. Ramachandran, B. Temple, A. N. Alexandrova, S. G. Chaney, and N. V Dokholyan, "Recognition of Platinum − DNA Adducts by HMGB1a," 2012.

[107] P. Virag, M. Perde-Schrepler, E. Fischer-Fodor, C. Tatomir, S. a Dorneanu, V. I. Cernea, and A. Irimie, "Superior cytotoxicity and DNA cross-link induction by oxaliplatin versus cisplatin at lower cellular uptake in colorectal cancer cell lines.," *Anticancer. Drugs*, vol. 23, no. 10, pp. 1032–8, Nov. 2012.

[108] N. J. Wheate, S. Walker, G. E. Craig, and R. Oun, "The status of platinum anticancer drugs in the clinic and in clinical trials.," *Dalton transactions (Cambridge, England : 2003)*, vol. 39, no. 35. pp. 8113–27, 21-Sep-2010.

[109] B. a Chan and J. I. G. Coward, "Chemotherapy advances in small-cell lung cancer.," *J. Thorac. Dis.*, vol. 5, no. Suppl 5, pp. S565–S578, Oct. 2013.

[110] T. a Hensing, N. H. Hanna, H. H. Gillenwater, M. Gabriella Camboni, C. Allievi, and M. a Socinski, "Phase II study of BBR 3464 as treatment in patients with sensitive or refractory small cell lung cancer.," *Anti-cancer drugs*, vol. 17, no. 6. pp. 697–704, Jul-2006.

[111] J. L. Carr, M. D. Tingle, and M. J. McKeage, "Satraplatin activation by haemoglobin, cytochrome C and liver microsomes in vitro.," *Cancer Chemother. Pharmacol.*, vol. 57, no. 4, pp. 483–90, Apr. 2006.

[112] M. D. Hall and W. Hambley, "Platinum (IV) antitumour compounds : their bioinorganic chemistry," vol. 232, no. 2002, 2006.

[113] M. D. Hall, G. J. Foran, M. Zhang, P. J. Beale, and T. W. Hambley, "XANES determination of the platinum oxidation state distribution in cancer cells treated with platinum(IV) anticancer agents.," *J. Am. Chem. Soc.*, vol. 125, no. 25, pp. 7524–5, Jun. 2003.

[114] L. R. Kelland, B. a Murrer, G. Abel, C. M. Giandomenico, P. Mistry, and K. R. Harrap, "Ammine/amine platinum(IV) dicarboxylates: a novel class of platinum complex

exhibiting selective cytotoxicity to intrinsically cisplatin-resistant human ovarian carcinoma cell lines.," *Cancer Res.*, vol. 52, no. 4, pp. 822–8, Feb. 1992.

[115] P. Gramatica, E. Papa, and M. Luini, "Antiproliferative Pt (IV) complexes : synthesis , biological activity , and quantitative structure – activity relationship modeling," pp. 1157–1169, 2010.

[116] C. N. Sternberg, D. P. Petrylak, O. Sartor, J. A. Witjes, T. Demkow, J.-M. Ferrero, J.-C. Eymard, S. Falcon, F. Calabrò, N. James, I. Bodrogi, P. Harper, M. Wirth, W. Berry, M. E. Petrone, T. J. McKearn, M. Noursalehi, M. George, and M. Rozencweig, "Multinational, double-blind, phase III study of prednisone and either satraplatin or placebo in patients with castrate-refractory prostate cancer progressing after prior chemotherapy: the SPARC trial.," *J. Clin. Oncol.*, vol. 27, no. 32, pp. 5431–8, Nov. 2009.

[117] G. Z. Wang Z, "Targeting and delivery of platinum-based anticancer drugs," pp. 202–224, 2013.

[118] V. K. Ngan, K. Bellman, B. T. Hill, L. Wilson, and M. A. N. N. Jordan, "Mechanism of Mitotic Block and Inhibition of Cell Proliferation by the Semisynthetic Vinca Alkaloids Vinorelbine and Its Newer Derivative Vinflunine," vol. 60, no. 1, pp. 225–232, 2001.

[119] B. Y. A. M. Y. Maxmen, "Cancer research: Open ambition," *Nature*, pp. 8–10, 2012.

[120] B. Pachaiyappan and P. M. Woster, "Design of small molecule epigenetic modulators.," *Bioorg. Med. Chem. Lett.*, vol. 24, no. 1, pp. 21–32, Jan. 2014.

[121] J. Tan, S. Cang, Y. Ma, R. L. Petrillo, and D. Liu, "Novel histone deacetylase inhibitors in clinical trials as anti-cancer agents.," *J. Hematol. Oncol.*, vol. 3, p. 5, Jan. 2010.

[122] H. E. Carraway and S. D. Gore, "Addition of histone deacetylase inhibitors in combination therapy.," *J. Clin. Oncol.*, vol. 25, no. 15, pp. 1955–6, May 2007.

[123] K. Appleton, H. J. Mackay, I. Judson, J. a Plumb, C. McCormick, G. Strathdee, C. Lee, S. Barrett, S. Reade, D. Jadayel, A. Tang, K. Bellenger, L. Mackay, A. Setanoians, A. Schätzlein, C. Twelves, S. B. Kaye, and R. Brown, "Phase I and pharmacodynamic trial of the DNA methyltransferase inhibitor decitabine and carboplatin in solid tumors.," *J. Clin. Oncol.*, vol. 25, no. 29, pp. 4603–9, Oct. 2007.

[124] J. E. Delmore, G. C. Issa, M. E. Lemieux, P. B. Rahl, J. Shi, H. M. Jacobs, E. Kastritis, T. Gilpatrick, R. M. Paranal, J. Qi, M. Chesi, A. C. Schinzel, M. R. McKeown, T. P. Heffernan, C. R. Vakoc, P. L. Bergsagel, I. M. Ghobrial, P. G. Richardson, R. a Young, W. C. Hahn, K. C. Anderson, A. L. Kung, J. E. Bradner, and C. S. Mitsiades, "BET bromodomain inhibition as a therapeutic strategy to target c-Myc.," *Cell*, vol. 146, no. 6, pp. 904–17, Sep. 2011.

[125] X. Wu, J. Qi, J. E. Bradner, G. Xiao, and L.-F. Chen, "Bromodomain and extra-terminal (BET) protein inhibition suppresses HTLV-1 Tax-mediated tumorigenesis by inhibiting NF-κB signaling.," *J. Biol. Chem.*, Nov. 2013.

[126] C.-M. Chiang, “Brd4 engagement from chromatin targeting to transcriptional regulation: selective contact with acetylated histone H3 and H4.,” *F1000 Biol. Rep.*, vol. 1, no. December, p. 98, Jan. 2009.

[127] “Cancer cells acquire super-enhancers at driver genes.,” *Cancer discovery*, vol. 3, no. 12. p. OF12, Dec-2013.

[128] H. A. Hoke, C. Y. Lin, A. Lau, D. A. Orlando, C. R. Vakoc, J. E. Bradner, T. I. Lee, and R. A. Young, “Selective Inhibition of Tumor Oncogenes by Disruption of Super-Enhancers,” 2013.

[129] K. H. Bleicher, H.-J. Böhm, K. Müller, and A. I. Alanine, “Hit and lead generation: beyond high-throughput screening.,” *Nat. Rev. Drug Discov.*, vol. 2, no. 5, pp. 369–78, May 2003.

[130] J. P. Hughes, S. Rees, S. B. Kalindjian, and K. L. Philpott, “Principles of early drug discovery.,” *Br. J. Pharmacol.*, vol. 162, no. 6, pp. 1239–49, Mar. 2011.

[131] G. Francia, S. Man, B. Teicher, L. Grasso, and R. S. Kerbel, “Gene Expression Analysis of Tumor Spheroids Reveals a Role for Suppressed DNA Mismatch Repair in Multicellular Resistance to Alkylating Agents,” *Society*, vol. 24, no. 15, pp. 6837–6849, 2004.

[132] N. T. Elliott and F. A. N. Yuan, “A Review of Three-Dimensional In Vitro Tissue Models for Drug Discovery and Transport Studies,” vol. 100, no. 1, pp. 2–8, 2011.

[133] J. Friedrich, W. Eder, J. Castaneda, M. Doss, E. Huber, R. Ebner, and L. a Kunz-Schughart, “A reliable tool to determine cell viability in complex 3-d culture: the acid phosphatase assay.,” *J. Biomol. Screen. Off. J. Soc. Biomol. Screen.*, vol. 12, no. 7, pp. 925–37, Oct. 2007.

[134] F. I. Ghani, H. Yamazaki, S. Iwata, T. Okamoto, K. Aoe, K. Okabe, Y. Mimura, N. Fujimoto, T. Kishimoto, T. Yamada, C. W. Xu, and C. Morimoto, “Identification of cancer stem cell markers in human malignant mesothelioma cells.,” *Biochem. Biophys. Res. Commun.*, vol. 404, no. 2, pp. 735–42, Jan. 2011.

[135] J. Friedrich, C. Seidel, R. Ebner, and L. a Kunz-Schughart, “Spheroid-based drug screen: considerations and practical approach.,” *Nat. Protoc.*, vol. 4, no. 3, pp. 309–24, Jan. 2009.

[136] I. Dufau, C. Frongia, F. Sicard, L. Dedieu, P. Cordelier, F. Ausseil, B. Ducommun, and A. Valette, “Multicellular tumor spheroid model to evaluate spatio-temporal dynamics effect of chemotherapeutics: application to the gemcitabine/CHK1 inhibitor combination in pancreatic cancer.,” *BMC Cancer*, vol. 12, no. 1, p. 15, Jan. 2012.

[137] A. Ivascu and M. Kubbies, “Rapid generation of single-tumor spheroids for high-throughput cell function and toxicity analysis.,” *J. Biomol. Screen.*, vol. 11, no. 8, pp. 922–32, Dec. 2006.

[138] F. Hirschhaeuser, H. Menne, C. Dittfeld, J. West, W. Mueller-Klieser, and L. a Kunz-Schughart, “Multicellular tumor spheroids: an underestimated tool is catching up again.,” *J. Biotechnol.*, vol. 148, no. 1, pp. 3–15, Jul. 2010.

[139] A. S. Mikhail, S. Eetezadi, and C. Allen, “Multicellular tumor spheroids for evaluation of cytotoxicity and tumor growth inhibitory effects of nanomedicines in vitro: a comparison of docetaxel-loaded block copolymer micelles and Taxotere®.,” *PLoS One*, vol. 8, no. 4, p. e62630, Jan. 2013.

[140] R.-Z. Lin, R.-Z. Lin, and H.-Y. Chang, “Recent advances in three-dimensional multicellular spheroid culture for biomedical research.,” *Biotechnol. J.*, vol. 3, no. 9–10, pp. 1172–84, Oct. 2008.

[141] M. Carbone and M. a. Rdzanek, “Pathogenesis of Malignant Mesothelioma,” *Clin. Lung Cancer*, vol. 5, no. April, pp. S46–S50, Apr. 2004.

[142] K. Donaldson, □ C. A. P., and T. C. C, “Pulmonary toxicity of carbon nanotubes and asbestos - Similarities and differences.” Advanced Drug Delivery Reviews, pp. 2078–2086, 2013.

[143] W. S. Kamp DW, Graceffa P, Pryor WA, “The role of free radicals in asbestos-induced diseases.” pp. 293–315, 1992.

[144] J. C. Barrett, P. W. Lamb, and R. W. Wiseman, “Multiple Mechanisms for the Carcinogenic Effects of Asbestos and Other Mineral Fibers Asbestos and Multistage,” vol. 81, pp. 81–89, 1989.

[145] R. M. Rudd, “Malignant mesothelioma.,” *Br. Med. Bull.*, vol. 93, pp. 105–23, Jan. 2010.

[146] J. C. Wagner, C. A. Sleggs, and P. Marchand, “Diffuse pleural mesothelioma ans asbestos exposure in the North Western Cape province,” pp. 260–271, 1960.

[147] C. Bianchi and T. Bianchi, “Malignant mesothelioma: global incidence and relationship with asbestos.,” *Ind. Health*, vol. 45, no. 3, pp. 379–87, Jun. 2007.

[148] B. M. Robinson, “Malignant pleural mesothelioma : an epidemiological perspective,” vol. 1, no. 9, pp. 491–496, 2012.

[149] Y. Sekido, “Molecular pathogenesis of malignant mesothelioma.,” *Carcinogenesis*, vol. 34, no. 7, pp. 1413–9, Jul. 2013.

[150] R. M. Rudd, “Malignant mesothelioma.,” *Br. Med. Bull.*, vol. 93, pp. 105–23, Jan. 2010.

[151] S. P. Riaz, V. H. Coupland, M. Lüchtenborg, M. D. Peake, and H. Møller, “Mesothelioma incidence projections in South East England.,” *Eur. Respir. J.*, vol. 40, no. 4, pp. 965–8, Oct. 2012.

[152] “httpwww.asbestos.comworld-trade-center.” .

[153] V. Delgermaa, K. Takahashi, E.-K. Park, G. V. Le, T. Hara, and T. Sorahan, “Global mesothelioma deaths reported to the World Health Organization between 1994 and 2008.,” *Bull. World Health Organ.*, vol. 89, no. 10, pp. 716–24, 724A–724C, Oct. 2011.

[154] B. M. Robinson, “Malignant pleural mesothelioma: an epidemiological perspective.,” *Ann. Cardiothorac. Surg.*, vol. 1, no. 4, pp. 491–6, Nov. 2012.

[155] L. Fazzo, G. Minelli, M. De Santis, C. Bruno, and A. Zona, “Mesothelioma mortality surveillance and asbestos exposure tracking in Italy,” pp. 300–310, 2012.

[156] M. Carbone and H. Yang, “Molecular pathways: targeting mechanisms of asbestos and erionite carcinogenesis in mesothelioma.,” *Clin. Cancer Res.*, vol. 18, no. 3, pp. 598–604, Feb. 2012.

[157] M. S. Cooke, M. D. Evans, M. Dizdaroglu, and J. Lunec, “Oxidative DNA damage: mechanisms, mutation, and disease.,” *FASEB J.*, vol. 17, no. 10, pp. 1195–214, Jul. 2003.

[158] A. Marrogi, H. I. Pass, M. Khan, L. J. Metheny-Barlow, C. C. Harris, and B. I. Gerwin, “Human Mesothelioma Samples Overexpress Both Cyclooxygenase-2 (COX-2) and Inducible Nitric Oxide Synthase (NOS2): In Vitro Antiproliferative Effects of a COX-2 Inhibitor,” *Cancer Res.*, vol. 60, no. 14, pp. 3696–3700, Jul. 2000.

[159] Z. Coussens, LM Werb, “Inflammation and cancer,” vol. 420, no. 6917, pp. 860–867, 2010.

[160] a U. Dogan, Y. I. Baris, M. Dogan, S. Emri, I. Steele, A. G. Elmishad, and M. Carbone, “Genetic predisposition to fiber carcinogenesis causes a mesothelioma epidemic in Turkey.,” *Cancer Res.*, vol. 66, no. 10, pp. 5063–8, May 2006.

[161] R. L. Garcea and M. J. Imperiale, “Simian Virus 40 Infection of Humans,” vol. 77, no. 9, 2003.

[162] Z. Mohammad-Taheri, S. A. Nadji, F. Raisi, F. Mohammadi, M. Bahadori, and E. J. Mark, “No association between simian virus 40 and diffuse malignant mesothelioma of the pleura in Iranian patients: a molecular and epidemiologic case-control study of 60 patients.,” *American journal of industrial medicine*, vol. 56, no. 10. pp. 1221–5, Oct-2013.

[163] P. a Zucali, G. L. Ceresoli, F. De Vincenzo, M. Simonelli, E. Lorenzi, L. Gianoncelli, and a Santoro, “Advances in the biology of malignant pleural mesothelioma.,” *Cancer Treat. Rev.*, vol. 37, no. 7, pp. 543–58, Nov. 2011.

[164] A. J. Physiol, L. Cell, M. Physiol, K. Järvinen, P. Pietarinen-runtti, K. Linnainmaa, K. O. Raivio, C. M. Krejsa, T. Kavanagh, V. L. Kinnula, and B. E. Britigan, “Antioxidant defense mechanisms of human mesothelioma and lung adenocarcinoma cells Antioxidant defense mechanisms of human mesothelioma and lung adenocarcinoma cells,” *Am. J. Physiol.*, 2011.

[165] V. L. Kinnula, “Oxidant and antioxidant mechanisms of lung disease caused by asbestos fibres,” pp. 706–716, 1999.

[166] K. Kinnula, K. Linnainmaa, K. O. Raivio, and V. L. Kinnula, “Endogenous antioxidant enzymes and glutathione S . transferase in protection of mesothelioma cells against hydrogen peroxide and epirubicin toxicity,” vol. 77, pp. 1097–1102, 1998.

[167] O. D. Røe, E. Anderssen, H. Sandeck, T. Christensen, E. Larsson, and S. Lundgren, “Malignant pleural mesothelioma: genome-wide expression patterns reflecting general resistance mechanisms and a proposal of novel targets.,” *Lung Cancer*, vol. 67, no. 1, pp. 57–68, Jan. 2010.

[168] T. Berghmans, M. Paesmans, Y. Lalami, I. Lou, S. Luce, C. Mascaux, A. P. Meert, and J. P. Sculier, “Activity of chemotherapy and immunotherapy on malignant mesothelioma : a systematic review of the literature with meta-analysis,” vol. 38, 2002.

[169] N. J. Vogelzang, J. J. Rusthoven, J. Symanowski, C. Denham, E. Kaukel, P. Ruffie, U. Gatzemeier, M. Boyer, S. Emri, C. Manegold, C. Niyikiza, and P. Paoletti, “Phase III study of pemetrexed in combination with cisplatin versus cisplatin alone in patients with malignant pleural mesothelioma.,” *J. Clin. Oncol.*, vol. 21, no. 14, pp. 2636–44, Jul. 2003.

[170] J. Remon, P. Lianes, S. Martínez, and R. Querol, “Malignant mesothelioma : New insights into a rare disease,” *Cancer Treat. Rev.*, vol. 39, no. 6, pp. 584–591, 2013.

[171] C. W. Lee, N. Murray, H. Anderson, S. C. Rao, and W. Bishop, “Outcomes with first-line platinum-based combination chemotherapy for malignant pleural mesothelioma: a review of practice in British Columbia.,” *Lung cancer (Amsterdam, Netherlands)*, vol. 64, no. 3. pp. 308–13, Jun-2009.

[172] F. E. Mott, “Mesothelioma: a review.,” *Ochsner J.*, vol. 12, no. 1, pp. 70–9, Jan. 2012.

[173] L. Greillier, S. Marco, and F. Barlesi, “Targeted therapies in malignant pleural mesothelioma: a review of clinical studies,” *Anticancer. Drugs*, vol. 22, no. 3, pp. 199–205, Mar. 2011.

[174] F. Vandermeers, S. N. Sriramareddy, C. Costa, R. Hubaux, J. Cosse, and L. Willems, “Lung Cancer The role of epigenetics in malignant pleural mesothelioma,” *Lung Cancer*, vol. 81, no. 3, pp. 311–318, 2013.

[175] F. Vandermeers, P. Hubert, P. Delvenne, C. Mascaux, B. Grigoriu, A. Burny, A. Scherpereel, and L. Willems, “Valproate, in combination with pemetrexed and cisplatin, provides additional efficacy to the treatment of malignant mesothelioma.,” *Clin. Cancer Res.*, vol. 15, no. 8, pp. 2818–28, Apr. 2009.

[176] I. Zanellato, C. D. Boidi, G. Lingua, P.-G. Betta, S. Orecchia, E. Monti, and D. Osella, “In vitro anti-mesothelioma activity of cisplatin-gemcitabine combinations: evidence for sequence-dependent effects,” *Cancer Chemother. Pharmacol.*, Apr. 2010.

[177] T. Braumann, “Determination of hydrophobic parameters by reversed-phase liquid chromatography: theory, experimental techniques, and application in studies on quantitative structure-activity relationships.” J Chromatogr., pp. 191–225., 1986.

[178] P. Corporation, “Solution Cell Proliferation CellTiter 96 ® AQ ueous One Solution Cell Proliferation Assay.”

[179] www.promega.com, “CellTiter-Blue ® Cell Viability Assay Technical Bulletin.”

[180] M. Oliver, N. Harrison, J. Bishop, P. Cole, and G. Laurent, “A rapid and convenient assay for counting cells cultured in microwell plates: application for assessment of growth factors,” *J Cell Sci*, vol. 92, no. 3, pp. 513–518, Mar. 1989.

[181] E. Magnani and E. Bettini, “Resazurin detection of energy metabolism changes in serum-starved PC12 cells and of neuroprotective agent effect,” *Brain Res. Brain Res. Protoc.*, vol. 5, no. 3, pp. 266–272, Jul. 2000.

[182] T. L. Riss, R. A. Moravec, A. L. Niles, and L. Minor, “Cell Viability Assays-Assay Guidance Manual,” 2013.

[183] N. A. P. Franken, H. M. Rodermond, J. Stap, J. Haveman, and C. van Bree, “Clonogenic assay of cells in vitro,” *Nat. Protoc.*, vol. 1, no. 5, pp. 2315–2319, 2006.

[184] T. Chou and P. Talalayi, “QUANTITATIVE DOSE-EFFECT RELATIONSHIPS : THE COMBINED EFFECTS OF MULTIPLE.”

[185] G. P. Dimri, X. Lee, G. Basile, M. Acosta, G. Scott, C. Roskelley, E. E. Medrano, M. Linskens, I. Rubelj, and O. Pereira-Smith, “A biomarker that identifies senescent human cells in culture and in aging skin in vivo,” *Proc. Natl. Acad. Sci. U. S. A.*, vol. 92, no. 20, pp. 9363–9367, Sep. 1995.

[186] K. J. Wiechelman, R. D. Braun, and J. D. Fitzpatrick, “Investigation of the bicinchoninic acid protein assay: identification of the groups responsible for color formation.,” *Analytical biochemistry*, vol. 175, no. 1. pp. 231–7, 15-Nov-1988.

[187] M. J. B. Habig, WH Pabst, “Glutathione S-Transferases,” no. 22, pp. 7130–7139, 1974.

[188] J. Daubriac, J. Fleury-Feith, L. Kheuang, J. Galipon, a Saint-Albin, a Renier, M. Giovannini, F. Galateau-Sallé, and M.-C. Jaurand, “Malignant pleural mesothelioma cells resist anoikis as quiescent pluricellular aggregates.,” *Cell Death Differ.*, vol. 16, no. 8, pp. 1146–55, Aug. 2009.

[189] J. Klominek, K. Robért, A. Hjerpe, M. C. Lines, K. Robert, and B. Wickstrã, “Serum-dependent Growth Patterns of Two , Newly Established Human Mesothelioma Cell Lines Serum-dependent Growth Patterns of Two , Newly Established Human,” pp. 6118–6122, 1989.

[190] K.-U. Kim, S. M. Wilson, K. S. Abayasiriwardana, R. Collins, L. Fjellbirkeland, Z. Xu, D. M. Jablons, S. L. Nishimura, and V. C. Broaddus, “A novel in vitro model of human mesothelioma for studying tumor biology and apoptotic resistance.,” *Am. J. Respir. Cell Mol. Biol.*, vol. 33, no. 6, pp. 541–8, Dec. 2005.

[191] Y. T. Phung, D. Barbone, V. C. Broaddus, and M. Ho, “Rapid Generation of In Vitro Multicellular Spheroids for the Study of Monoclonal Antibody Therapy,” 2011.

[192] R. Chignola, a Schenetti, G. Andrighetto, E. Chiesa, R. Foroni, S. Sartoris, G. Tridente, and D. Liberati, “Forecasting the growth of multicell tumour spheroids: implications for the dynamic growth of solid tumours.,” *Cell Prolif.*, vol. 33, no. 4, pp. 219–29, Aug. 2000.

[193] R. Demicheli, R. Foroni, a Ingrosso, G. Pratesi, C. Soranzo, and M. Tortoreto, “An exponential-Gompertzian description of LoVo cell tumor growth from in vivo and in vitro data.,” *Cancer Res.*, vol. 49, no. 23, pp. 6543–6, Dec. 1989.

[194] S. Aizawa, K. Ookawa, T. Kudo, J. Asano, M. Hayakari, and S. Tsuchida, “Characterization of cell death induced by ethacrynic acid in a human colon cancer cell line DLD-1 and suppression by N-acetyl-L-cysteine.,” *Cancer Sci.*, vol. 94, no. 10, pp. 886–93, Oct. 2003.

[195] K. Järvinen, Y. Soini, K. Kahlos, and V. L. Kinnula, “Overexpression of γ-glutamylcysteine synthetase in human malignant mesothelioma,” *Hum. Pathol.*, vol. 33, no. 7, pp. 748–755, Jul. 2002.

[196] S.-S. Byun, S. W. Kim, H. Choi, C. Lee, and E. Lee, “Augmentation of cisplatin sensitivity in cisplatin-resistant human bladder cancer cells by modulating glutathione concentrations and glutathione-related enzyme activities.,” *BJU Int.*, vol. 95, no. 7, pp. 1086–90, May 2005.

[197] W. H. Ang, I. Khalaila, C. S. Allardyce, L. Juillerat-Jeanneret, and P. J. Dyson, “Rational design of platinum(IV) compounds to overcome glutathione-S-transferase mediated drug resistance.,” *J. Am. Chem. Soc.*, vol. 127, no. 5, pp. 1382–3, Feb. 2005.

[198] S. Awasthi, S. K. Srivastava, F. Ahmad, H. Ahmad, and G. a Ansari, “Interactions of glutathione S-transferase-pi with ethacrynic acid and its glutathione conjugate.,” *Biochimica et biophysica acta*, vol. 1164, no. 2. pp. 173–8, 10-Jul-1993.

[199] I. Zanellato, I. Bonarrigo, M. Sardi, M. Alessio, E. Gabano, M. Ravera, and D. Osella, “Evaluation of platinum-ethacrynic Acid conjugates in the treatment of mesothelioma,” *ChemMedChem*, vol. 6, no. 12, pp. 2287–2293, Dec. 2011.

[200] W. H. Ang, S. Pilet, R. Scopelliti, F. Bussy, L. Juillerat-Jeanneret, and P. J. Dyson, “Synthesis and characterization of platinum(IV) anticancer drugs with functionalized aromatic carboxylate ligands: influence of the ligands on drug efficacies and uptake.,” *J. Med. Chem.*, vol. 48, no. 25, pp. 8060–9, Dec. 2005.

[201] M. D. Hall, S. Amjadi, M. Zhang, P. J. Beale, and T. W. Hambley, “The mechanism of action of platinum(IV) complexes in ovarian cancer cell lines.,” *J. Inorg. Biochem.*, vol. 98, no. 10, pp. 1614–24, Oct. 2004.

[202] S. B. Giaccone G, O’Brien ME, Byrne MJ, Bard M, Kaukel E, “Phase II trial of ZD0473 as second-line therapy in mesothelioma..pdf.” Eur J Cancer. 2002, 2002.

[203] S. R. A. Khan, S. Huang, S. Shamsuddin, S. Inutsuka, K. H. Whitmire, H. Siddik, and A. R. Khokhar, "Synthesis , Characterization and Cytotoxicity of New Platinum (IV) Axial Carboxylate Complexes : Crystal Structure of Potential Antitumor Agent [Pt (trans -1 R , 2 R -Diaminocyclohexane) trans (acetate) 2 Cl 2]," vol. 8, pp. 515–521, 2000.

[204] M. Ravera, E. Gabano, I. Zanellato, I. Bonarrigo, E. Escribano, V. Moreno, T. Calvet, and D. Osella, "Synthesis, characterization and antiproliferative activity on mesothelioma cells of bis(carboxylato)platinum(IV) complexes based on picoplatin," *Dalt. Trans.*, 2012.

[205] P. Filippakopoulos, J. Qi, S. Picaud, Y. Shen, W. B. Smith, O. Fedorov, E. M. Morse, T. Keates, T. T. Hickman, I. Felletar, M. Philpott, S. Munro, M. R. McKeown, Y. Wang, A. L. Christie, N. West, M. J. Cameron, B. Schwartz, T. D. Heightman, N. La Thangue, C. a French, O. Wiest, A. L. Kung, S. Knapp, and J. E. Bradner, "Selective inhibition of BET bromodomains.," *Nature*, vol. 468, no. 7327, pp. 1067–73, Dec. 2010.

[206] W. W. Lockwood, K. Zejnullahu, J. E. Bradner, and H. Varmus, "Sensitivity of human lung adenocarcinoma cell lines to targeted inhibition of BET epigenetic signaling proteins.," *Proc. Natl. Acad. Sci. U. S. A.*, vol. 109, no. 47, pp. 19408–13, Nov. 2012.

[207] A. Kitamura, K. Matsushita, Y. Takiguchi, H. Shimada, Y. Tada, M. Yamanaka, K. Hiroshima, M. Tagawa, T. Tomonaga, H. Matsubara, M. Inoue, M. Hasegawa, Y. Sato, D. Levens, K. Tatsumi, and F. Nomura, "Synergistic effect of non-transmissible Sendai virus vector encoding the c-myc suppressor FUSE-binding protein-interacting repressor plus cisplatin in the treatment of malignant pleural mesothelioma," 2011.

[208] S. Adhikary and M. Eilers, "Transcriptional regulation and transformation by Myc proteins.," *Nat. Rev. Mol. Cell Biol.*, vol. 6, no. 8, pp. 635–45, Aug. 2005.

[209] A. M. Havelka, M. Berndtsson, M. H. Olofsson, M. C. Shoshan, and S. Linder, "Mechanisms of action of DNA-damaging anticancer drugs in treatment of carcinomas: is acute apoptosis an 'off-target' effect?," *Mini Rev. Med. Chem.*, vol. 7, no. 10, pp. 1035–1039, Oct. 2007.

[210] I. B. Roninson, "Tumor cell senescence in cancer treatment.," *Cancer Res.*, vol. 63, no. 11, pp. 2705–15, Jun. 2003.

[211] J. W. Shay and I. B. Roninson, "Hallmarks of senescence in carcinogenesis and cancer therapy.," *Oncogene*, vol. 23, no. 16, pp. 2919–33, Apr. 2004.

[212] S. Mannava, K. C. Moparthy, L. J. Wheeler, K. I. Leonova, A. Joseph, A. B. Smiraglia, A. E. Berman, S. Flanagan, S. Donna, N. C. Zeitouni, A. V Gudkov, C. K. Mathews, and A. Mikhail, "Ribonucleotide reductase and thymidylate synthase or exogenous deoxyribonucleosides reduce DNA damage and senescence caused by C - MYC depletion," vol. 4, no. 12, pp. 917–922, 2012.

[213] A. Catalano, L. Graciotti, L. Rinaldi, G. Raffaelli, S. Rodilossi, P. Betta, W. Gianni, S. Amoroso, and A. Procopio, "Preclinical evaluation of the nonsteroidal anti-inflammatory agent celecoxib on malignant mesothelioma chemoprevention.,"

International journal of cancer. Journal international du cancer, vol. 109, no. 3. pp. 322–8, 10-Apr-2004.

[214] T. Roth, C. Eckert, H.-H. Fiebig, and M. Jung, "Comparative action of cobalt carbonyl complexes on cancer cells using human tumor xenografts," *Anticancer Res.*, vol. 22, no. 4, pp. 2281–2284, Aug. 2002.

[215] C. Stenger, T. Naves, M. Verdier, and M. Ratinaud, "The cell death response to the ROS inducer , cobalt chloride , in neuroblastoma cell lines according to p53 status," pp. 601–609, 2011.

[216] I. García-Arnandis, M. I. Guillén, F. Gomar, M. A. Castejón, and M. J. Alcaraz, "Control of cell migration and inflammatory mediators production by CORM-2 in osteoarthritic synoviocytes," *PLoS One*, vol. 6, no. 9, p. e24591, 2011.

[217] A. J. Atkin, S. Williams, P. Sawle, R. Motterlini, J. M. Lynam, and I. J. S. Fairlamb, "μ2-Alkyne dicobalt(0)hexacarbonyl complexes as carbon monoxide-releasing molecules (CO-RMs): probing the release mechanism," *Dalt. Trans.*, no. 19, pp. 3653–3656, May 2009.

[218] L. Li, A. Hsu, and P. K. Moore, "Actions and interactions of nitric oxide, carbon monoxide and hydrogen sulphide in the cardiovascular system and in inflammation--a tale of three gases!," *Pharmacol. Ther.*, vol. 123, no. 3, pp. 386–400, Sep. 2009.

[219] I. Ott, K. Schmidt, B. Kircher, P. Schumacher, T. Wiglenda, and R. Gust, "Antitumor-Active Cobalt−Alkyne Complexes Derived from Acetylsalicylic Acid: Studies on the Mode of Drug Action," *J Med Chem*, vol. 48, no. 2, pp. 622–629, 2005.

[220] "Crosstalk of reactive oxygen species and NF-κB signaling.pdf." .

[221] M. D. Díaz-Muñoz, I. C. Osma-García, C. Cacheiro-Llaguno, M. Fresno, and M. A. Iñiguez, "Coordinated up-regulation of cyclooxygenase-2 and microsomal prostaglandin E synthase 1 transcription by nuclear factor kappa B and early growth response-1 in macrophages," *Cell. Signal.*, vol. 22, no. 10, pp. 1427–1436, Oct. 2010.

[222] F. Scalera, J. Borlak, B. Beckmann, J. Martens-Lobenhoffer, T. Thum, M. Täger, and S. M. Bode-Böger, "Endogenous nitric oxide synthesis inhibitor asymmetric dimethyl L-arginine accelerates endothelial cell senescence," *Arterioscler. Thromb. Vasc. Biol.*, vol. 24, no. 10, pp. 1816–1822, Oct. 2004.

[223] J. Clària and C. N. Serhan, "Aspirin triggers previously undescribed bioactive eicosanoids by human endothelial cell-leukocyte interactions," *Proc. Natl. Acad. Sci. U. S. A.*, vol. 92, no. 21, pp. 9475–9479, Oct. 1995.

[224] J. E. Keeble and P. K. Moore, "Pharmacology and potential therapeutic applications of nitric oxide-releasing non-steroidal anti-inflammatory and related nitric oxide-donating drugs," *Br. J. Pharmacol.*, vol. 137, no. 3, pp. 295–310, Oct. 2002.

[225] A. Sparatore, E. Perrino, V. Tazzari, D. Giustarini, R. Rossi, G. Rossoni, K. Erdmann, K. Erdman, H. Schröder, and P. Del Soldato, "Pharmacological profile of a novel

H(2)S-releasing aspirin.,” *Free Radic. Biol. Med.*, vol. 46, no. 5, pp. 586–92, Mar. 2009.